The Surface Structure and the Chemical Activity of $V_2O_3(0001)$ Model Catalysts

vorgelegt von Master of Science in Chemistry
Mohammad Abu Haija
aus Jordanien

von der
Fakultät II – Mathematik und Naturwissenschaften
der Technischen Universität Berlin
zur Erlangung des akademischen Grades
Doktor der Naturwissenschaften
Dr. rer. nat.

genehmigte Dissertation

Promotionsausschuss:

Vorsitzender: Prof. Dr. M. Schoen
Berichter: Prof. Dr. H.-J. Freund
Berichter: Prof. Dr. G. H. Findenegg
Berichter: Prof. Dr. Hildebrandt

Tag der wissenschaftlichen Aussprache: 14. August 2006

Berlin 2006

D 83

Abstract

Results of a systematic study of various aspects of the well-defined $V_2O_3(0001)$ model catalyst system are presented. This study deals with the preparation, the characterization and the chemical activity of the $V_2O_3(0001)$ model catalyst. Experiments are carried out under UHV conditions using a variety of surface sensitive techniques such as low energy electron diffraction (LEED), thermal desorption spectroscopy (TDS), x-ray photoelectron spectroscopy (XPS), ultraviolet photoelectron spectroscopy (UPS), near-edge x-ray absorption fine structure (NEXAFS), infrared reflection-absorption spectroscopy (IRAS), and high resolution electron energy loss spectroscopy (HREELS).

In the present study, the $V_2O_3(0001)$ model catalyst is prepared as a thin film with a thickness of ~100 Å on Au(111) and W(110) substrates. The surface of $V_2O_3(0001)$ can be terminated by a layer of vanadyl groups or by a layer of vanadium atoms. Characterization studies of these surfaces are performed focusing on their geometric and electronic properties which are correlated with their chemical activities. The chemical activities of the differently terminated $V_2O_3(0001)$ surfaces are investigated by adsorption of a variety of probe molecules. Chemisorbed species are identified and investigated in terms of stability, geometric and electronic properties as well as reaction paths. The investigated molecules are oxygen, carbon monoxide, carbon dioxide, water, propane and propene. The influence of the surface termination on the adsorption and the reaction of these molecules is addressed. In this way, the structure-activity relationship is established.

The vanadyl terminated $V_2O_3(0001)$ surface is found to be chemically inert towards all the investigated molecules whereas the vanadium terminated $V_2O_3(0001)$ surface is found to be chemically active. The difference between the chemical activities of the two surface terminations is a result of their differing geometric and electronic properties. These properties permit strong interactions with the vanadium terminated surface only, leading to dissociative adsorption in some cases. Unlike the surface vanadium atoms on the vanadyl terminated surface, the surface vanadium atoms on the vanadium terminated surface are freely accessible to the adsorbed molecules and exhibit a lower oxidation state. The adsorption of O_2 on the vanadium terminated surface leads to the formation of vanadyl groups and negatively charged peroxo (O_2^{2-}) species. Annealing the peroxo-covered surface restores the vanadyl terminated layer. CO interacts strongly with the vanadium terminated surface and adsorbs in a tilted geometry on the surface. Annealing the CO-covered surface leads to the formation of vanadyl groups, most likely via CO dissociation. The adsorption of CO_2 on the vanadium terminated surface induces the formation of strongly bonded, bent $CO_2^{\delta-}$ species in addition to weakly bonded, linear CO_2 species. $CO_2^{\delta-}$ adsorbs in C_{2v} symmetry in which the O–O axis is parallel to the surface. Upon annealing it decomposes to CO and O with the oxygen atoms forming vanadyl groups. H_2O dissociates on the vanadium terminated surface and forms OH species which are stable up to ~600 K. The adsorption of C_3H_8 and C_3H_6 on the vanadium terminated surface leads to the formation of oxidized hydrocarbon species.

Contents

Chapter 1

Introduction

This chapter provides a justification for the experimental approach of the present study. The utility of studying model catalyst systems in order to obtain a fundamental understanding of heterogeneous catalytic processes is addressed. After a brief literature overview of vanadium oxide systems, the objectives and the structure of the present thesis are described.

1.1 Why model catalysts?

Transition metal oxides display a broad variety of physical and chemical properties [1,2]. Many oxides undergo phase transitions accompanied by interesting structural and electronic behavior. One of the areas where metal oxides are employed to a large extent is heterogeneous catalysis. In such an area, oxide materials function either as catalysts or as supports for active components [3].

In the early 1960s, heterogeneous catalysts were viewed as a *black box* that converted reactant molecules to desirable products [4]. Although heterogeneous catalysts were investigated over many decades, open questions related to their catalytic properties still exist. This is mainly due to the very limited knowledge about their microscopic properties. Heterogeneous catalyst surfaces usually consist of different components and exhibit a high density of defects, a complicated morphology and different crystallographic surfaces. Moreover, parameters such as the method of preparation and the thermal treatment can greatly influence the surface and the catalytic properties of the catalysts. Therefore, an accurate characterization of these surfaces or of intermediate species, which may form on such surfaces during a catalytic reaction, represents a difficult task. Thus, a challenge in the field of heterogeneous catalysis is to achieve an atomic level understanding of catalytic reaction processes.

The need for a scientific understanding of catalytic reaction processes motivated the development of the *surface science approach* to heterogeneous catalysis. Within this approach, studies of elementary reaction steps are commonly conducted on well-defined

model catalyst systems under ultra-high vacuum (UHV) conditions. These studies are performed by using a set of surface science techniques to precisely characterize surfaces. A large number of well-defined model catalyst systems, ranging from single-crystal surfaces of metals to thin films of oxides, were intensively investigated over the last 35 years. The results of these efforts are available in a number of review articles and books [5-12]. The use of well-defined model catalysts is now an established procedure for studying the elementary steps of industrial catalytic reactions under well-defined conditions. However, the UHV methodology obviously differs from that of technical catalysis where elevated pressures and high-surface area materials are typically utilized. In order to bridge the so-called *pressure and material gaps* between model and technical catalysis, surface science methodologies are extended to investigate model catalyst systems with increasing degree of complexity under more realistic reaction conditions [13,14].

An essential part of many model catalysts is a single crystalline oxide surface. However, the preparation of clean oxide surfaces turned out to be very difficult [15]. The availability of high quality single-crystal oxides is rather limited. Even when they are available, a number of experimental problems associated with the preparation of their surfaces might appear. Such problems are mainly related to the sample mounting, heating and temperature controlling [16]. An important development in the surface science of oxides is the use of thin film growth techniques to prepare high-quality oxide surfaces [17-20]. Commonly, the oxide film is grown on a well-ordered metal substrate with a good lattice match to the desired oxide overlayer. The oxide film may also be prepared by direct oxidation of a metallic (or bimetallic) substrate. An overview of some well-ordered thin oxide films described in the literature is available in reference [16]. The thin film methodology facilitates the use of a wide range of surface spectroscopic and structural probes to characterize model catalyst surfaces and to identify stable surface species. In fact, the oxide films do not tend to charge if they are not too thick [21].

The understanding of the surface chemistry of the oxide model catalysts is of considerable importance for the development of a clear atomic picture of chemical interactions at their surfaces. A common approach to this goal is the study of adsorption of molecules on these surfaces using surface sensitive techniques. A particular emphasis in this approach is placed on the identification and characterization of relevant surface

intermediate species [22]. The geometric and electronic structure of the intermediate species as well as their reactivity can then be investigated in more details. The information provided by the adsorption studies are essential for understanding the fundamental mechanisms in heterogonous catalysis. With this purpose in mind, numerous investigations of adsorption and reaction of molecules on model catalyst surfaces were performed in recent years [18,23-26].

1.2 Vanadium oxides

The vanadium-oxygen system is a very complex one. In this system, many compounds may form such as the single valency oxides in the form of VO, VO_2, V_2O_3 and V_2O_5, and the mixed valency oxides in the form of $V_{2n}O_{5n-1}$ (Wadsley phase) and V_nO_{2n-1} (Magnéli phase). Vanadium oxides are intensively studied due to their unique physical and chemical properties. They are widely employed in many technological applications such as catalysis, electronic materials, battery electrodes, and gas chromatography [27-29]. Moreover, they have attractive characteristics for the detection of toxic and flammable gases [30,31] and they are even components of medical implants [32]. In order to cover such a wide rage of applications, a number of different techniques were developed [33-36] to prepare different forms of vanadium oxides [37-41]. The special and rich chemistry of vanadium oxides results from two interrelated factors [29,42]. The first factor is that vanadium ions can exist in various formal oxidation states ranging from +2 to +5. The second factor is that the ions can exhibit different coordination geometries such as octahedra, pentagonal bypyramids, square pyramids and tetrahedra, which can share corners, edges and faces, presenting a notable variety of structural arrangements.

Vanadium oxides and supported vanadium oxides are excellent catalysts used in a large number of chemical reactions (examples are provided in Appendix B). Vanadium oxide-based catalysts are used for the manufacture of important chemicals and for the reduction of environmental pollution [43]. The authors also emphasized the importance of these catalysts by an extensive open literature search on oxide catalysts which demonstrated that about 28% of the published articles in the period 1967-2000 dealt with vanadium in supported metal oxide catalysis. Despite of this importance, many fundamental questions concerning the catalytic performance of vanadium oxide

catalysts, especially the nature of the active species are still under debate [43-45]. These unresolved issues are mainly due to the lack of a reliable understanding of the microscopic structure of vanadium oxide catalyst surfaces. The main reason for this lack of understanding is the high complexity these surfaces. Such an understanding can be achieved by utilizing the surface science approach; namely, when vanadium oxide model catalysts that exhibit well-defined surface properties are investigated.

In attempts to contribute to a fundamental understanding of vanadium oxides, many research groups utilized the surface science approach by studying the growth and properties of vanadium oxide layers prepared on a number of surfaces. For instance, vanadium oxide layers were prepared on surfaces of metals such as Au(111) [46,47], W(110) [47], Cu(100) [48], Cu_3Au(100) [49], Ni(110) [50], Pt(111) [51-53] and Rh(111) [54,55], and on surfaces of oxides such as TiO_2 [56,57], Al_2O_3(0001) [58], CeO_2(111) [59] and MgO(100) [60]. Within this approach, single phase vanadium oxide layers may serve as model systems for vanadium oxide-based catalysts and may provide a molecular level understanding of their chemical activity. The V_2O_3(0001) model catalyst, in particular, was investigated at the fundamental level by a number of experimental [47,54] and theoretical [61-64] studies. The aim of these studies was to understand the geometric and electronic properties of the V_2O_3(0001) surface. The understanding of the V_2O_3(0001) surface can be further enhanced by studying its chemical activity [65,66]. In this way, the correlations between the structure and the reactivity of the V_2O_3(0001) surface can be established.

1.3 The present thesis

The present thesis provides a systematic investigation of the preparation, the characterization and the reactivity of well-defined V_2O_3(0001) model catalysts prepared as thin films on Au(111) and W(110) substrates under UHV conditions. The surface of V_2O_3(0001) was found to exhibit two different terminations: a termination by vanadyl groups and a termination by vanadium atoms. The geometric, electronic and vibrational properties of these differently terminated surfaces were investigated using a variety of surface science techniques including low energy electron diffraction (LEED), thermal desorption spectroscopy (TDS), X-ray photoelectron spectroscopy (XPS), ultraviolet photoelectron spectroscopy (UPS), near-edge X-ray absorption fine structure

(NEXAFS), infrared reflection-absorption spectroscopy (IRAS), and high resolution electron energy loss spectroscopy (HREELS).

A central theme of the present work was the study of the surface chemistry of the V_2O_3(0001) model catalyst. This study allowed the establishment of correlations between the surface structure of V_2O_3(0001) and its chemical activity. The chemical activity of the differently terminated V_2O_3(0001) surfaces was investigated via adsorption of a number of selected gases on these surfaces. The adsorption properties were found to depend on the V_2O_3(0001) surface termination as a consequence of the different electronic and structural properties of the different terminations. Chemisorbed species were identified by using the previously mentioned surface sensitive techniques. The stability of these species, their geometric and electronic properties, as well as their reaction paths were also investigated. These adsorption studies provided empirical insights into the fundamental mechanisms of the adsorption and reaction of gas molecules on the V_2O_3(0001) surface.

The present thesis is organized as follows: Chapter 2 provides a description of the experimental aspects in the present study. It starts with a description of the utilized surface science techniques followed by a description of the employed UHV systems. Chapter 3 gives a detailed description of the preparation and the characterization of the V_2O_3(0001) model catalyst. The V_2O_3(0001) surface geometric and electronic properties are discussed focusing on the two different studied surface terminations: the vanadyl and the vanadium termination. Comparative spectroscopic data collected for both terminations are also discussed in detail. In addition to that, spectroscopic data recorded at temperatures near to the metal–insulator transition of V_2O_3 are presented. The adsorption studies are discussed in chapters 4 to 8. These chapters deal with the interaction of the V_2O_3(0001) model catalysts with oxygen, carbon monoxide, carbon dioxide, water, propane and propene. The way how the surface termination influences the adsorption and the reaction of these gases is addressed. Finally, chapter 9 summarizes the results of the work presented in this thesis and gives some suggestions for possible future work.

Chapter 2

Experimental Aspects

This chapter specifies the various analytical techniques and systems utilized in the present study. The experiments presented in this work were carried out under ultra-high vacuum (UHV) conditions and, therefore, the experimental setup is essentially determined by the conditions of both UHV and the used spectroscopies.

2.1 Experimental techniques

A truly microscopic understanding of surface phenomena requires probing the surface properties experimentally at the molecular level. The following pages provide a brief description of a range of surface analytical techniques that were employed in the present study. A list of these experimental techniques is presented in Table 2.1. These techniques are capable of providing detailed information concerning the geometric structure, electronic properties, chemical composition and chemistry of surfaces. Combining these techniques may provide a rather detailed set of complementary information on the sample under investigation. A detailed and comprehensive description of these techniques is available in the literature; see for example references [67-69]

Table 2.1: List of the surface science techniques employed in this work

Acronym	Name	Primary Surface Information
LEED	Low Energy Electron Diffraction	Surface structure
TDS	Thermal Desorption Spectroscopy	Surface reactivity and activation energy
XPS	X-ray Photoelectron Spectroscopy	Composition, chemical state and electronic structure.
UPS	Ultraviolet Photoelectron Spectroscopy	Valence band structure
NEXAFS	Near-Edge X-ray Absorption Fine Structure	Composition, chemical state and electronic structure.
IRAS	Infrared Reflection-Absorption Spectroscopy	Chemical identification
HREELS	High Resolution Electron Energy Loss Spectroscopy	Chemical identification

2.1.1 Low Energy Electron Diffraction (LEED)

LEED is a standard technique in surface science. It is fast and provides a simple and convenient characterization of the long-range order of periodic surface structures. Figure 2.1(a) illustrates schematically a typical experimental arrangement necessary to perform a LEED experiment in which a monochromatic electron beam, whose energy Ep can be varied (typically in the range 20-300 eV), is generated by an electron gun. The beam is incident upon a sample that must be an electrical conductor connected to ground in order to prevent charging. After undergoing diffraction, electrons back-scattered from the periodic surface travel toward a series of grids (G1-4) as shown in Figure 2.1(a). The outer grid (G4) nearest to the sample is grounded to ensure that the electrons travel in a field free region. The inner grid (G1) is also grounded in order to screen out the high electric field due to the high voltages on the fluorescent screen (S). The inner pair of grids (G2 and G3) serves as a cut-off filter and is held at a negative potential (- Ep + ΔV), where ΔV is typically within the range 0-10 V. This guarantees that only elastically scattered electrons reach the screen which is biased at a high positive voltage (~5 keV) in order to accelerate the transmitted electrons to ensure that they cause light emission from the screen. The diffracted electrons give rise to a pattern consisting of bright spots on a dark background. These spots reflect the symmetry and crystalline order of the surface. Typically, the LEED pattern is recorded by a digital camera connected to a computer. The LEED pattern may also be viewed by the eyes.

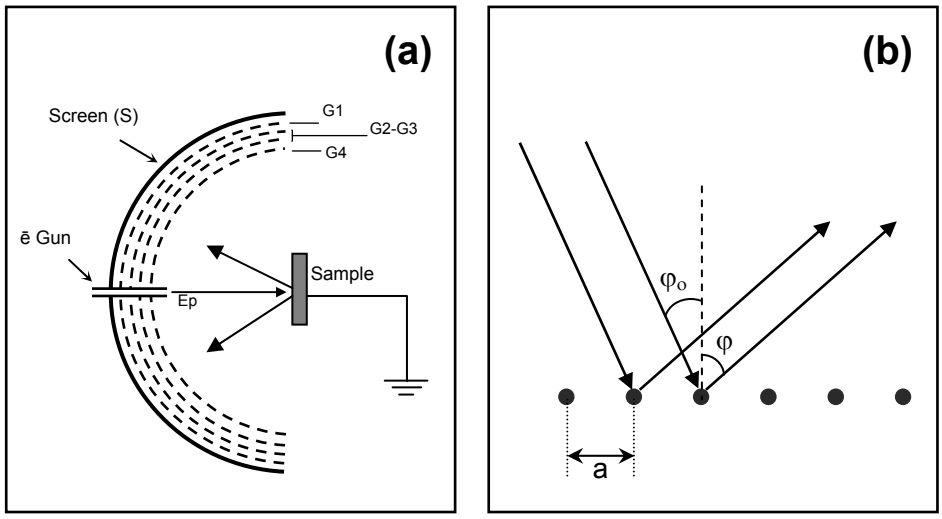

Figure 2.1: left: Scheme of a four-grid LEED apparatus. Right: Scheme of the diffraction process.

Electrons are diffracted by ordered surfaces. In LEED, electrons with energies between 20 and 300 eV are elastically scattered (i.e. without loss of energy) from a surface and the diffraction pattern is then analyzed. For these energies a number of spots can be seen on the screen with reasonable distances between them. The wavelength λ of an electron of momentum p may be calculated from the de Broglie formula:

$$\lambda = \frac{h}{p} = \frac{h}{m\upsilon}$$

This equation is the basis for the mathematical description of interference patterns of electrons at diffracted crystal surfaces. The waves associated with the scattered electrons undergo a constructive interference if the path difference between waves scattered from different scatterers is equal to an integral multiple of the wavelength λ. This is described by the following equation:

$$a(\sin\varphi - \sin\varphi_o) = n\lambda$$

where a is the distance between the periodically arranged scatterers, and φ_o and φ are the angles of incident and reflected electrons, respectively (see Figure 2.1(b)). If this condition is satisfied, constructive interference occurs and a sharp electron intensity maximum is observed.

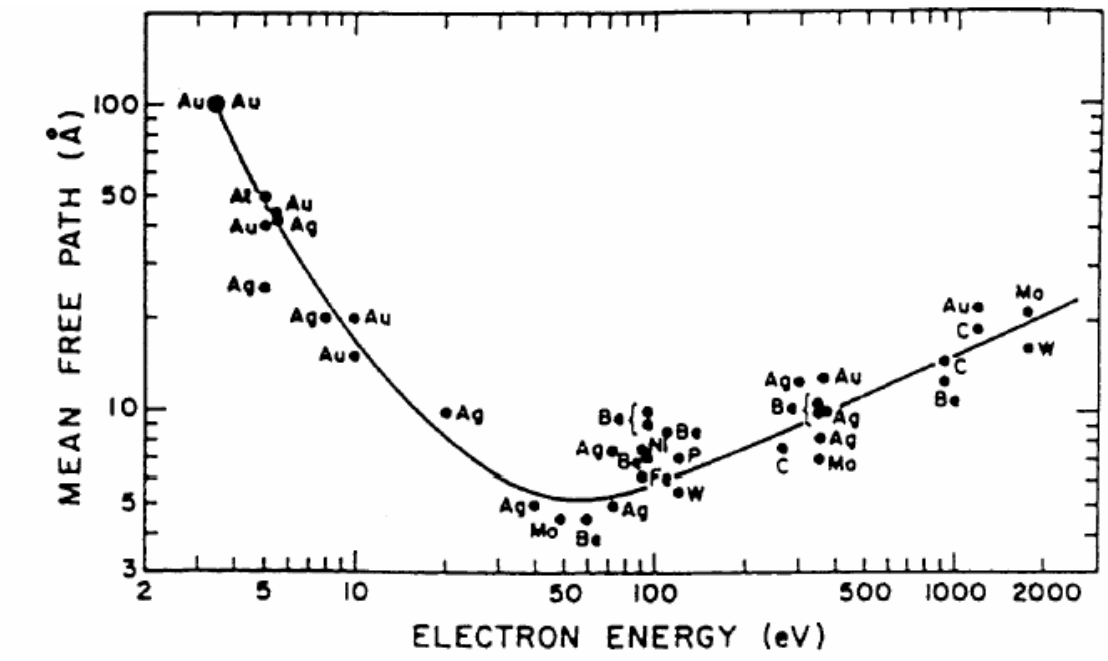

Figure 2.2: Universal curve for the electron free path [70].

The employed electron energies make LEED a very surface sensitive technique. This can be described in terms of the mean free path of an electron traveling through a solid matter as a function of the electron energy. This path is shown in Figure 2.2 for a large number of elements. The curve in Figure 2.2 is called the universal curve of the inelastic mean free path in a solid. This curve exhibits a minimum of about 5 Å in the energy range of about 50-100 eV. This implies that for electron energies in this range only the first few atomic layers of the solid are sampled.

2.1.2 Thermal Desorption Spectroscopy (TDS)

TDS [71] is one of the most commonly used techniques to investigate gas-solid interactions. TDS provides important information, qualitative and quantitative, about the species desorbing from a surface, which permits to draw conclusions on interactions and reactions of adsorbed species on the surface and with the surface.

Adsorption is the term used to describe the process whereby a molecule binds to a surface. In TDS, molecules (adsorbates) adsorbed on a surface (adsorbent) are thermally activated through heating the substrate. The heating leads to desorption or reaction of adsorbates, or both. The rate of desorption is followed by monitoring the amount of adsorbates desorbed into the gas phase as a function of temperature. The experimental requirements for a TDS experiment include the following:

(i) A method of heating the sample in a way that the heating rate is constant.

(ii) A method of monitoring the sample temperature. This could be achieved by spot-welding a thermocouple junction to the edge of the sample.

(iii) A detector to monitor the desorbing products. Typically, this consists of a quadrapole mass spectrometer.

By identifying the molecules that desorb and the desorption kinetics involved, conclusions can be drawn about the thermally activated processes that occur on the surface. Qualitatively, the desorbed products must be related to the adsorbed species. In a simple case, the adsorbed molecule desorbs as the temperature rises. In a more complicated case, the adsorbate may fragment and recombine or rearrange itself to form new molecules. The analysis of the desorption spectrum provides a general, easily-obtained view of ‘where some of the action is’ by identifing the temperature ranges at

which interesting events leading to desorption occur. These ranges can then be investigated in more details using other analytical techniques.

TDS also provides a great deal of quantitative information when the detected desorbing species are related to the kinetics of surface species. Kinetic parameters for molecular desorption or reaction on surfaces can be determined by analyzing the desorption spectra within the framework of an assumed model. The desorption process is often described by using approximate forms of a general rate equation called the Polanyi-Wigner equation:

$$r(\theta) = -\frac{d\theta}{dt} = v(\theta)\theta^n \exp\left(-\frac{E(\theta)}{RT}\right)$$

where $r(\theta)$ is the rate of desorption, θ is the surface coverage, t is the time, v is the pre-exponential factor, n is the reaction order, $E(\theta)$ is the activation energy, R is the gas constant, and T is the temperature. If the temperature increases linearly by heating, i.e., if $\beta = dT/dt$ = constant, the equation can be written as:

$$r(\theta) = -\frac{d\theta}{dT}\beta = v(\theta)\theta^n \exp\left(-\frac{E(\theta)}{RT}\right)$$

At $T = T_{max}$ (the thermal desorption maximum) and for $n = 1$ (first-order desorption), Redhead [72] gave the following equation:

$$\frac{E}{RT_{\max}^2} = \left(\frac{v_1}{\beta}\right)\exp\left(-\frac{E}{RT_{\max}}\right)$$

Here, β and T_{max} are determined experimentally, v_1 is commonly assumed to be 10^{13} s^{-1} and, thus, E can directly be calculated. It is worth noting that θ is not involved in the previous equation. This means that the peak temperature is independent on the surface coverage. However, the peak temperature will depend on the surface coverage if $n = 2$ (second-order desorption):

$$\frac{E}{RT_{\max}^2} = \left(\frac{2v_2\theta}{\beta}\right)\exp\left(-\frac{E}{RT_{\max}}\right)$$

Sometimes, zero-order desorption processes occur. This is typically the case for multilayer desorption.

2.1.3 X-ray Photoelectron Spectroscopy (XPS)

A very important and widely used technique to obtain information about the electronic structure of a sample is the photoelectron spectroscopy (PES). The PES process, shown in Figure 2.3(a), involves the ionization of a sample atom or molecule by a beam of monoenergetic photons $h\nu$, in which the sample loses an electron $\bar{e}$. The electron energy distribution [the number of electrons detected as a function of their kinetic energy] can be measured by using an electrostatic energy analyzer consisting of two electrically isolated concentric hemispheres with a potential difference between them (see Figure 2.3(b)). The electrostatic field separates electrons by allowing only electrons of a chosen kinetic energy to pass to the detector. Recording the number of photoelectrons as a function of their kinetic energy yields a spectrum of distinct peaks which reflect the occupied orbitals of the electronic system under investigation. Because the number and binding energies of the occupied orbitals are different for different chemical elements, the photoelectron spectra differ as well. They can serve as *fingerprints* of the different elements, making PES a very useful analytical tool. The intensity of the photoelectron peaks is determined by Fermi's golden rule: the emission rate is proportional to the square of the matrix element $\langle\Psi_f|H'|\Psi_i\rangle$ where $\langle\Psi_f|$ and $|\Psi_i\rangle$ are the wavefunctions of the final and initial states respectively, and H′ is the perturbation (photon beam) responsible for the transition. The transition rate depends on the initial and final states and the perturbation. The perturbation describes the electron-photon interaction and can be given as [73]:

$$H' = \frac{e}{mc}\boldsymbol{A}\cdot\boldsymbol{p}$$

where e and m refer to the charge and mass of the electron, and c is the light velocity. $\boldsymbol{A}$ is the vector potential of the incident radiation and $\boldsymbol{p}$ is the momentum operator. According to Fermi's golden rule, the transition probability per unit time between initial and final states with energies E_i and E_f, respectively can be written as:

$$R = \frac{2\pi}{\hbar}\left|\left\langle\Psi_f\left|H'\right|\Psi_i\right\rangle\right|^2\delta\left(E_f - E_i - \hbar\omega\right)$$

More detailed discussions about experimental and theoretical approaches to PES are given in the literature; see for example references [73,74].

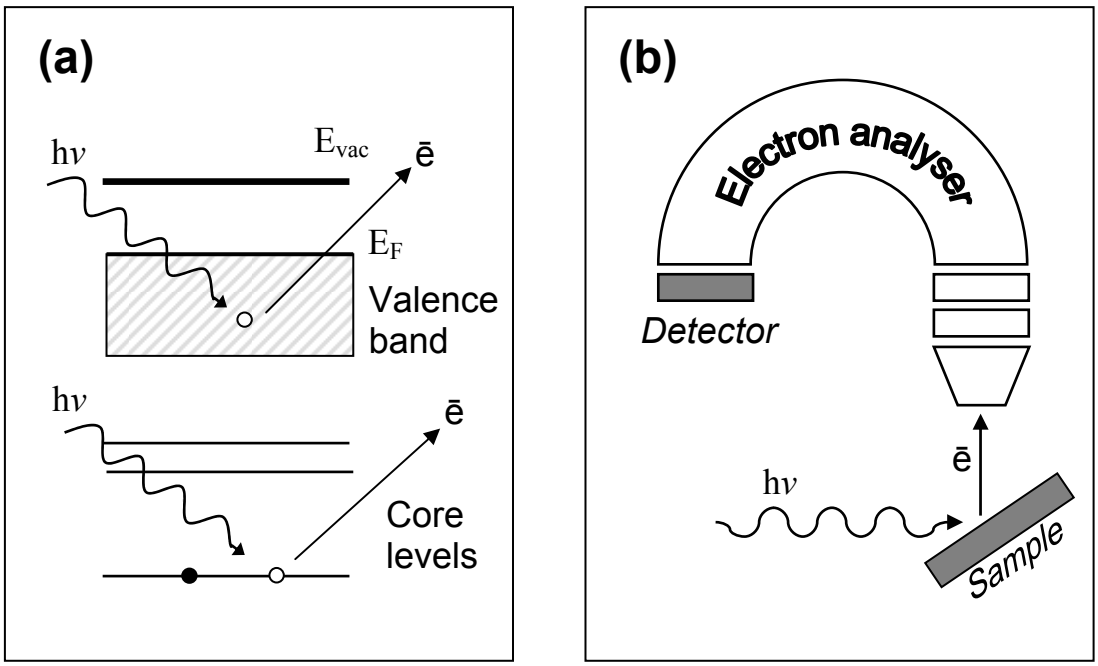

Figure 2.3: Left: Schematic illustration of the photoelectric process in a solid. Right: Setup for a typical PES experiment.

Since the introduction of synchrotron radiation sources, photoelectron spectroscopy of core levels (XPS) reached a position as one of the major techniques for the study of solids, surfaces and thin films. The XPS technique provides information about the atomic composition of a sample as well as about the chemical environment or oxidation state of surface species. For this reason, XPS is often referred to as *electron spectroscopy for chemical analysis* or ESCA

The basis of the XPS technique lies in Einstein's explanation of the photoelectric effect, where photons can induce electron emission from a solid provided that the photon energy is greater than the work function (Φ) of the solid. In XPS, a monochromatic beam of X-rays of energy $h\nu$ is incident upon a solid surface and is absorbed by an electron of binding energy E_1 (Figure 2.4(a)). This electron is then emitted into the vacuum with a kinetic energy E_{kin} as follows:

$$E_{kin} = h\nu - E_B - \Phi$$

Some of the photon energy $h\nu$ is consumed to overcome the potential energy barrier $(E_B+\Phi)$ associated with the attraction of the electron by the nucleus, while the remaining energy is transformed into the kinetic energy of the photoemitted electron. In addition to synchrotron radiation, Al K_α (1486.6 eV) and Mg K_α (1253.6 eV) radiation is often the photon energies of choice for XPS.

The binding energy E_B is formally defined as the difference between the total energy of the ionic final state E_f and the total energy of the neutral initial state E_i:

$$E_B = E_f - E_i$$

The simplest approach to the binding energy calculation assumes that Koopman's theorem is valid, i.e. electron orbitals remain frozen during the photoemission process. In other words, Koopman's theorem assumes that the energy of the electrons remaining after photoemission is exactly the same as in the initial state. This simply implies that the binding energy E_B would be just the negative orbital energy ε of the emitted electron.

$$E_B = -\varepsilon$$

In reality, the situation is more complicated. Koopman's theorem neglects relaxation and the change in correlation that occurs upon the photoemission process. Since a core electron is missing in the final state, other electrons in the system try to *screen* the generated core hole. They rearrange due to the attraction by the positively charged core hole. The associated *relaxation energy* causes a corresponding increase of the kinetic energy of the ejected electron. Relaxation occurs for both electrons on the atom containing the core hole (intra-atomic relaxation) and on the surrounding atoms (extra-atomic relaxation).

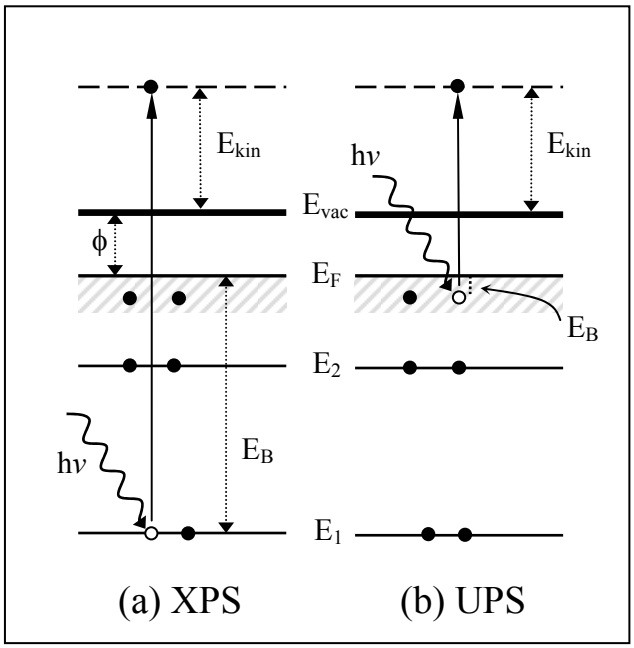

Figure 2.4: Schematic view for XPS (left) and UPS (right) processes.

The precise binding energy of the core levels of an atom or molecule will depend critically on the species to which this atom or molecule is bonded. Charge transfer may leave atoms with partial positive (or negative) charges, leading to a shift in core levels to higher (or lower) binding energies associated with increased (or decreased) Coulombic attraction between core electrons and the nucleus. As a result, atoms in a high formal oxidation state will yield XPS peaks at higher binding energies relative to the same atom in a low oxidation state. The magnitude of this so-called *chemical shift* depends on the local environment surrounding the atom under investigation.

The physical basis for the chemical shifts is illustrated by the so-called *charge potential model*. This model relates the binding energy E_i of a particular core level on an atom i to an energy reference $E_i°$, the charge q_i on the atom i, and the charge q_j on the surrounding atoms j at distances r_{ij}, as follows:

$$E_i = E_i^o + kq_i + V_i \ , \qquad where\ V_i = \sum_{j \neq i} q_j / r_{ij}$$

k is the proportionality constant. The binding energy of all core levels of a certain atom should be affected to the same extent by the charge q_i. The chemical shift between states 1 and 2 can be written as:

$$\Delta E_B = E_B(2) - E_B(1) = k\left[q_i(2) - q_i(1)\right] + \left[V_i(2) - V_i(1)\right]$$

Chemical shifts in XPS may reach values of several electron volts and, therefore, they are experimentally accessible even with the limited resolution of conventional x-ray photoelectron spectrometers [68]. A compilation of data for a large number of elements is provided in reference [75].

One of the objectives of XPS measurements is to provide a compositional analysis of a surface. The binding energies of the discrete core levels depend on the atom type. Thus, the observation of peaks at certain binding energies in a XPS spectrum can be taken as an indication of the presence of a particular element. However, extra features may appear in the XPS spectrum, so-called *satellite* peaks. They are due an interaction between the ejected photoelectron and other electrons in the atom. This may give rise to shake-up or shake-off processes which involve excitation of valence electrons into unoccupied states or into the vacuum, respectively. The energy of either process is supplied from the kinetic energy of the initially ejected photoelectron.

The inelastic scattering of photoelectrons in solids makes XPS a surface sensitive technique. This is described in terms of the previously mentioned mean free electron path (see Figure 2.2). For surface experiments, choosing the right photon energy to create photoelectrons with a kinetic energy in the range of 50-100 eV will result in a high surface sensitivity. In this energy range, the probability that electrons emerge from the sample without having been inelastically scattered is high only for electrons from the first few atomic layers (i.e. the surface region). Another widely utilized method to enhance the surface sensitivity is to detect electrons at a grazing angle of emission. By varying the angle of emission, it is possible to change the sampling depth for an electron in a solid. For example, the photoelectrons will travel a distance *d* in a solid if the XPS measurement is carried out at the normal emission angle ($\theta = 0°$), whereas rotating the sample to a grazing emission angle (for example $\theta = 70°$) will make the photoelectrons travel a longer distance in the solid ($x = d/cos\theta$). This situation is schematically represented in Figure 2.5. Clearly, the larger the angle of emission is, the larger the path length for electrons will be. Consequently, a higher surface sensitivity is achieved for a grazing detection angle.

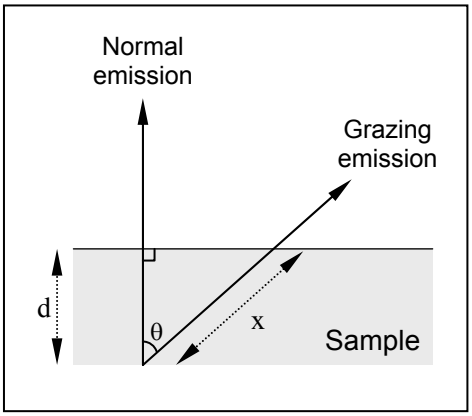

Figure 2.5: Schematic representation of the geometry of XPS spectra taken at normal and grazing angles.

2.1.4 Ultraviolet Photoelectron Spectroscopy (UPS)

UPS is a surface sensitive technique that involves the same principles and the same type of measurements as XPS, but UV photons are used for excitation instead of X-ray photons. Whereas XPS is used to study the strongly bound core electrons, UPS is used to study the weakly bound valence electrons which control a wide range of surface properties such as chemical bond formation. In most cases, however, XPS is not well

suited to study valence electronic states. X-ray photon sources lead to a poor energy resolution of valence peaks, while lower energy UV photons exhibit a much narrower energy width and hence are more useful for studying valence states. Additionally, the photon energy in XPS is far above the photoionisation threshold so that the cross-section is usually small. UPS is used to identify molecular species on surfaces and to characterize their decomposition and reaction. This is achieved by identifying characteristic electron binding energies associated with the bonds of the molecules. UPS may also allow geometric information of adsorbed species to be derived by exploiting dipole selection rules.

UPS is usually performed using a Helium lamp emitting 21.2 eV (HeI radiation) or 40.8 eV (HeII radiation) photons, but nowadays much work is performed using synchrotron radiation. Figure 2.4(b) illustrates the process of photoemission from the valence band of a solid using monochromatic UV photons of energy $h\nu$. The kinetic energy analysis of the photoemitted electron can be performed with an electron energy analyzer as described previously for the XPS technique. The binding energy can be calculated by following equation which is also valid for XPS:

$$E_{kin} = h\nu - E_B - \Phi$$

UPS can also be used to determine the work function of a solid. The work function Φ is defined as the minimum energy required to remove an electron from the solid and is simply calculated by subtracting the total width of the photoelectron spectrum ΔE from the photon energy $h\nu$:

$$\Phi = h\nu - \Delta E$$

with the spectrum being recorded normal to the surface. The precision of this method is about 0.05 eV, if the Fermi edge and the low energy cut-off are determined with an appropriate resolution [68]. However, some care must be exercised to avoid the emission of secondary electrons from the walls of the chamber and other parts of the spectrometer. To avoid these secondaries, the sample is typically placed at a negative bias voltage of some volts with respect to the analyzer. In this way, the whole spectrum emitted from the sample is shifted to a region where no spurious secondary electrons are detected. Another reason for the application of a voltage is that electrons with very low energies are sensitive to electric fields which may deflect them before they enter the analyzer. The applied voltage will accelerate the electrons and thus reduce this problem.

2.1.5 Near-Edge X-ray Absorption Fine Structure (NEXAFS)

NEXAFS [76] is a powerful research tool that is used for a variety of scientific studies. The NEXAFS technique was developed in the 1980s to clarify the structure of molecules bonded to surfaces. NEXAFS provides information about the structural, chemical and electronic properties of the sample under investigation.

NEXAFS measures the excitation probability as a function of photon energy near to the core level excitation thresholds. NEXAFS experiments require the photon energy to vary, and thus require the use of synchrotron radiation. The photon energy varies in an energy range close to an absorption edge, where core electrons are excited to an unoccupied state. These transitions lead to pronounced fine structures, the so-called NEXAFS *resonances*. The X-ray absorption process is illustrated in Figure 2.6(a). A typical K-edge spectrum of a diatomic molecule (e.g. CO) is shown in Figure 2.6(b). The spectrum is dominated by two intense features: a low energy feature (labeled π*) and a high energy feature (labeled σ*). The low energy feature is the *π* resonance*, that corresponds to a transition to a π* antibonding orbital of the molecule. The high energy feature is the *σ* shape resonance*, that corresponds to a transition to a σ* state. The term 'shape resonance' refers to the fact that the excited state is stabilized against immediate decay by a hump in the potential shape. Several sharp but weak resonances are observed between the π* and σ* resonances, which correspond to excitations to Rydberg orbitals.

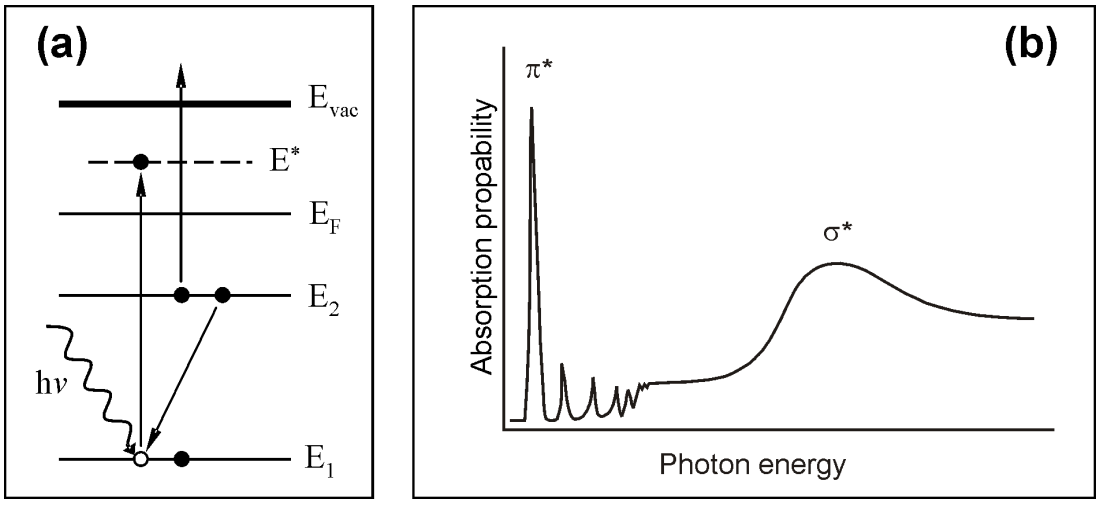

Figure 2.6: Left: Schematic view for X-ray absorption process. Right: K-edge spectrum of a diatomic molecule [76].

The intensity of NEXAFS resonance depends on the relative orientation of the electric field vector of the photon with respect to the direction of a specific molecular orbital. For example, the dipole selection rules governing K-shell NEXAFS resonance intensities are simple [76]: the resonance intensity associated with a specific molecular orbital final state is largest if the **E** vector points in the direction of that molecular orbital, and the intensity vanishes if **E** is perpendicular to the direction of the orbital. If the photons are linearly polarized, then ordered structures will produce spectra that essentially depend on the angle of the photon incidence. Therefore, the intensity variation of NEXAFS resonances, as a function of the orientation of the electric field vector **E** of the photons, allows NEXAFS to be used to determine the molecular orientation of adsorbates on a surface. This is the case when dealing with a simple adsorbed molecule like CO which exhibits a certain symmetry. However, for more complicated molecules the situation may not be as clear cut.

There are various detection methods employed in NEXAFS experiments. At first sight, the most obvious way is the determination of the ratio of the X-ray transmitted I through a sample (of thickness x) to that incident I_o on the sample [77,78]. This directly gives the absorption coefficient μ:

$$\frac{I}{I_o} = e^{-\mu x}$$

This method is not surface sensitive since nearly all photons are adsorbed in the bulk of the sample. Alternatively, most of the surface science NEXAFS experiments involve *Yield mode* measurements which are associated with the annihilation of the created core hole by the emission of fluorescent photons or Auger electrons. The detection techniques is called Auger electron yield (AEY) if the Auger electrons are monitored, whereas it is called fluorescent yield (FY) if the fluorescent photons are monitored. The AEY measurements are surface sensitive whereas the FY measurements are bulk sensitive. Other electron yield detections are the partial electron yield (PEY) and the total electron yield (TEY). The PEY measurement uses a partial yield detecor to monitor the emitted electrons. This device detects only electrons with energies greater than a set threshold. In TEY measurements, the signal is collected by monitoring the sample to ground current. All emitted electrons contribute to the TEY signal, independent of their energy. In TEY, potentially bulk information is obtained since the signal is dominated by the low energy electrons (see Figure 2.2).

2.1.6 Infrared Reflection-Absorption Spectroscopy (IRAS)

Vibrational spectroscopy is a powerful tool that probes the bonding of atoms and molecules adsorbed on a surface. Many surfaces are impenetrable to infrared radiation and, therefore, transmission experiments are not possible. Most of the surface science studies use the so-called *reflection mode*; and the technique is commonly called infrared reflection-absorption spectroscopy (IRAS). The IRAS technique provides a wealth of information regarding adsorbate systems due to its sensitivity and extremely high resolution ($\leq$ 2 cm^{-1}). For instance, CO molecules bonding to sites with different coordination, e.g., on-top, bridge bonded, or higher coordinated sites, will exhibit different vibrational frequencies due to different degree of back-donation of substrate electrons into the lowest unoccupied orbital of CO [79]. The frequencies can be determined with IRAS and conclusions about the type of adsorption sites can be drawn.

Figure 2.7 illustrates a typical experimental set-up for a vacuum IRAS experiment. Infrared radiation is focused through an IR-transparent window (usually an alkali halide) onto the sample surface at grazing incidence. The sample, acting as a mirror, reflects the beam out of a second vacuum-sealed window. Then the beam is focused onto a photoconductive semiconductor detector such as mercury cadmium telluride (MCT). Typically, the path of the IR beam that is external to the UHV chamber is purged with dry nitrogen to minimize interference from gas phase absorption bands associated with atmospheric H_2O and CO_2 (it may also be pumped).

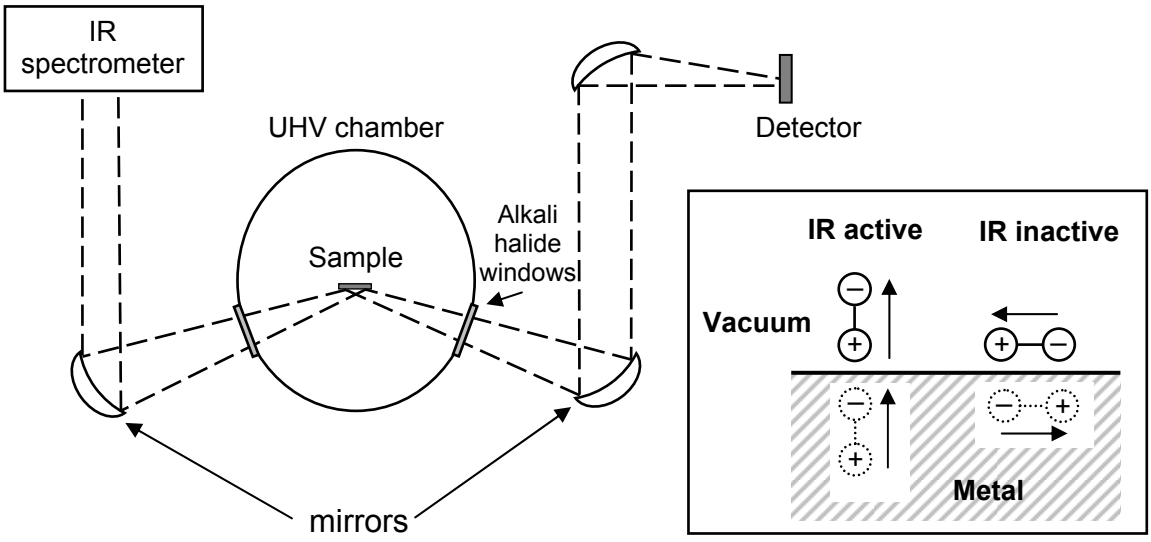

Figure 2.7: Left: Schematic diagram of the experimental configuration used in IRAS. Right: Illustration of surface selection rule for observation of IRAS in terms of molecular and image dipoles.

When a molecule is exposed to IR radiation, it absorbs specific frequencies of radiation. IR radiation can only be absorbed by bonds within a molecule if the radiation has exactly the right energy to induce a vibration of a bond. Such a vibration is said to be IR-active if it gives rise to an oscillating dipole moment. In IRAS, the absorption of IR radiation by thin films and molecules on metal surfaces is markedly enhanced at high angles of incidence and is effectively limited to the p-polarised radiation [69,80]. The observation of vibrational modes of surface species on a metallic substrate with IRAS is subjected to the surface selection rule. When a molecule is adsorbed on a substrate, the molecule induces image charges with opposite signs in the substrate. Only vibrational modes with a non-zero component of the dipole moment perpendicular to the surface are IR-active and, as a result, an absorption band is observed. In contrast, for a dipole aligned parallel to the surface, the dipole moment is canceled by the dipole moment of the image charges and no IR absorption band is observed. Figure 2.7 illustrates this phenomenon.

IRAS is mainly used to characterize the nature of bonding between a surface and adsorbates, to identify the chemical nature of adsorbed species, and to obtain information about bonding within the adsorbed species from characteristic frequencies. The adsorption of a molecule implies a frequency shift with respect to the gas-phase value. The main effects which describe the frequency shift of an adsorbed molecule are the wall effect, the self-image shift and the chemical shift [79,81]. Considering an isolated adsorbed CO molecule, the wall effect leads to a higher frequency shift (blue-shift) [79]. This results form the Pauli repulsion between the carbon lone-pair electrons and the surface charge distribution. The self-image shift, on the other hand, leads to a red-shift due to the interaction between the dipole moment of the adsorbed CO and its image [79]. As a result of the chemical bonding of CO to the substrate, a red shift is observed depending on the extent of the charge transferred (backdonation) from the substrate to the unoccupied $2\pi^*$ molecular orbital of the adsorbed CO. In addition to these effects, an increase of the adsorbate coverage results in a shift to higher frequencies [79]. This is due to intermolecular interactions such as (i) dipole-dipole interactions between neighboring molecules, which result from the vibrational coupling of the molecule's dipole with its own image dipole in addition to the coupling with dipoles of neighboring molecules and their image dipoles, (ii) chemical shifts which may result from a competition for backdonation electrons between the adsorbed

molecules or it may result from direct molecular interactions between the adsorbed molecules, and (iii) Stark effects whereby the vibrational frequency of an adsorbed molecule can be influenced by the presence of an electric field which may be produced by neighboring dipoles; an adsorbed dipole parallel (or anti-parallel) to the electric field leads to a red-shift (or blue-shift).

2.1.7 High Resolution Electron Energy Loss Spectroscopy (HREELS)

Another method of exciting atomic and molecular vibrations at surfaces is with an electron beam. In HREELS, the exciting electron beam is highly monochromatic and exhibits a typical primary beam energy between 1 and 10 eV. The electron beam is scattered on a sample surface and the scattered electrons are detected by an electron energy analyzer. This scenario is illustrated in Figure 2.8. A fraction of the electrons suffers energy losses owing to the excitation of surface vibrations, leading to the observation of energy loss peaks.

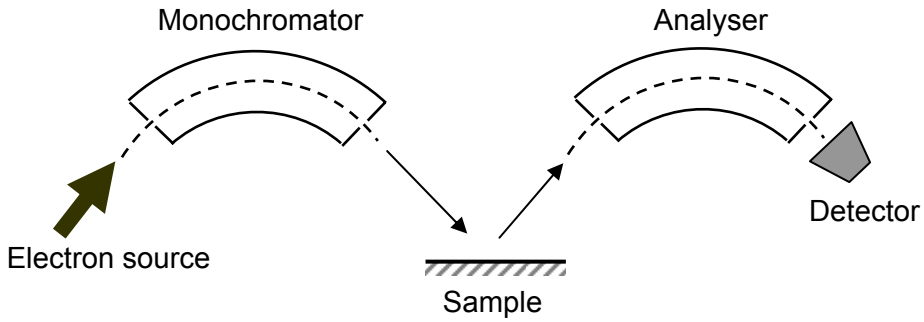

Figure 2.8: Schematic experimental arrangement for HREELS.

Similar to IRAS, HREELS provides sensitive fingerprints of the structure and stoichiometry of an oxide surface. A major advantage of HREELS with respect to IRAS is its ability to monitor vibrational modes that cannot be observed by IRAS. In HREELS, the vibrational excitation may take place by a number of independent mechanisms such as dipole scattering, impact scattering and negative ion resonance [82]. The dipole scattering is caused by a long range interaction between the electric field of the incoming electrons and the surface vibrational dipoles. In dipole scattering, the highest scattering intensity is observed in specular direction, i.e. the direction where the angle of incidence equals the angle of reflection. The dipole scattering of electrons

follows the selection rules that hold for excitations by IRAS. Therefore, only vibrations with a dynamic dipole moment perpendicular to the surface can be observed with the dipole scattering. Consequently, HREELS can help to identify the geometric structure of adsorbed molecules on a surface. The impact scattering, on the other hand, is a short range mechanism by which a direct collision between the adsorbate and the electron leads to vibrational excitations. Vibrations excited by the impact scattering are best observed off-specular. In the impact scattering regime, vibrational modes which are parallel and perpendicular to the surface may be excited [69]. More details about the selection rules of the dipole and impact scattering and about the applications of these selection rules are available in the literature [82,83]. The last mechanism is the negative ion resonance which involves the formation of a temporary negative ion caused by electron capture. After the decay, the electron may leave behind a molecule in a vibrationally exited state.

2.2 Experimental setup

2.2.1 The UHV systems

Three different UHV systems were mainly used in this work. Each system consists of two stainless steel chambers which can be separated by a gate valve. The upper chamber is the preparation chamber where samples can be prepared. The lower chamber is the analysis chamber where measurements are performed. The preparation chamber is equipped with a manipulator which allows sample transfer from the preparation chamber to the analysis chamber. Additionally, each preparation chamber is commonly equipped with an evaporator for metal deposition, an ion gun for sputtering, a gas doser, LEED optics and a mass spectrometer. In all these systems, only pressures in the low 10^{-10} mbar range are employed in order to provide well-defined conditions for the sample preparation and analysis.

The first UHV system is primarily suited for ARUPS measurements. The system consists of a preparation chamber and an analysis chamber. The UPS measurements were performed in the analysis chamber using a rotatable VSW HA 100 hemispherical analyzer and a Specs UVS 300 helium discharge lamp as source for UV radiation. The

incidence angle of the UV radiation was usually 45° with respect to the surface normal. The resolution of the analyzer was about 100 meV.

The second UHV system is used for PES and NEXAFS measurements using synchrotron radiation. Most of the synchrotron radiation measurements presented in this thesis were carried out on the beamline UE52-PGM at the BESSY II synchrotron radiation center in Berlin, Germany [84]. The UE52-PGM beam line delivers photons within the energy range of 90 to 1500 eV. The system is attached to this beam line and consists of two chambers connected by a gate valve. XPS and UPS spectra were obtained in the analysis chamber using a Scienta SES200 analyzer which was mounted at an angle of 55° with respect to the incident photon beam. Figure 2.9 shows a schematic representation of the geometry of all PES measurements discussed in the present thesis. The photon impinges on the surface with an incidence angle α and the electron is detected at the angle θ. The tunability of the radiation source allows the photon energy to be set so that the ionization cross-sections for each element can be optimized for maximum sensitivity. For example, a photon energy of 630 eV was used for the V 2p and O 1s levels, while 380 eV was used for the C 1s level. A photon energy of 120 eV was employed to excite valence band electrons. Kinetic energies of electrons at these photon energies are about 100 eV, which is close to the kinetic energy corresponding to the minimum inelastic mean free path of about 5 Å (see the universal curve, Figure 2.2). Thus, the resulting photoemission spectra should provide a maximum surface sensitivity. The overall energy resolution in the XPS measurements was usually better than 100 meV. In all PES measurements the energy scale was calibrated relative to the energy of the W $4f_{7/2}$ level by taking spectra of the tungsten filament used for sample heating, or relative to the Au $4f_{7/2}$ energy by taking spectra of the clean gold crystal.

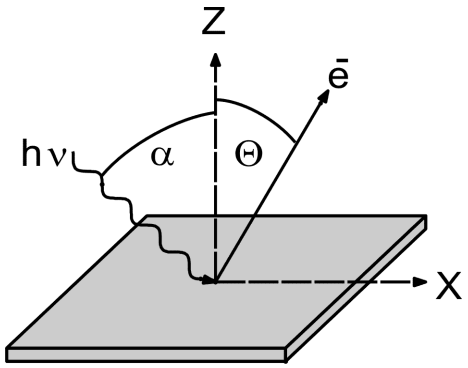

Figure 2.9: Geometry of the PES measurements employed in this work.

NEXAFS spectra were taken in the same analysis chamber by measuring the current flowing between the ground potential and the sample (total yield detecttion TYD), or by using a partial yield detector (PYD) mounted below the sample. The energy resolution in NEXAFS measurements was usually better than 100 meV.

The third UHV system was dedicated for IRAS, HREELS and TDS measurements. The IRAS spectra were obtained in reflection-absorption geometry using a modified Mattson RS-1 FTIR spectrometer. Similar to the previous two systems, this system consists of a preparation chamber and an analysis chamber. It has an infrared interferometer which was operated at about 7×10^{-3} mbar, and a liquid nitrogen cooled MCT detector which was operated under constant nitrogen pressure. The IR beam was admitted into the UHV chamber through a KBr window. Then the beam was reflected through a second KBr window and was focused into the detector. In this work, the angle of incidence of the IR light relative to the sample normal was about 85°. Typically, 2000 scans were accumulated for the clean surface and 500 scans for the adsorbate-covered surface. The IRAS spectra of an adsorbate covered surface were divided by the IR spectrum of the clean surface recorded right before the gas exposure. All IRAS spectra presented in this thesis were collected at a resolution of 2 cm^{-1}.

TDS experiments were conducted in the same chamber using a computer-controlled quadrupole mass spectrometer (HIDEN HAL RC 201). The ionizer of the mass spectrometer was enclosed in an individually pumped Feulner cup [85] with a nozzle entrance at the end. For TDS measurements, the nozzle entrance was facing the sample with a distance of ~0.5 mm between the sample surface and the nozzle entrance. With this setup, only molecules desorbing from the sample surface were detected (other desorbing molecules were geometrically shielded). All TDS spectra presented in this thesis were recorded after gas exposure at 90 K. A heating rate of 0.5 K/s was used unless stated otherwise in the text.

HREELS spectra were recorded in the lower chamber which was equipped with a Specs Delta 0.5 spectrometer. All spectra presented in this thesis were recorded in specular geometry ($angle_{in}$ = $angle_{out}$ = 65° with respect to the surface normal). The incident beam energy was 5 eV and the resolution was about 30 cm^{-1}.

2.2.2 Sample setup

The UHV chambers used in this work were equipped with a precise sample manipulator capable of performing *x*, *y* and *z* translation and rotation about the *z* axis. At the end of the manipulator rod, an electrically isolated sample holder was attached (schematically depicted in Figure 2.10). Single-crystal metal substrates, either W(110) or Au(111), were mounted between tantalum foils fixed in narrow slits at the edges of the substrates. The tantalum foils were gently spot-welded between two parallel tungsten wires. The heating of both substrates could be performed either by heat radiation from a glowing tungsten filament right behind the substrate or by electron bombardment using the same filament after applying a positive voltage (up to 1000 V) to the substrate. The gold substrate could also be heated resistively. Sample temperatures were measured with either W-5%Re/W-26%Re or Ni-Cr/Ni thermocouples. The W-5%Re/W-26%Re thermocouple was spot-welded to the side of the W(110) crystal, while the Ni-Cr/Ni thermocouple was fixed inside a hole at the side of the Au(111) crystal. The samples could be cooled down to ~90 K by filling the manipulator rod with liquid nitrogen.

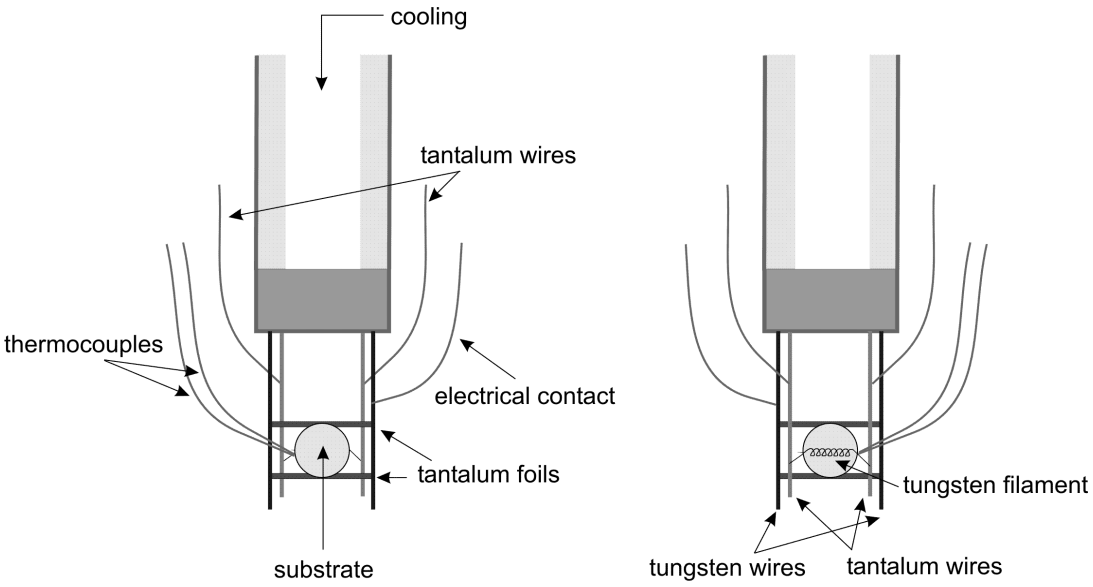

Figure 2.10: Schematic representation of the front (left) and the back (right) of the sample holder**.**

Chapter 3

Vanadium Oxide Model Catalyst

This chapter describes the $V_2O_3(0001)$ model catalyst system; beginning with a brief literature overview of the V_2O_3 system, moving on to the preparation of the $V_2O_3(0001)$ films on W(110) and Au(111) substrates, and ending with the characterization of these films using a variety of surface science techniques such as LEED, IRAS, HREELS, UPS, XPS and NEXAFS. Particular emphasis is given to the characterization of the surface of $V_2O_3(0001)$ which can be terminated by a layer of vanadyl groups or by a layer of vanadium atoms. The metal–insulator transition of the $V_2O_3(0001)$ films is also discussed.

3.1 Introduction

In the family of vanadium oxides, much attention was drawn to vanadium sesquioxide, V_2O_3. Mott [86] stated about V_2O_3 that 'there are almost as many theories for this material as there are theorists who have discussed it'. Indeed, V_2O_3 is one of the transition metal oxides that were studied extensively for many years [87]. V_2O_3 exhibits a complex phase diagram [88]. It undergoes a metal–insulator transition (MIT) as a function of temperature, doping (Cr, Al, Ti), and pressure [89]. The MIT is accompanied by a change of the crystal structure and the magnetic properties. However, the precise mechanism responsible for these transitions remains unclear [90-93].

As a result of its interesting physical and chemical properties, V_2O_3 was extensively investigated by a number of experimental [94-103] and theoretical [104-106] studies. V_2O_3 was used in the so-called chemical valve membrane [107]. In chemical processes catalyzed by vanadium oxide catalysts, V_2O_5 may undergo reduction forming V_2O_3 [108,109] which may play an important role in the chemical process. Indeed, a catalytic V_2O_3 phase was suggested to be responsible for the high catalytic performance in oxidative dehydrogenation of ethane [110] and propane [111].

In V_2O_3, each vanadium atom is surrounded by an octahedron of oxygen atoms. The formal oxidation state of the vanadium ion is +3 exhibiting a $3d^2$ electronic

configuration. The electronic structure of V_2O_3 was the object of many PES investigations [97,101,103,112-116]. Valence band studies, using ultraviolet photoemission spectroscopy, showed that the V 3d states lie within ~3 eV from the Fermi level (E_F) and the O 2p band was located between ~4 and ~10 eV binding energy. The V 3d states showed significant changes across the MIT. Core level PES was also applied to study the electronic states of V_2O_3. Early core level studies [97,113-115] indicated the presence of strong hybridization between the O 2p and V 3d states. A schematic illustration of the electronic structure of V_2O_3 is displayed in Figure 3.1.

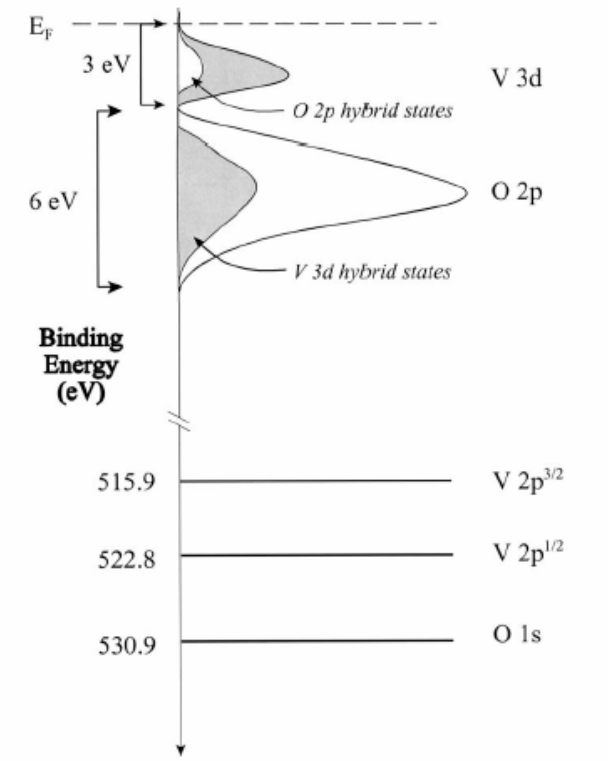

Figure 3.1: Schematic illustration of the electronic structure of V_2O_3 [117].

The *ideal* bulk-terminated (0001) surface of V_2O_3 may exhibit three different possible terminations as shown in Figure 3.2: (i) an oxygen termination (Corundum(0001)–O); (ii) a single metal layer (Corundum(0001)–Me); and (iii) a double metal layer (Corundum(0001)–2Me). The single metal layer termination would be the only stable termination due to electrostatic considerations [118]. The other two terminations are polar surfaces which are unstable and therefore they should not exist. However, stabilization of a polar surface might be possible by charge rearrangement at the surface which may occur via various routes such as reconstruction [19]. A recent theoretical study [64], related to the stability of these bulk terminated V_2O_3(0001)

surfaces, suggested that the double layer terminated surface is highly unstable and that the single layer terminated surface is stable only at very low chemical potentials of oxygen, i.e. at very reducing conditions. The oxygen terminated surface is stable under an oxygen-rich ambient.

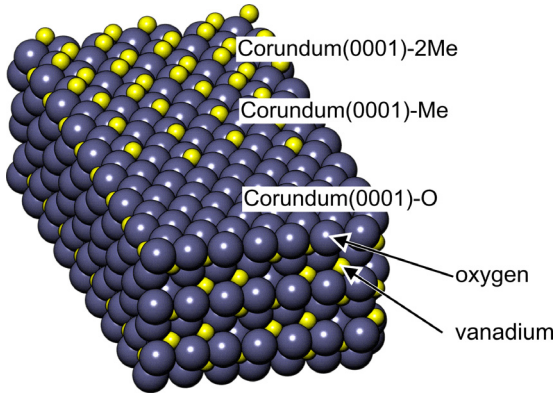

Figure 3.2: Different ideal terminations of the $V_2O_3(0001)$ surface.

Information about the termination of the *real* $V_2O_3(0001)$ surface may be obtained from a comparison with other well studied corundum surfaces, like $Cr_2O_3(0001)$ [19,119-122]. Due to the similarity of the bulk phases of V_2O_3 and Cr_2O_3, it might be reasonable to assume similar surface geometries. The $Cr_2O_3(0001)$ surface was examined in great detail and found to be terminated by a half metal layer corresponding to the one denoted by Corundum(0001)–Me in Figure 3.2. Additionally, exposure of the $Cr_2O_3(0001)$ surface to oxygen was found to result in the formation of chromyl groups. It may be assumed that the real $V_2O_3(0001)$ surface is also terminated by a half metal layer at low oxygen chemical potential. The formation of other surface terminations, like an oxygen terminated surface, can be expected at higher oxygen pressure [47,54]. One of the questions to deal with in this study is: how is the $V_2O_3(0001)$ surface terminated under UHV conditions? A direct and clear answer to this question is given in more details in the following two sections. It should be mentioned, however, that this surface was previously demonstrated to exhibit different terminations by Dupuis [47,123].

In what follows, a comprehensive experimental study using synchrotron radiation based techniques (UPS, XPS and NEXAFS) and vibrational spectroscopies (IRAS and HREELS) was conducted to control the preparation of well-defined $V_2O_3(0001)$ thin films. Using these surface sensitive techniques, the $V_2O_3(0001)$ films are found to be terminated by a layer of vanadyl (V=O) groups under typical UHV

conditions [47]. Very recently, experimental [54] and theoretical [64] investigations came to a similar conclusion. The vanadyl terminated surface is found to be stable in UHV up to ~1000 K. Electron irradiation of this surface leads to the removal of the oxygen atoms from the vanadyl layer and results in a surface terminated by vanadium atoms [47].

3.2 Preparation of the V_2O_3(0001) films

The preparation of well-defined oxide surfaces plays a key role in surface science studies on these materials. Ordered oxide surfaces can be prepared by cutting and polishing single crystal oxides followed by sputtering and annealing in vacuum or in oxygen atmosphere. Such a process usually produces a sufficient number of defects at the surface and in the bulk. An alternative way to prepare oxide surfaces with better quality is the cleavage of single crystal oxides. However, single crystal oxides may cause severe experimental problems. They are often insulators which may prevent electron spectroscopy measurements. Other common experimental problems are related to the sample mounting, heating and temperature controlling. These experimental problems can be avoided by the growth of thin film oxides onto conducting metal substrates [15].

Establishing the preparation procedure of an oxide film includes time-consuming processes of trying different recipes which may take several weeks. These processes mainly involve a set of preliminary experiments to control the preparation conditions such as the substrate temperature, evaporation rate, and oxygen pressure. Preliminary experiments related to the preparation of V_2O_3(0001) thin films are not discussed here. Instead of that, a description of the most optimized preparation procedure is provided. In the present work, well-ordered V_2O_3(0001) films were grown on Au(111) and W(110) substrates. The preparation of these films was conducted in two steps, comprising the preparation of a clean substrate and the growth of a vanadia film.

The first step is the preparation of the clean substrate. Cleaning Au(111) was achieved in UHV by cycles of Argon sputtering and annealing at 1050 K. Removing carbon from W(110) was achieved by cycles of annealing at 1800 K in 10^{-6} mbar of oxygen for a few minutes followed by another annealing step at 2300 K without oxygen. The cycles were repeated until clean and well-ordered substrates were obtained.

The cleanliness and the order of a substrate surface were usually checked by XPS and LEED.

The vanadium was evaporated from a vanadium wire with 2 mm diameter using a well degassed water-cooled electron beam evaporator. The applied evaporation rate was about 1 Å/min as measured by a quartz crystal microbalance. In the second step of the preparation, about 50 Å of vanadium were deposited onto the respective substrate at 600 K in 1×10^{-7} mbar of oxygen followed by annealing at 670 K in 1×10^{-7} mbar of oxygen for 15 minutes. Annealing in vacuum at 850 K for 10 minutes ended the preparation. The resulting oxide film with a thickness of ~100 Å was found to be terminated by a layer of vanadyl groups (see the following section). These films were subjected to electron irradiation in UHV leading to the formation of another surface termination, namely the vanadium terminated $V_2O_3(0001)$ surface (section 3.4).

3.3 Characterization of the $V_2O_3(0001)$ films

3.3.1 LEED

The first indication that the prepared V_2O_3 layers are ordered comes from LEED. Figure 3.3 displays LEED patterns taken at different stages of the preparation. The hexagonal periodicity of the surface is recognized after annealing the film at 670 K, although the spots are somewhat broad (Figure 3.3(a) and (b)). Further annealing to 850 K leads to sharp reflexes corresponding to a $V_2O_3(0001)$ film with a high degree of long-range order (Figure 3.3(c) and (d)).

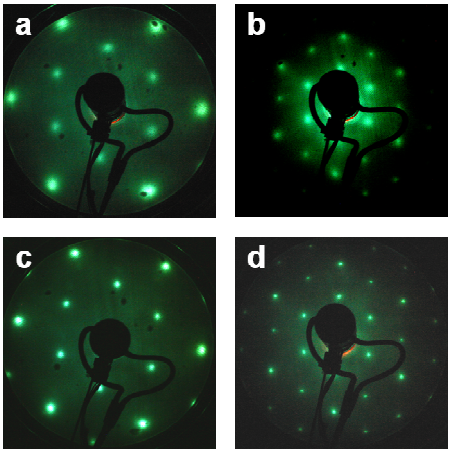

Figure 3.3: LEED patterns of 100 Å thick $V_2O_3(0001)$/Au(111) films: (a) and (b) after annealing to 670 K at 50 and 125 eV, respectively; (c) and (d) after annealing to 850 K at 50 and 125 eV, respectively.

3.3.4 IRAS and HREELS

Vibrational properties of the $V_2O_3(0001)$ film were investigated by HREELS and IRAS measurements. A typical IR spectrum of the $V_2O_3(0001)$ film divided by a spectrum of the clean Au(111) substrate is displayed in Figure 3.4(a). The spectrum is dominated by one peak centered at 1040 cm^{-1}. Additional information about this peak is provided by HREELS measurements where the same peak position was also observed (bottom spectrum in Figure 3.4(b)). Identification of the origin of this feature is possible by a comparison with a spectrum of the chromyl terminated $Cr_2O_3(0001)/Cr(110)$ surface (top spectrum in Figure 3.4(b)) [47]. The spectrum of the $Cr_2O_3(0001)$ surface exhibits a similar peak (marked with a vertical line) which was assigned to chromyl groups consisting of oxygen atoms doubly bonded to the underlying chromium atoms [124,125]. Consequently, the peak at 1040 cm^{-1} in the $V_2O_3(0001)$ spectrum can be attributed to the excitation of vanadyl (V=O) stretching vibrations which clearly indicates that the $V_2O_3(0001)$ layer is covered by vanadyl groups. Recently, vanadyl groups were also identified on the surface of a $V_2O_3(0001)$ film grown on Rh(111) [54]. The HREELS spectrum shown in Figure 3.4(b) is in good agreement with spectra reported for the $V_2O_3(0001)$ film on Rh(111) [54]. Recent theoretical calculations predicted the presence of vanadyl groups on the $V_2O_3(0001)$ surface [64].

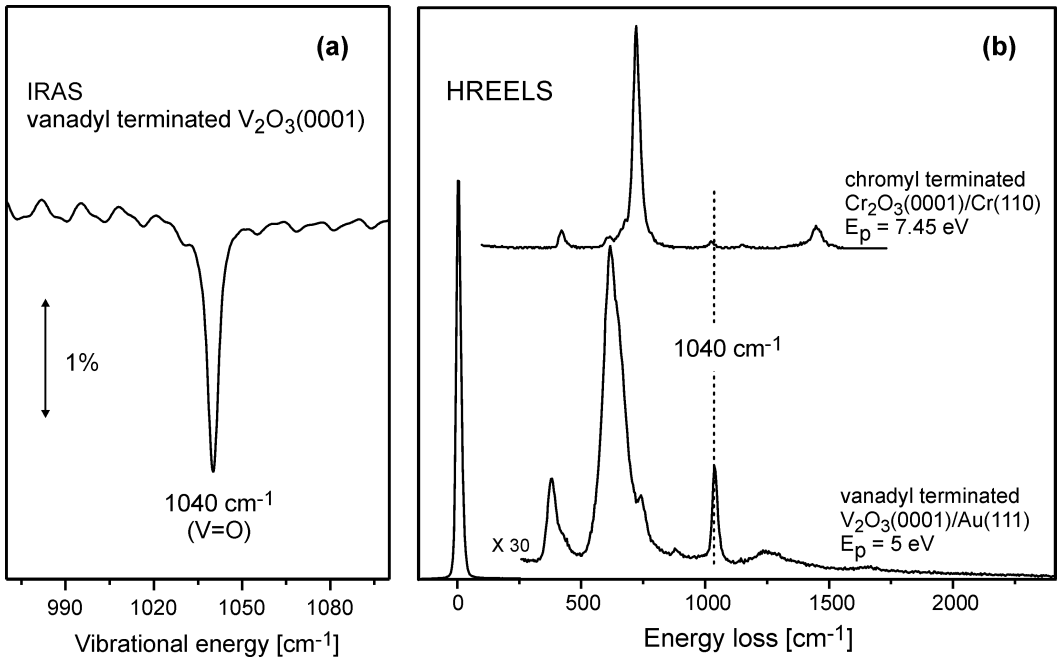

Figure 3.4: Left: IRAS spectrum of vanadyl terminated $V_2O_3(0001)/Au(111)$ divided by a spectrum of clean Au(111). Right: HREELS spectrum of vanadyl terminated $V_2O_3(0001)/Au(111)$ (bottom) in comparison with a spectrum of a chromyl terminated $Cr_2O_3(0001)/Cr(110)$ (top) [47].

3.3.2 UPS and XPS

The composition and chemical state of the $V_2O_3(0001)$ layers were examined by XPS and UPS measurements. Figure 3.5(a) shows typical XPS spectra of the V 2p and O 1s region of the vanadyl terminated $V_2O_3(0001)$ surface. The spectra were recorded in different experimental geometries: normal emission ($\theta = 0°$) to enhance bulk sensitivity and grazing emission ($\theta = 70°$) to enhance surface sensitivity. For comparison, a spectrum of $V_2O_5(001)$ is shown at the bottom in Figure 3.5(a) [47]. The V 2p signal is spin-orbit split into $2p_{3/2}$ and $2p_{1/2}$ states, and followed by the O 1s emission at ~530 eV. The spectra clearly show that the peak position of the O 1s core level does not significantly depend on the vanadium oxidation state, in agreement with data found in the literature [97,126]. The V 2p features were fitted in order to facilitate their interpretation. According to Zimmermann et al. [114] the V $2p_{1/2}$ state near to the O 1s level (labeled Sat.) is attributed to a V 2p satellite. The intensities of the V $2p_{3/2}$ and V $2p_{1/2}$ states at 515.15, 517.15, 522.4, and 524.4 eV (marked with vertical lines) in the spectra of the $V_2O_3(0001)$ surface depend on the emission angle. Clearly, the states at higher binding energies get more intense at the grazing emission angle $\theta = 70°$. This means that the features at 517.15 and 524.4 eV are surface states originating from the surface vanadium atoms while the features at 515.15 and 522.4 eV are bulk states originating from the bulk vanadium atoms [47]. V 2p and O 1s core level spectra with similar angular dependence were recently reported by Schoiswohl et al. [54] for vanadyl terminated $V_2O_3(0001)$ films on Rh(111).

Comparing the spectrum of $V_2O_5(001)$ in Figure 3.5(a) with that of $V_2O_3(0001)$ at $\theta = 70°$ reveals that the binding energy of the surface V $2p_{3/2}$ state in the $V_2O_3(0001)$ spectrum is close to that of the V $2p_{3/2}$ state of $V_2O_5(001)$. This may indicate that the outermost vanadium atoms on the $V_2O_3(0001)$ surface are in a higher oxidation state than the bulk vanadium atoms. This may be the reason why the V $2p_{3/2}$ binding energy of surface vanadium atoms is higher than the V $2p_{3/2}$ binding energy of the bulk vanadium atoms.

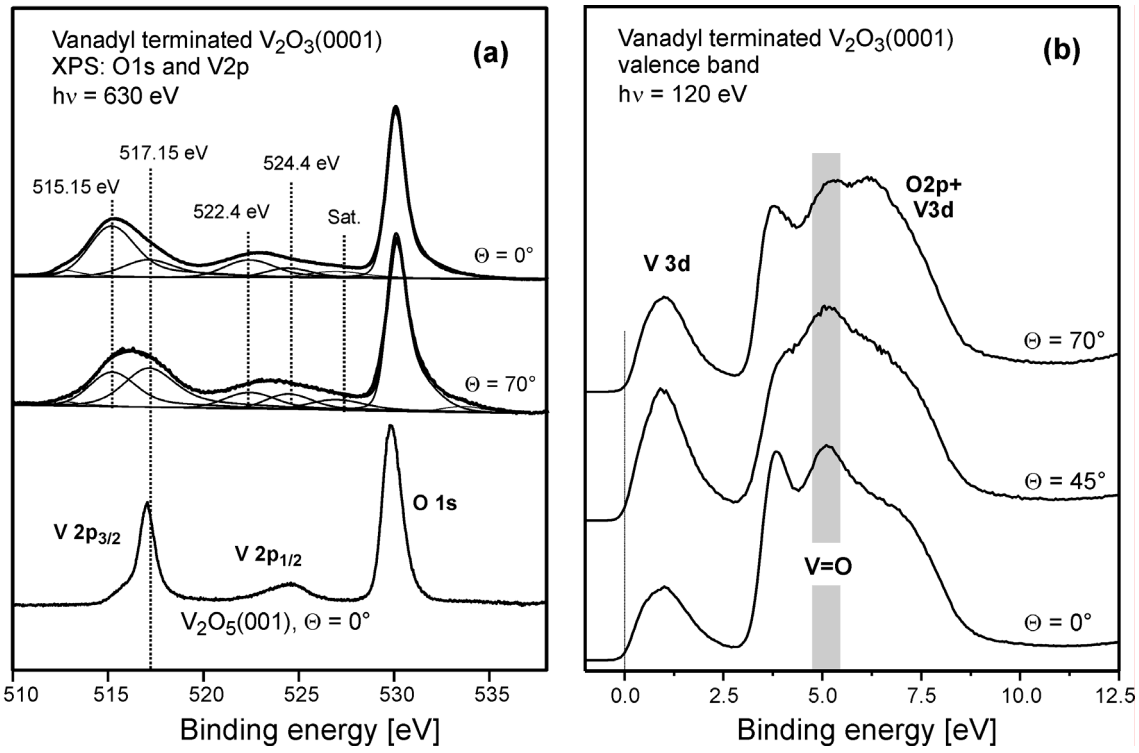

Figure 3.5: Left: V 2p and O 1s core levels spectra of vanadyl terminated V_2O_3(0001)/W(110). At the bottom a spectrum of V_2O_5(001) single-crystal is shown [47]. Right: valence band spectra of vanadyl terminated V_2O_3(0001)/W(110). Both panels show spectra obtained for different electron detection angles.

Typical valence band spectra of the vanadyl terminated V_2O_3(0001) surface are displayed in Figure 3.4(b). The spectra exhibit two clearly separated spectral regions which can be associated with the V 3d band (between E_F and ~2.5 eV) and the O 2p band with some hybridized V 3d contribution (between ~3.0 and 9.5 eV). The spectra exhibit clear angular dependence, similar to what was observed for vanadyl terminated V_2O_3(0001)/Rh(111) [54]. The band at about 5 eV is associated with the vanadyl groups [47,54,64].

3.3.3 NEXAFS

Unlike XPS, NEXAFS is sensitive to the unoccupied electronic states. A combination of the two techniques gives a rather complete view of the electronic structure of the sample under investigation. Figure 3.6 displays NEXAFS spectra of the V2p ($L_{2,3}$) and O 1s (K) regions of the vanadyl terminated V_2O_3(0001) surface. Features below 527 eV are the V 2p related absorption features and those above 527 eV are related to the O 1s features.

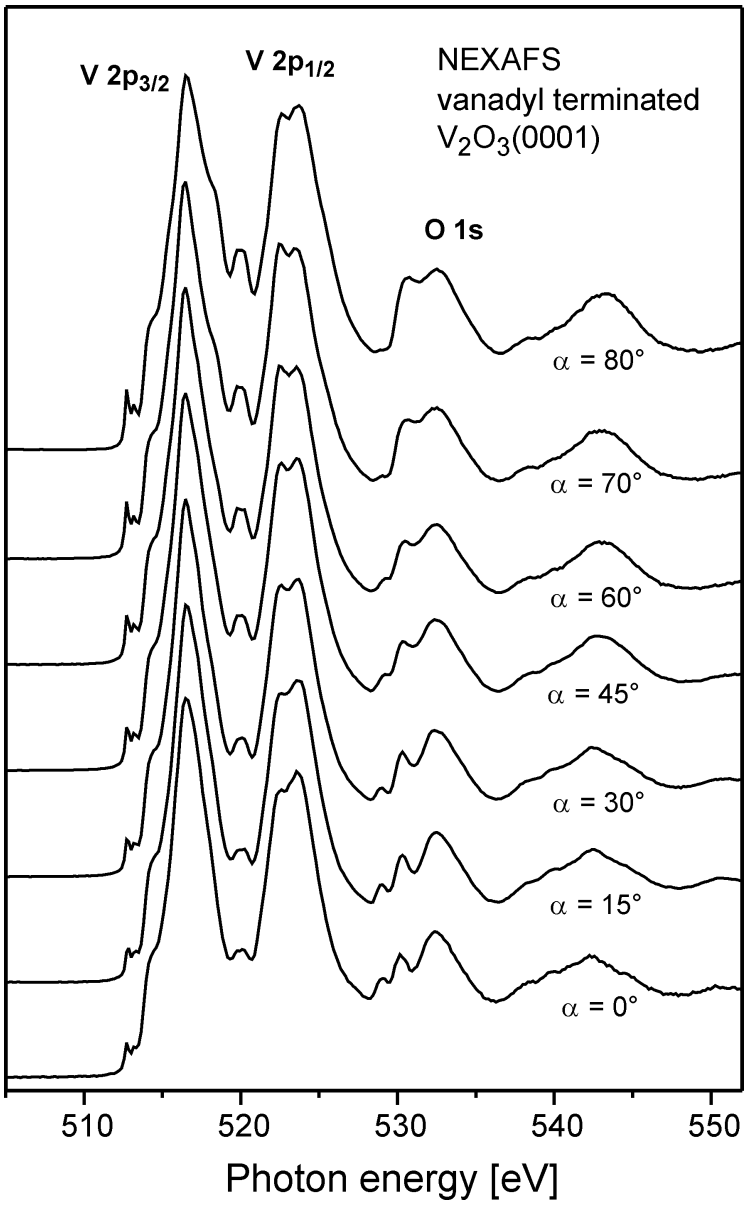

Figure 3.6: NEXAFS spectra of vanadyl terminated V_2O_3(0001)/W(110) recorded at different light incidence angles as indicated.

No O 1s → O 2p NEXAFS intensity is to be expected for V_2O_3 in a purely ionic picture since the O 2p levels are fully occupied and cannot accommodate additional charge. In contrast, the spectra show a quite noticeable O 1s absorption signal. Since the oxygen–vanadium bond contains covalent parts, density of unoccupied V 3d levels is mixed into the O 2p levels and the O 1s → O 2p (actually O 1s → O 2p plus V 3d) transition becomes possible. This is the origin of the structure between 530 and 535 eV [47]. The broad structure centered around 542 eV is attributed to a O 1s → O 3p transition [127]. The structure of the O 1s NEXAFS features reflects details of the hybridization and its intensity is governed by the degree of hybridization, the

occupation of the V 3d levels, and the dipole selection rules. The dipole selection rules are responsible for the dependence of the spectral features on the light incidence angle. Calculated NEXAFS spectra [127] were found to be consistent with the present NEXAFS spectra (discussed in the following section).

The vanadium L-edge NEXAFS spectra in Figure 3.6 correspond to electronic transitions from V 2p to V 3d states. The spectrum shows two peaks centered at around 516 and 523 eV due to the vanadium $2p_{3/2}$ and $2p_{1/2}$ levels, respectively. The line shape and the peak energies of the vanadium L-edge are sensitive to the chemical environment and can be used as fingerprints of the oxidation state [128-130]. The present NEXAFS spectra are in good agreement with data found in the literature [114,129,131].

Taking the previously discussed LEED, XPS, UPS, NEXAFS, IRAS and HREELS results together, it is evident that well-ordered $V_2O_3(0001)$ thin films can be prepared on W(110) and Au(111) substrates. These films are terminated by a layer vanadyl (V=O) groups.

3.4. Vanadium terminated $V_2O_3(0001)$

In an attempt to search for other stable terminations of the $V_2O_3(0001)$ surface, the oxygen atoms of the vanadyl groups of the vanadyl terminated $V_2O_3(0001)$ surface were removed by electron irradiation in UHV [47]. At the beginning of this work, electron irradiation was achieved by biasing the sample at 100 V and exposing it to electrons emitted from the glowing tungsten filament mounted behind the sample for few seconds at 600 K [47]. Later on, the electron irradiation was performed by an external tungsten filament positioned at ~1 cm in front of the sample. An electron current of 2 mA with a kinetic energy of 500 eV was incident onto the sample surface for 30 seconds (this procedure was repeated four times) or an electron current of 5 mA for 30 seconds (only one time) was used.

As pointed out in the previous section, under typical preparation conditions in an oxygen atmosphere, the $V_2O_3(0001)$ surface is terminated by a layer of vanadyl (V=O) groups. Electron irradiation leads to the removal of the vanadyl oxygen atoms of this layer; the resulting surface is terminated by vanadium atoms. Consequently, the question arises whether the state of the $V_2O_3(0001)$ surface before the electron irradiation can be restored or not. Indeed, the removal of the oxygen of the vanadyl

groups is found to be a reversible process: annealing the vanadium terminated surface in an oxygen atmosphere restores the vanadyl terminated surface. This oxidation process is discussed in more details in chapter 4. Model structures of the two differently terminated $V_2O_3(0001)$ surfaces, vanadyl and vanadium, are sketched in Figure 3.7. The vanadyl terminated surface (Figure 3.7(a)) may be regarded as the ideal vanadium terminated surface (Figure 3.7(b)) with one additional oxygen bonded on top of each outermost vanadium atom forming vanadyl (V=O) groups. These models are supported by recent STM studies [132].

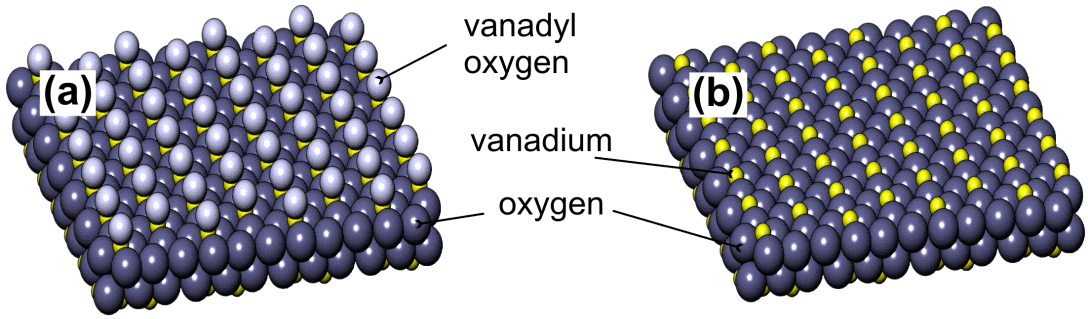

Figure 3.7: Tentative models of the vanadyl terminated (left) and the vanadium terminated $V_2O_3(0001)$ (right) surfaces.

A question that can be asked now is: what are the differences in the chemical/physical properties of the two terminations, vanadyl and vanadium $V_2O_3(0001)$ surfaces? Before answering this question, it is worthwhile to mention that the $Cr_2O_3(0001)$ surface was found to be terminated by chromium atoms after annealing at 1000 K [120]. At this point, it is reasonable to check whether the oxygen of the vanadyl groups of the $V_2O_3(0001)$ surface can be removed thermally or not. Experimentally, oxygen atoms of the vanadyl groups are found to be stable up to ~1000 K, as described in the following experiment: a vanadyl terminated $V_2O_3(0001)$ surface was thermally annealed (without electron irradiation) at different temperatures by using a glowing tungsten filament mounted right behind the sample. UPS and XPS spectra (Figure 3.8) recorded after each annealing step were taken under surface sensitive conditions (electron kinetic energy of ~100 eV and electron detection at $\theta = 70°$). Under these conditions, changes occurring in the surface region should be detectable. Neither the UPS nor the XPS spectra indicate any temperature-induced changes of the $V_2O_3(0001)$ film structure up to 1000 K. Thus, vanadyl groups are thermally stable on the surface until at least 1000 K. After annealing at 1070 K, the substrate core level (W

3d) is detected, which suggests that tungsten diffuses through the film. Nevertheless, the vanadyl terminated surface is maintained up to 1000 K. Similar findings were reported for vanadyl terminated V_2O_3(0001)/Rh(111) [54]. Theoretically, Kresse et al. [64] demonstrated that the vanadyl termination is the favorable termination of the V_2O_3(0001) surface under UHV conditions. Moreover, the authors [64] predicted that removal of vanadyl groups to produce the vanadium terminated surface by heating is impossible under UHV conditions.

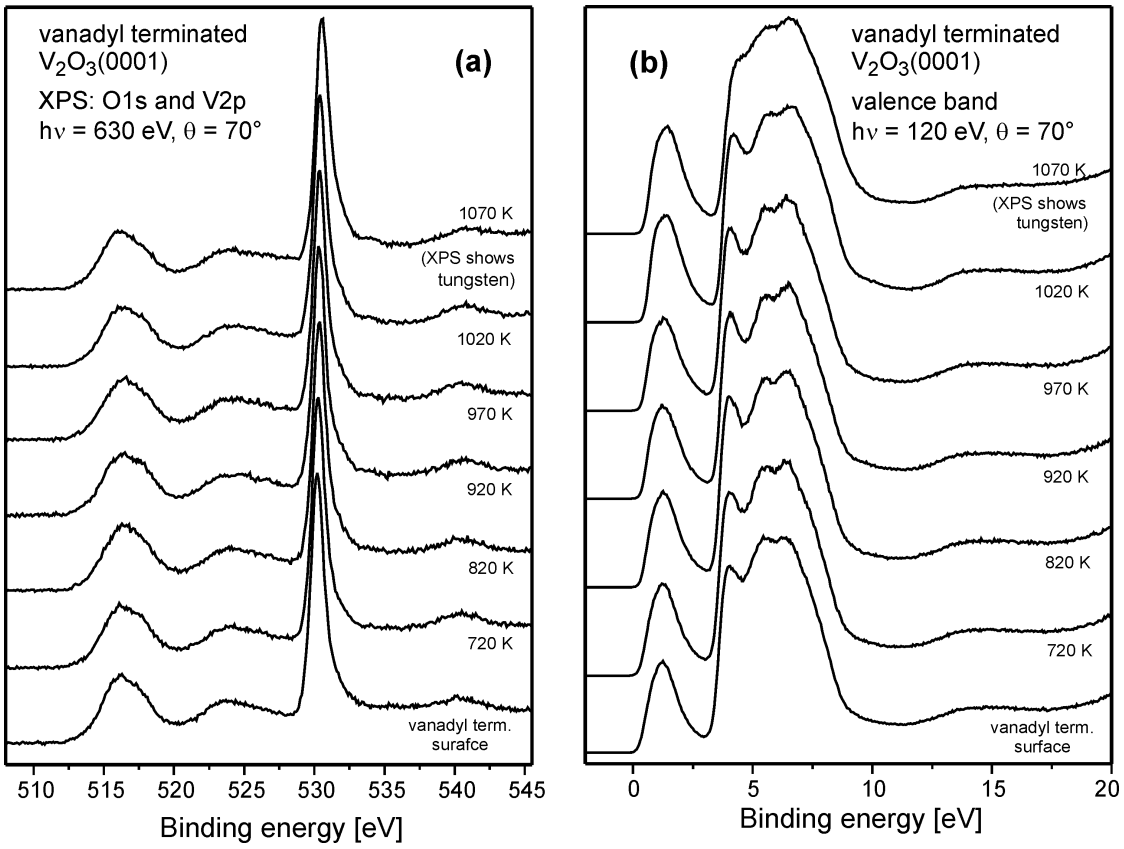

Figure 3.8: Photoelectron spectra taken after annealing vanadyl terminated V_2O_3(0001)/W(110) at different temperatures by thermal radiation from a glowing tungsten filament. Left: O 1s and V 2p core level spectra. Right: valence band spectra. The surface sensitivity was enhanced by recording the spectra at an electron detection angle of 70°.

A hint on the differences between the two surface terminations of V_2O_3(0001) is given by HREELS and IRAS measurements. Figure 3.9(b) compares a HREELS spectrum taken for the vanadyl terminated surface (top spectrum) with a spectrum of the vanadium terminated surface (bottom spectrum). The spectra are normalized to each other by adjusting the peak of the elastically reflected electrons to the same height. One obvious difference between the two spectra is that the loss intensities differ. This may be attributed to different electron reflection properties of the two surfaces or to the

spectrometer settings. Another difference is that the peak at 1040 cm^{-1}, which is characteristic for the vanadyl species, exhibit less intensity in the spectrum of the vanadium terminated surface compared to the spectrum of the vanadyl terminated one. This may suggest that vanadyl groups are removed from the vanadium terminated surface. A peak at 1040 cm^{-1} is also observed in Figure 3.9(a) which displays an IR spectrum of the vanadyl terminated surface divided by a spectrum of the vanadium terminated one. The presence of this peak in Figure 3.9(a) also indicates that the vanadyl groups can be removed by electron irradiation [47].

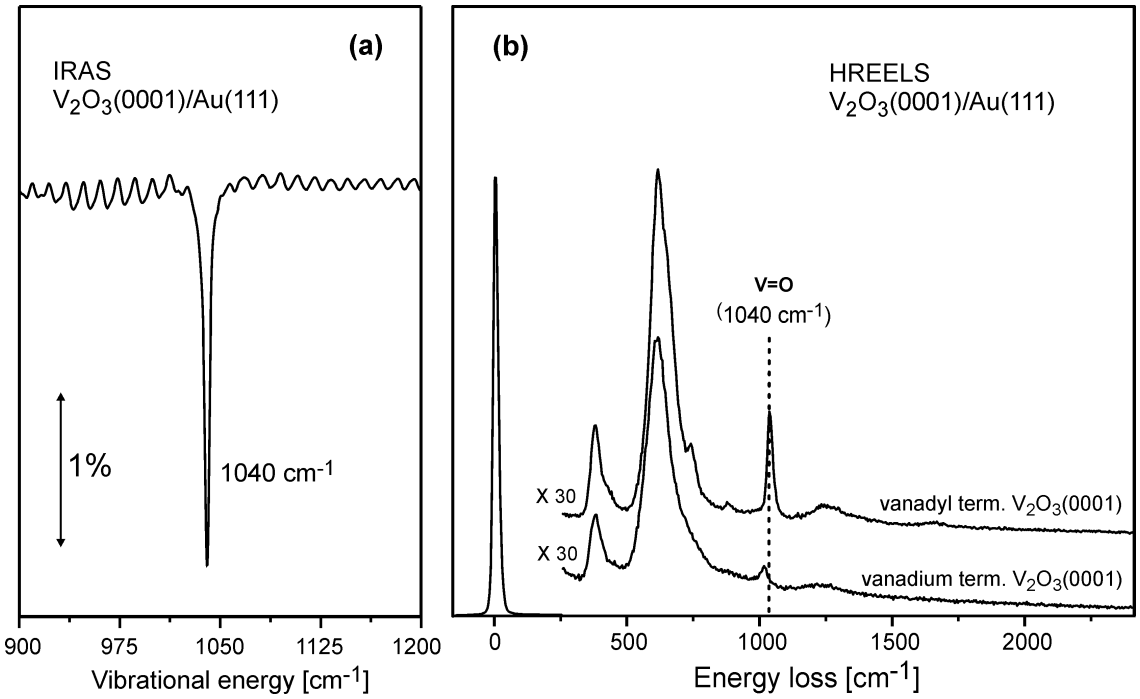

Figure 3.9: Left: IRAS spectrum of vanadyl terminated V_2O_3(0001)/Au(111) divided by a spectrum of vanadium terminated V_2O_3(0001)/Au(111). Right: HREELS spectra of vanadium terminated (bottom) and vanadyl terminated (top) V_2O_3(0001)/Au(111)**.**

The effect of reduction can also be seen in core level XPS data. Figure 3.10(a) compares surface sensitive O 1s and V 2p core level spectra taken for the vanadyl terminated surface (top spectrum) and the vanadium terminated surface (bottom spectrum). In the O 1s region, the spectrum of the vanadium terminated surface exhibits a small feature at 531.7 eV. This peak is not due to a surface contamination as demonstrated XPS and UPS investigations. Indeed, the peak at 531.7 eV may be associated with a vanadium–oxygen compound with different structural properties. In the V 2p region, the intensities of the V 2p surface states in the spectrum of the vanadyl

terminated surface are reduced in the spectrum of the vanadium terminated one. This may indicate not all the vanadyl groups could be removed by electron irradiation. Another possible explanation is that these V 2p states may have a different origin in the case of the vanadium terminated surface.

Valence band spectra of the vanadyl terminated surface and spectra of the vanadium terminated one are displayed in Figure 3.10(b). The band near to the Fermi energy between 0 and 3 eV binding energy is essentially occupied with V 3d electrons which are not involved in the V–O binding. Thus, the occupation of this band reflects the oxidation state. Since vanadium has five electrons and its formal oxidation state in V_2O_3 is +3, the levels close to the Fermi energy should contain two electrons in a simple ionic picture. Reduction of the vanadium atoms should lead to an increase of the occupation and, therefore, to an increase in the intensity of the V 3d band. The spectra in Figure 3.10(b) show that the intensity of the V 3d band is smaller for the vanadyl terminated surface than for the vanadium terminated one, indicating a higher oxidation state of the vanadyl terminated surface. This is compatible with the above discussion according to which the formal oxidation increases when going from the vanadium terminated surface to the vanadyl terminated one.

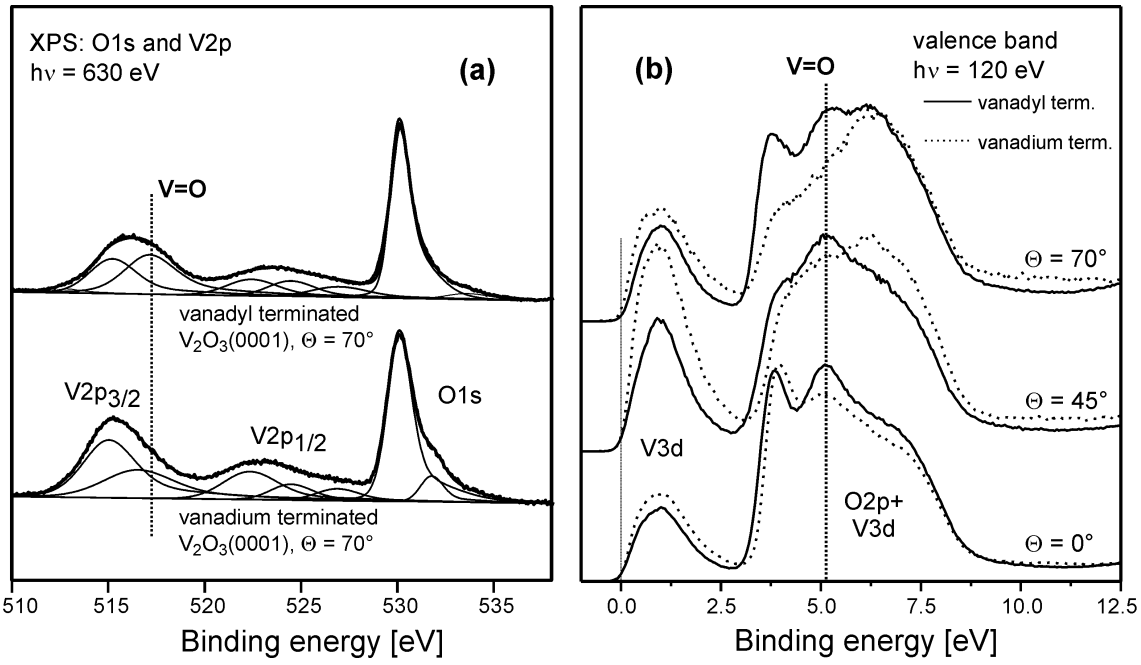

Figure 3.10: Left: V 2p and O 1s core level spectrum of vanadium terminated V_2O_3(0001)/W(110) (bottom) in comparison with a spectrum of vanadyl terminated V_2O_3(0001)/W(110) (top). Right: valence band spectra of vanadium terminated V_2O_3(0001)/W(110) in comparison with spectra of the vanadyl terminated V_2O_3(0001)/W(110).

Another effect is the shift of the intensity induced by the O 2p + V 3d levels to a higher binding energy upon removal of the vanadyl oxygen atoms (Figure 3.10(b)). This shift also reflects changes of the oxidation state. Hermann and Witko calculated densities of states for V_2O_3, VO_2, and V_2O_5 [29]. Their data showed that the O 2p + V 3d hybrid states shift to smaller binding energy with increasing oxidation state. This is the reason for the shift of the O 2p + V 2p states in Figure 3.10(b) upon removal of the vanadyl groups. Another point to be noted is that the band at ~5 eV, which is associated with the vanadyl species, exhibit less intensity in the spectrum of the vanadium terminated surface compared to the spectrum of the vanadyl terminated one [47]. This can be attributed to the removal of the vanadyl groups from the vanadium terminated surface.

NEXAFS measurements were performed on the vanadyl terminated and vanadium terminated $V_2O_3(0001)$ surfaces. The NEXAFS spectra were recorded using two different methods. One method was to collect the photoelectric current flowing between the sample and the ground potential (total yield detection TYD). This signal is not particularly surface sensitive due to the large number of low-energy secondary electrons which contribute to the signal. The other method employed a partial yield detector (PYD) which was mounted below the sample. The PYD only detected electrons leaving the surface at grazing angle. Electrons with energies below 50 eV were eliminated from the signal by setting the mesh in front of the PYD to a voltage of -50 eV. Thus, the NEXAFS signal collected by the PYD was significantly more surface sensitive than that collected by the TYD. A direct comparison between the spectra obtained with these two methods should reveal structures due to the surface of $V_2O_3(0001)$. A set of data and difference spectra are displayed in Figure 3.11.

The NEXAFS difference spectra (denoted by (3) in Figure 3.11(a)-(d)) show structures due to the surface. Assuming that the difference spectra of the vanadium terminated and the vanadyl terminated surfaces contain bulk intensity in about equal amounts, then the intensity due to the bulk should vanish in the difference of these spectra. These difference spectra are displayed in panels (e) and (f). Intensity due to the surface states of the vanadyl terminated surface should lead to maxima (marked with vertical lines), and intensity due to the vanadium terminated surface should induce minima.

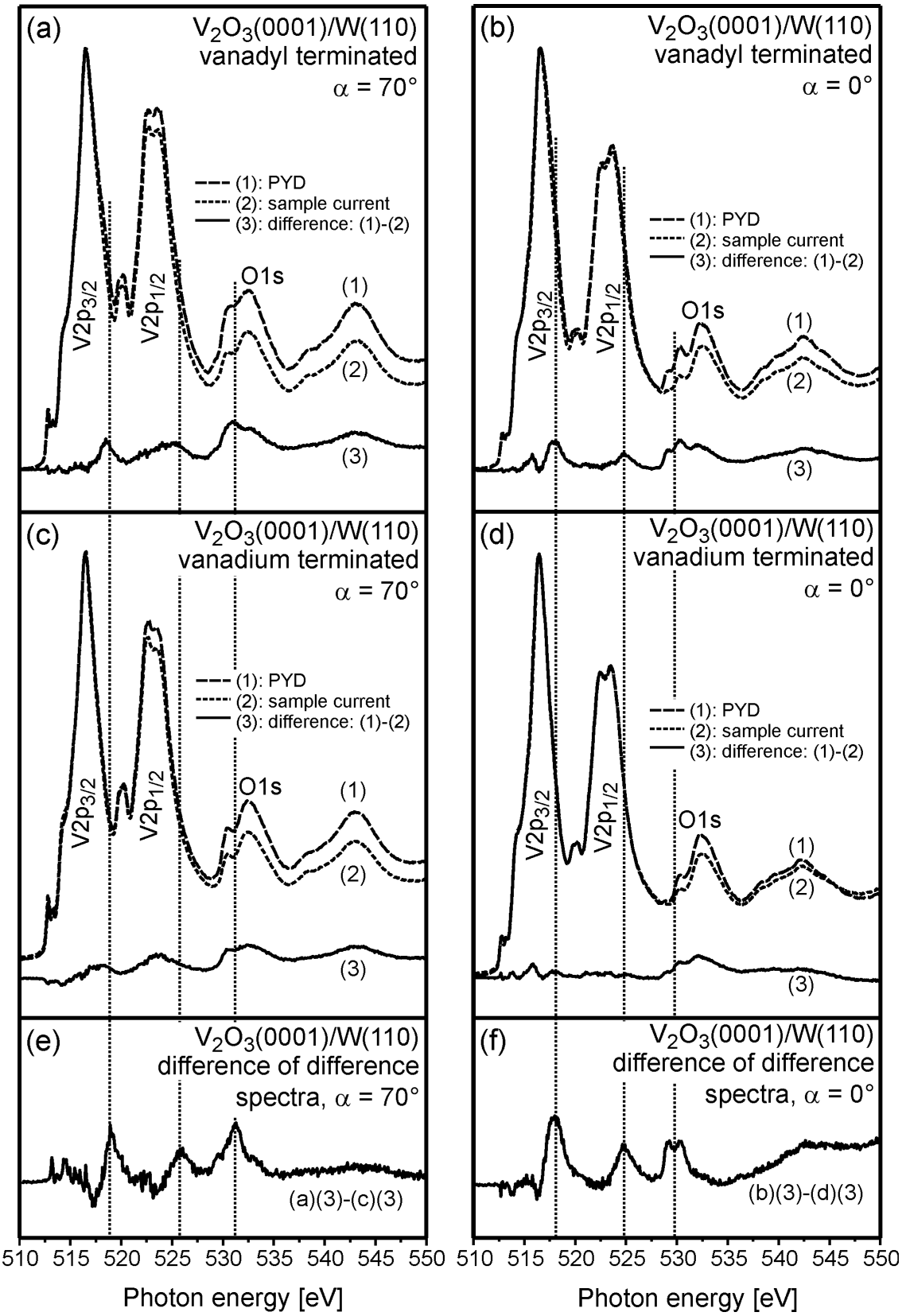

Figure 3.11: NEXAFS spectra of vanadium terminated and vanadyl terminated V_2O_3(0001)/W(110). Spectra were recorded in two different light incidence angles using the sample current mode and with a partial yield detector (PYD).

In the V L-edge region, additional V 2p induced intensity is observed at the high-energy side of the two V 2p peaks of the vanadyl terminated oxide. The shift of this intensity with respect to the bulk V 2p intensity is about 2 eV. This shift is the same as that of the V 2p surface XPS peak of the vanadyl terminated surface with respect to the bulk XPS peak (see Figure 3.5(a)). The V 2p induced NEXAFS peaks in the difference spectra can be attribute to excitations of the vanadium atoms of the vanadyl groups.

The intensity in the O 1s region is higher for the vanadyl terminated surface. This means that the number of unoccupied O 2p + V 3d states is higher for the vanadyl terminated surface, which may indicate a higher oxidation state as discussed previously. The additional intensity for the vanadyl terminated surface is not uniformly distributed over the O 1s → O 2p structure but concentrated on the low energy part. Part of this intensity should be attributed to the oxygen atoms of the vanadyl groups while the other part could be related to the oxygen atoms beneath the surface vanadium atoms. Indeed, this was recently confirmed by theoretical calculations [127] in which the contributions of different oxygen species in the O 1s region were identified.

Depending on its termination, the $V_2O_3(0001)$ surface may contain differently coordinated oxygen atoms. The half metal layer terminated surface contains both threefold O(3) and fourfold O(4) coordinated oxygen species near the surface, while the vanadyl terminated surface also contains singly O(1) coordinated vanadyl oxygen species. Recent calculated NEXAS spectra [127] revealed a clear difference between the two $V_2O_3(0001)$ surface terminations, in good agreement with the present experimental results. According to these calculations [127], the O 1s → O 2p peak (Figure 3.11(c) and (d) for both angles α) can be associated with electronic transitions originating from O(3) and O(4) 1s orbitals. The O(3) transitions are spread over the full peak region while the O(4) transitions are located at the high energy side. For the vanadyl terminated surface, the authors [127] attributed the O 1s → O 2p peak (Figure 3.11(a) and (b) for both angles α) to electronic transitions originating from O(1), O(3) and O(4) 1s orbitals. The central feature (at ~531 eV) was assigned to electronic transitions originating at the O(1) species.

In order to determine the work function of the vanadyl terminated and vanadium terminated surfaces, the HeI line at 21.22 eV was used as the excitation source for UPS measurements. Figure 3.12 compares the valence band spectrum of the vanadyl

terminated surface with the spectrum of the vanadium terminated one. The spectra were taken at normal emission and the samples were biased at -5 eV during the measurements. The work function was found to be 5.3 eV for the vanadium terminated surface and 6.3 eV for the vanadyl terminated $V_2O_3(0001)$ surface. The latter value is close to the value of ~6 eV reported for $V_2O_3(0001)$ single crystals [133]. Figure 3.12 reveals a difference of ~1.0 eV between the two terminations. A similar result was found by Dupuis [123]. The 1 eV difference is associated with the vanadyl groups. Presumably, the removal of the negatively charged oxygen ions from the vanadyl terminated surface leads to a decrease in the work function.

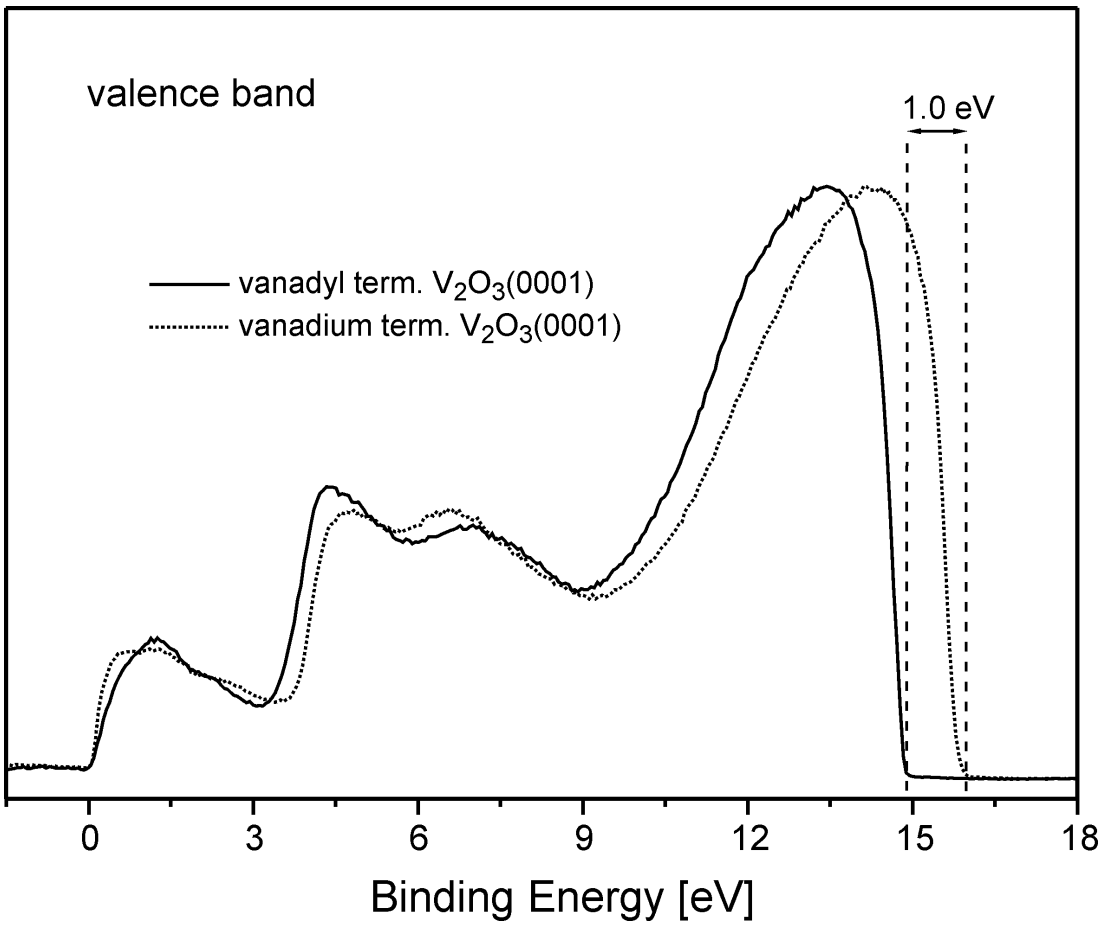

Figure 3. 12: Valence band spectra (HeI) of vanadyl terminated (solid line) and vanadium terminated (dotted line) $V_2O_3(0001)$/W(110). The difference of the low energy cut-off energies corresponds to the difference of the work function (~1.0 eV) between the two surfaces. The spectra were taken at normal emission and the samples were biased at -5 eV.

3.5 The metal-insulator transition in V_2O_3(0001) films

The metal-insulator transition (MIT) in V_2O_3 was intensively investigated and discussed for many years. V_2O_3 exhibits a complex phase diagram with paramagnetic metal, paramagnetic insulator, and antiferromagnetic insulator (AFI) regions as a function of temperature and pressure [88]. The mechanism driving the MIT of V_2O_3 remains unclear [90-93].

Pure stoichiometric V_2O_3 undergoes a paramagnetic metal to antiferromagnetic insulator transition with decreasing temperature at ~155 K. In the present study, UPS, HREELS and NEXAFS measurements were carried out at temperatures in the range of 90 to 300 K in order to investigate the MIT in V_2O_3(0001) films. UPS spectra of the V 3d band of the vanadyl terminated V_2O_3(0001) surface taken at 80, 185 and 300 K are displayed in Figure 3.13(a). The clearest change in the spectra across the temperature range is the shift of the high energy cut-off of the V 3d structure towards lower binding energy upon cooling from 300 to 85 K. Such behavior may be considered as an indication of the MIT occurring in the V_2O_3(0001) film [134-136]. Due to the surface sensitivity of the UPS, the spectra in Figure 3.13(a) indicate that the MIT takes place also in the surface region. At this point, it is worth to mention that a temperature-dependent broadening in XPS spectra of metals was reported [137-139] which may also be responsible for the spectral changes observed in the UPS spectra.

Figure 3.13(b) shows NEXAFS spectra of the vanadyl terminated V_2O_3(0001) surface recorded at 300 K and 80 K. The vanadium L-edge spectrum at 300 K is hardly changed upon cooling to 80 K. However, a number of spectral changes (indicated by arrows) at about 514, 520 and 523 eV can be observed. Similar changes were reported for different V_2O_3 single crystals [140-142] and V_2O_3 thin films [143] and were associated with the MIT. The authors [140-142] attributed the changes to orbital ordering. The changes in the presented NEXAFS spectra (Figure 3.13(b)) can be associated with the MIT occurring in the V_2O_3(0001) film. To some extent, a temperature-dependent broadening effect may also be responsible for these changes.

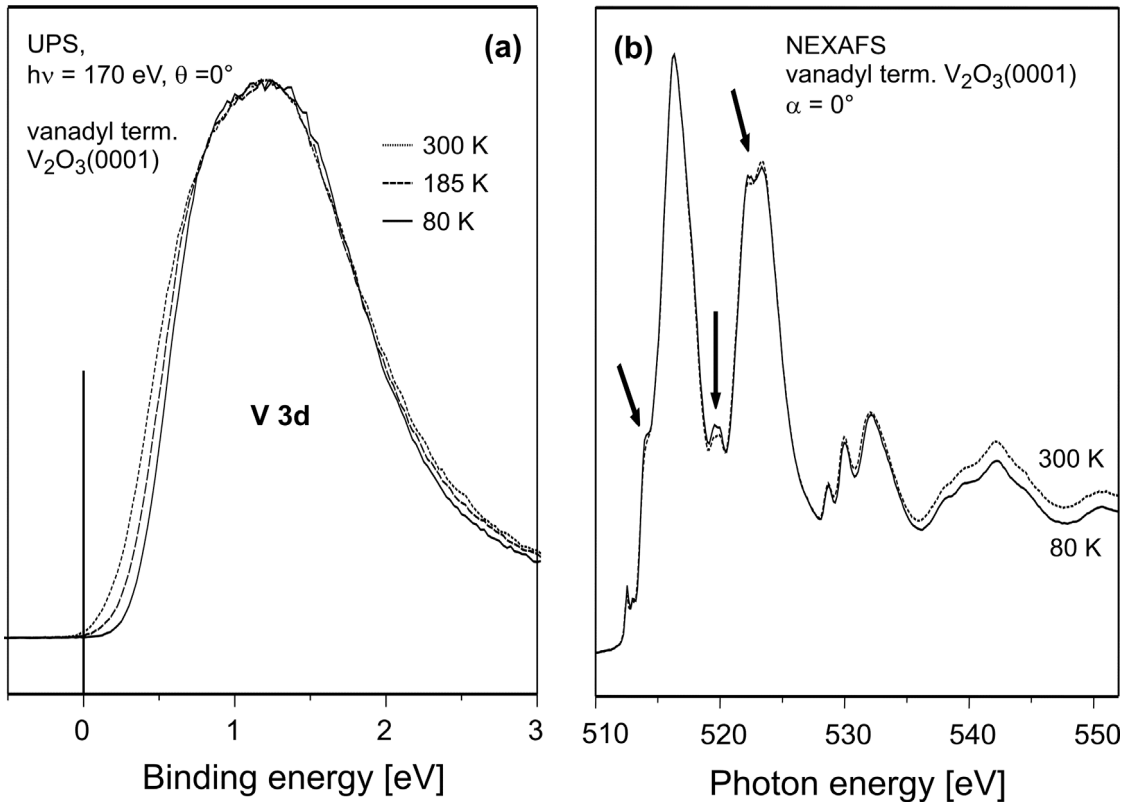

Figure 3.13: V3d valence band (left) and NEXAFS (right) spectra of vanadyl terminated V_2O_3(0001)/W(110). Spectra were recorded at different temperatures as indicated.

Figure 3.14(a) presents HREELS spectra of the vanadyl terminated V_2O_3(0001) surface recorded at 300 K and 90 K. The spectra change markedly upon cooling to 90 K. The most noticeable change is related to the structure at 620 cm^{-1} which shifts to 668 cm^{-1} and increases remarkably in intensity upon cooling. New peaks at 275 and 543 cm^{-1} appear, whereas the peaks at 382, 1040, 1335 and 1700 cm^{-1} gain intensity. These changes in the HREELS spectra can be attributed to the MIT. The loss feature at 620 cm^{-1} originates from vibrational modes due to the three oxygen atoms below the vandyl group [64]. The observed changes in this feature may reflect structural changes in the V_2O_3 film due to the MIT. The loss feature at 543 cm^{-1} observed in the spectrum at 90 K is probably hidden in the 300 K spectrum by the broad feature at 620 cm^{-1}. The two features at about 1335 cm^{-1} (≈ 668×2) and 1700 cm^{-1} (≈ 668+1040) can be attributed to multiple losses. Very recently, similar observations in HREELS spectra were reported by Pfuner et al. [134] upon cooling of V_2O_3(0001) films from 300 to 100 K. The authors [134] also attributed the spectral changes to the MIT in these films.

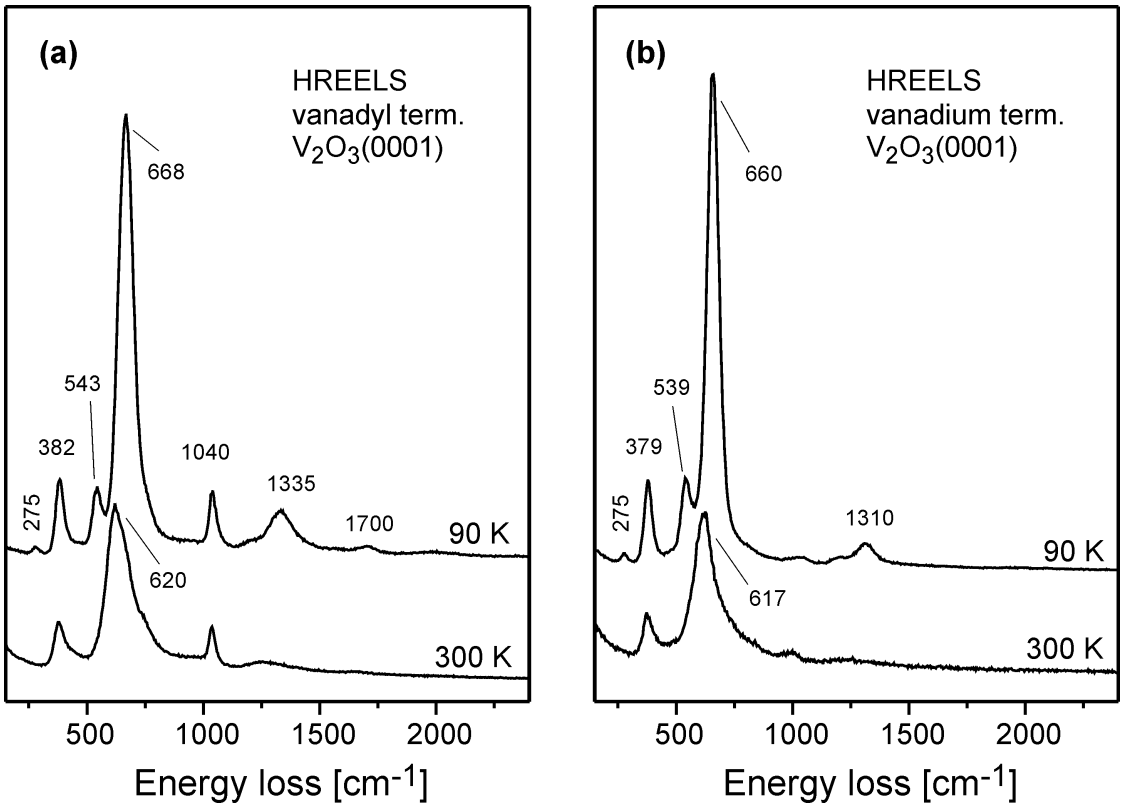

Figure 3.14 HREELS spectra of vanadyl terminated (left) and vanadium terminated (right) $V_2O_3(0001)$/Au(111). Spectra were recorded at 90 and 300 K.

Similar HREELS measurements were performed for the vanadium terminated $V_2O_3(0001)$ surface. The HREELS spectra are shown in Figure 3.14(b). Clearly, the spectra change upon cooling due to the MIT. Similar to Figure 3.14(a), the most pronounced change in Figure 3.14(b) is related to the structure at 617 cm^{-1}, which shifts to 660 cm^{-1} and increases remarkably in intensity upon cooling. New peaks at 275 and 539 cm^{-1} appear, whereas the peaks at 379 and 1310 cm^{-1} gain intensity. Unlike the spectrum of the vanadyl terminated surface, no feature is observed at about 1700 cm^{-1} in the spectrum of the vanadium terminated surface (Figure 3.14(b)) which does not exhibit the vanadyl stretching vibration at 1040 cm^{-1}.

As mentioned earlier, the precise mechanism giving rise to this phase transition is unclear. Theoretical calculations might be needed to explain the present data.

3.6 Summary

Well-ordered $V_2O_3(0001)$ thin films grown on W(110) and Au(111) with a thickness of ~100 Å were investigated with respect to their surface properties. The geometric, electronic and vibrational structure of these films was characterized by means of a variety of surface sensitive techniques including LEED, XPS, UPS, NEXAFS, IRAS and HREELS.

Typical preparation conditions were: ~50 Å of vanadium were deposited onto the respective substrate at 600 K in 1×10^{-7} mbar O_2 followed by annealing at 670 K in 1×10^{-7} mbar O_2 and then annealing in vacuum at 850 K. Under these conditions, the $V_2O_3(0001)$ films are terminated by a layer of vanadyl groups. These groups are stable on the surface up to temperatures $\geq$ 1000 K. The oxygen atoms of the vanadyl layer may be removed by electron irradiation in UHV leading to a surface terminated by vanadium atoms. Annealing the vanadium terminated surface in an oxygen atmosphere restores the vanadyl terminated surface.

Sharp reflexes are observed by LEED indicating a high degree of a long-range order of the $V_2O_3(0001)$ films. IRAS and HREELS spectra of the vanadyl terminated $V_2O_3(0001)$ surface exhibit a peak at 1040 cm^{-1} due to the excitation of vanadyl (V=O) stretching vibrations which disappears after the electron irradiation as a result of removing of the vanadyl oxygen atoms.

Under very surface sensitive conditions, a V 2p surface state is observed in XPS data of the vanadyl terminated surface. Its binding energy indicates that the oxidation state of the vanadium atoms on the vanadyl terminated surface is higher than the oxidation state of the bulk vanadium atoms. This result is corroborated by ARUPS data which show that the V 3d induced intensity is smaller for the vanadyl terminated surface than for the vanadium terminated one. NEXAFS difference spectra also exhibit intensities due to the V 2p and O 1s surface states of the vanadyl terminated surface.

The vanadyl and vanadium terminated surfaces exhibit work functions of 6.3 and 5.3 eV, respectively. The low work function of the vanadium terminated surface may be associated with the removal of the negatively charged oxygen ions. The metal insulator transition of the $V_2O_3(0001)$ films was also investigated. The MIT of these films was evidenced by UPS, NEXAFS and HREELS.

Chapter 4

Adsorption of Oxygen

This chapter describes the oxidation of the vanadium terminated $V_2O_3(0001)$ surface and explains how oxygen interacts with this surface. Using TDS, UPS, XPS, IRAS and HREELS, the adsorbed oxygen species were identified and their behavior was examined.

4.1 Introduction

The interaction of oxygen with oxide catalysts is an important step in the course of catalytic hydrocarbon oxidation reactions [144,145]. Iwamoto and Lunsford pointed out that the nature of the surface oxygen species formed during the interaction of oxygen with oxide surfaces significantly influences the hydrocarbon oxidation reaction [146]. Therefore, an understanding of the nature of chemisorbed oxygen species on oxide surfaces is very important for understanding of catalytic reactions involving oxygen.

In general, the adsorption state of oxygen is classified into two types: molecular (O_2) and atomic (O) adsorption states. Adsorbed species such as O_2^-, O_2^{2-}, O^- and O^{2-} were identified on oxide surfaces [124,125,146-153], and their characterization and reactivity were documented [154,155]. The formation of radical-ion forms of molecularly adsorbed oxygen is only observed on reduced oxide surfaces [148]. Their formation is caused by stabilization of oxygen molecules on coordinatively unsaturated cations where the degree of oxidation is lower than that of regular sites. The oxygen adsorption process in this case is accompanied by an electron transfer from a site with excess electron density into the adsorbed oxygen molecule. Charged molecular oxygen species are unstable at high temperatures as they tend to decompose upon heating and to re-oxidize the surface of the catalyst [148].

4.2 Results and discussion

4.2.1 IRAS and HREELS

As verified in section 3.4, electron irradiation of the vanadyl terminated surface leads to the removal of the oxygen atoms from the vanadyl layer and results in a surface terminated by vanadium atoms. This process is reversible: the vanadyl terminated surface can be prepared by annealing the vanadium terminated surface in O_2 atmosphere. In order to understand this process, the interaction of O_2 with the vanadium terminated surface was investigated in more details. Figure 4.1 shows a series of IRAS spectra taken from vanadium terminated $V_2O_3(0001)$ after exposure to O_2 at 90 K. Two bands at 951 and 1030 cm^{-1} are observed at 90 K. The band at 1030 cm^{-1} is assigned to the vanadyl species [47]. The observation of this band at 90 K indicates that at this temperature a fraction of the adsorbed oxygen molecules dissociates to form vanadyl groups.

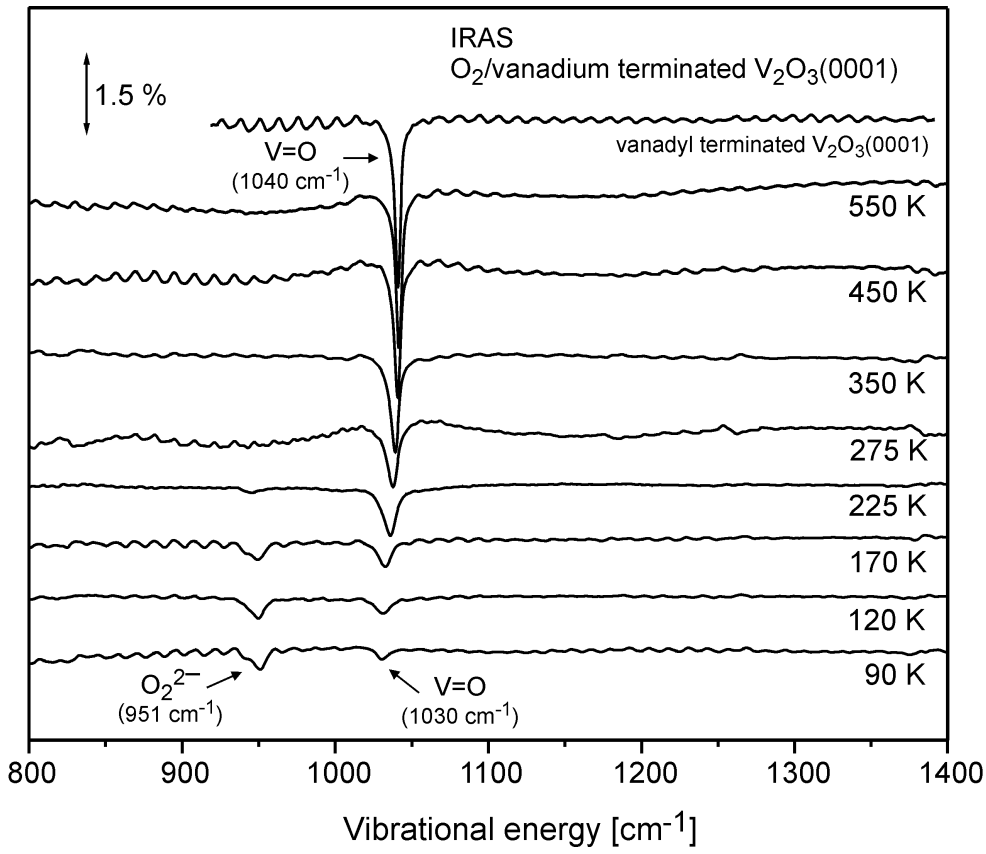

Figure 4.1: IRAS spectra of O_2 adsorbed on vanadium terminated $V_2O_3(0001)$/Au(111) as a function of the annealing temperature after dosing 15 L at 90 K. At the top, a spectrum of vanadyl terminated $V_2O_3(0001)$ is shown for comparison purposes.

Upon annealing, the vanadyl feature at 1030 cm^{-1} increases in intensity and shifts to 1040 cm^{-1}. The shift form 1030 to 1040 cm^{-1} is possibly associated with surface ordering induced by annealing. It is obvious from the IRAS data that the vanadyl groups are fully recovered upon annealing the O_2-dosed surface up to 550 K, as is evident from the similarity of the topmost spectra in Figure 4.1. The band at 951 cm^{-1} is detected up to 170 K and then it disappears at higher temperatures. Based on its vibrational energy, this band can be attributed to peroxo (O_2^{2-}) species. Typically, peroxo (O_2^{2-}) species have characteristic vibrations in the range of 900-1100 cm^{-1} while superoxo (O_2^{-}) species have vibrations in the range of 1100-1150 cm^{-1} [156]. The observation of peroxo (O_2^{2-}) species was also reported on oxide systems such as SnO_2 [152], CeO_2 [157], $SrTiO_3$ [158], Li doped NiO thin films [159,160] and other oxides [147,148]. For adsorption of O_2 on Cr_2O_3(0001) [124,125], the adsorbed oxygen species were found to exhibit an IR band at 963 cm^{-1} which is most likely also due to peroxo species.

Very recent theoretical calculations [66] supported the interpretation that peroxo species form on the V_2O_3(0001) surface. These calculations predicted an IR-active mode for η^2-peroxo species on V_2O_3(0001) at 960 cm^{-1}, which is consistent with the present experimental results. Moreover, these calculations suggested that the peroxo species are lying more or less flat on the surface. Only modes with changes of the dipole moment perpendicular to the surface can be observed by IRAS (see section 2.1.6). Although the peroxo species are lying flat on the surface, the peroxo bond represents a $V^{\delta+}$–$O_2^{\delta-}$ dipole perpendicular to the surface as suggested by the calculations [66]. The dipole moment changes when the O–O bond is compressed or stretched since the O–O stretching mode has a component that changes the V–O bond distances. Furthermore, the charge separation between V and O_2 changes with the O–O distance; it gets smaller (or larger) with decreasing (or increasing) the distance.

Additional information is provided by HREELS measurements. The HREELS spectra are displayed in Figure 4.2. The spectrum of the clean vanadium terminated surface exhibits a number of losses due to the optical phonons of the oxide. Oxygen adsorption on the vanadium terminated surface leads to additional losses at 950 and 1027 cm^{-1}, in good agreement with the presented IRAS spectra. Additionally, a shoulder is found at ~765 cm^{-1} for the O_2-dosed surface and for the vanadyl terminated surface but not for the clean vanadium terminated surface. Theoretical calculations predicted

that this feature may be assigned to a surface localized mode on the vanadyl terminated surface and the peroxo covered surface [66].

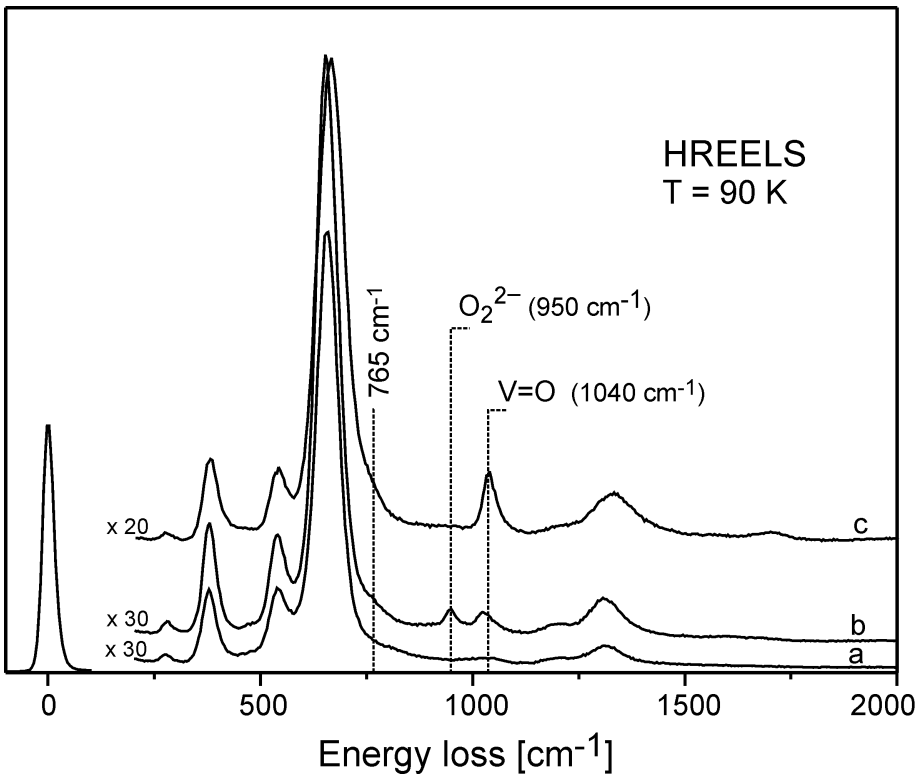

Figure 4.2: HREELS spectra of clean vanadium terminated V_2O_3(0001)/Au(111) (a) and after O_2 adsorption (15 L) on vanadium terminated V_2O_3(0001)/Au(111) at 90 K (b). A spectrum of clean vanadyl terminated V_2O_3(0001)/Au(111) (c) is shown for comparison. HREELS spectra were recorded at 90 K.

4.2.2 TDS

Figure 4.3 shows a thermal desorption spectrum of O_2 (mass 32) measured after adsorption of oxygen on vanadium terminated V_2O_3(0001) at 90 K. Two desorption features are observed by monitoring mass 32: a low-temperature desorption feature with a maximum temperature around 115 K followed by a broad feature between 125 and 250 K. Based on the present data, the origin of the desorption feature at 115 K is not clear. It may be attributed to molecules that did not originate from the sample surface. The intensity of the high-temperature feature is about a factor of 100-200 weaker than the signal observed with the same setup for a monolayer of molecular propane desorbing from the vanadium terminated V_2O_3(0001) surface. Thus, it may be assumed that this feature is due to desorption of some minority species, possibly interacting with surface defects or to a reaction path with low probability. This observation essentially

means that nearly all of the oxygen atoms of the adsorbed peroxo species are used for the formation of vanadyl groups. As mentioned previously, a comparison of the intensities of the vanadyl vibrations in the two topmost spectra in Figure 4.1 clearly shows that annealing the oxygen covered surface leads to a surface that is fully covered by vanadyl groups. Since one surface vanadium atom binds to one oxygen atom to form one vanadyl group, the coverage of the surface vanadium atoms with O_2^{2-} should be about 0.5, i.e only every second surface vanadium atom carries an O_2^{2-} group according to the TDS data.

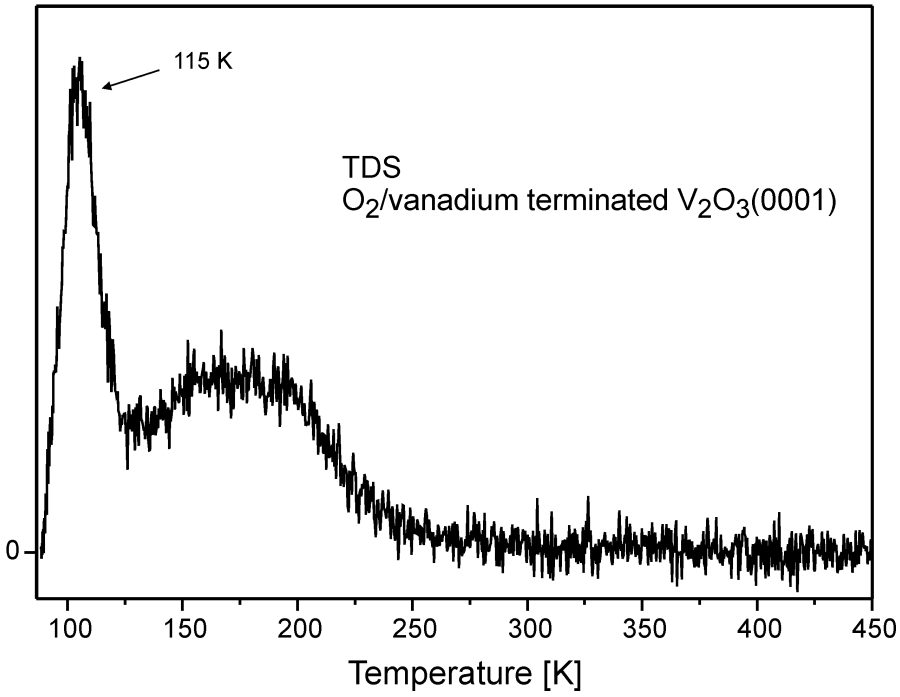

Figure 4.3: TDS spectrum of O_2 (mass 32) after adsorption of O_2 (saturation coverage) on vanadium terminated V_2O_3(0001)/Au(111) at 90 K. The heating rate was 0.5 Ks^{-1}

4.2.3 UPS and XPS

Valence band and XPS spectra for the interaction of oxygen with vanadium terminated V_2O_3(0001) are presented in Figure 4.4. Oxygen adsorption at 80 K immediately leads to a significant decrease of the V 3d intensity (Figure 4.4(b)) which means that the oxidation state of the surface vanadium atoms increases (see section 3.4). A shift of the V 2p levels to higher binding energy upon oxygen dosage at 80 K (Figure 3.4(a)) is also compatible with increasing vanadium oxidation state.

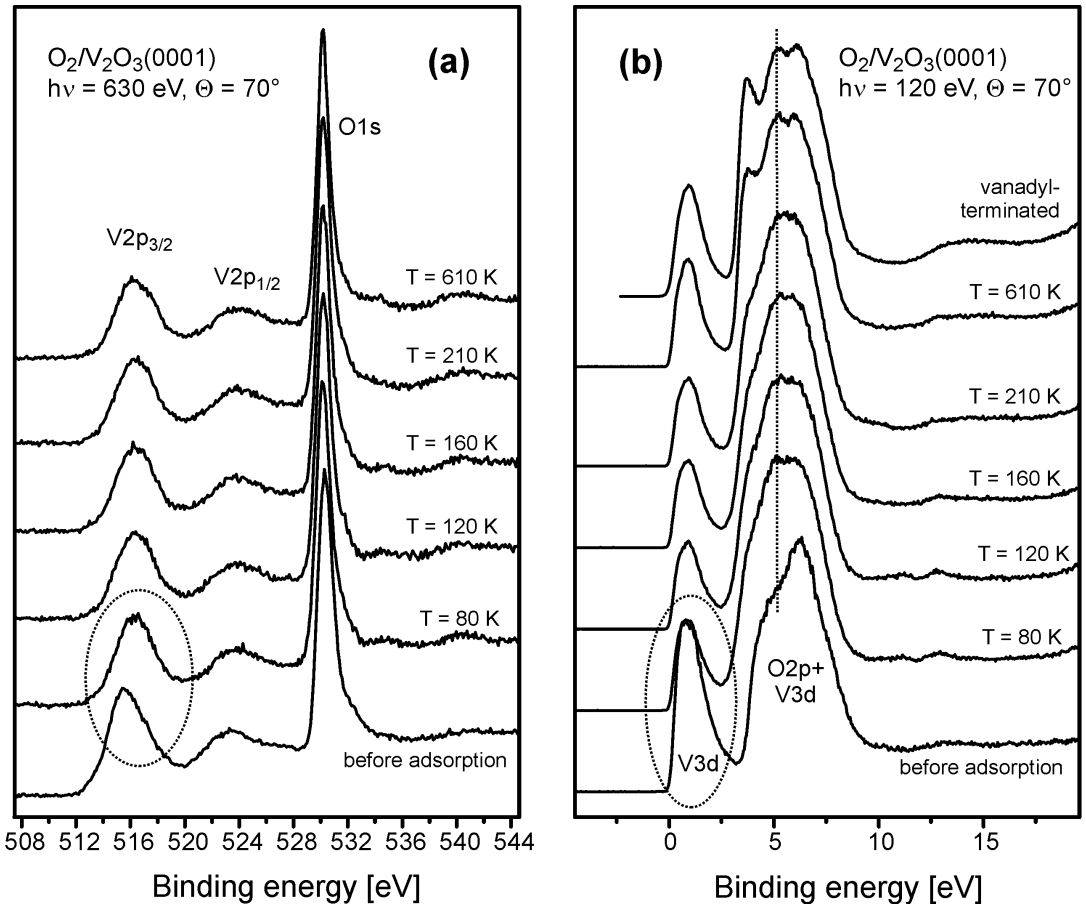

Figure 4.4: Photoelectron spectra of O_2 on vanadium terminated V_2O_3(0001)/W(110) as a function of the annealing temperature after dosing 10 L at 80 K. Left: O 1s and V 2p core level spectra. Right: valence band spectra and at the top a spectrum of vanadyl terminated V_2O_3(0001)/W(110) is shown.

It is also obvious from the UPS spectra that vanadyl species form upon annealing the O_2-dosed surface up to 610 K. This is evident from the similarity of the valence band structures of the two topmost spectra in Figure 4.4(b). The peak at about 5 eV is assigned to vanadyl groups (see section 3.4). Additionally, UPS spectra recorded at temperatures between 80 and 210 K are noticeably different from the valence band spectrum of the vanadyl terminated surface shown at the top. This is due to the presence of both peroxo species and vanadyl groups on the surface at low temperatures. Figure 4.4(b) also reveals that the V 3d intensity at temperatures between 80 and 210 K, where the surface is covered by O_2^{2-}, is smaller than the case of the vanadyl terminated surface. This suggests that the average oxidation state of the surface vanadium atoms is even higher for peroxo coverage than for vanadyl termination which is somewhat at variance with the coverage of ~0.5 concluded from the previously discussed TDS data. Thus, the situation with respect to the peroxo coverage remains somewhat unclear but it may be stated that the coverage is likely between 0.5 and 1.

4.3 Summary

By applying a variety of surface sensitive techniques, the interaction of oxygen with the vanadium terminated $V_2O_3(0001)$ surface was investigated. The obtained results indicate that oxygen interacts strongly with this surface. Oxygen adsorption at 90 K occurs both dissociatively and molecularly, as shown by IRAS and HRELLS. In addition to the formation of vanadyl groups, negatively charged adsorbed oxygen species in the form of peroxo (O_2^{2-}) are also formed at 90 K. Upon annealing, the peroxo species dissociate and the resulting oxygen atoms bond to the surface vanadium atoms forming vanadyl groups. As demonstrated by IRAS, the vanadyl terminated surface is fully recovered after annealing the O_2-dosed vanadium terminated $V_2O_3(0001)$.

Chapter 5

Adsorption of Carbon Monoxide

This chapter deals with the adsorption of CO on $V_2O_3(0001)$ surfaces and explains the influence of the different surface terminations on the interaction with CO. XPS, IRAS and NEXAFS were used to exploit CO as a probe molecule for the surface bonding properties. The adsorbed CO species and their molecular geometry were investigated.

5.1 Introduction

CO adsorption on metal and metal oxide surfaces was studied extensively. It is generally accepted that CO binds weakly to the cations of the metal oxide surfaces and serves as a probe molecule for Lewis acid sites on oxides [148,161]. The first explanation of the bonding mechanism for the chemisorption of CO was presented by Blyholder [162]. Recalling that the HOMO and LUMO of CO are 5σ and 2π* respectively, the CO–metal bonding can be described in terms of electron donation (from the CO 5σ orbital to unoccupied metal orbitals) and back-donation (from the metal to the CO 2π* empty orbitals). The extent of back-donation is directly correlated to the strength of the M–CO bond and to the tendency for the CO molecule to decompose on the surface. The C–O bond is weakened by the charge in the antibonding 2π* molecular orbital.

The vibrational frequency shift of adsorbed CO relative to the gas phase value can provide important information about the nature of the CO interaction with the surface. For example, the back-donation weakens the C–O bond which may lower the C–O stretching frequency below the gas phase value [163]. On the other hand, the C–O stretching frequency tends to increase due to the Pauli repulsion between the electron charge distribution of CO and that of the surface [164]. The C–O stretching frequency is different for different adsorption sites that may exhibit different back-donation properties [165]. Details about the frequency shift are given in section 2.1.6.

5.2 Results and Discussion

5.2.1 XPS

Figure 5.1 compares the C ls XPS spectra recorded after CO adsorption on vanadyl terminated and on vanadium terminated V_2O_3(0001) at 80 K. The temperature dependence of these spectra clearly shows that CO interacts strongly with the vanadium terminated surface and very weakly with the vanadyl terminated one. This is similar to observations made for TiO_2 [166,167]. For this oxide, it was reported that CO adsorbs weakly on oxidized titania and adsorbs more strongly when the oxide is reduced. Figure 5.1(a) reveals a C 1s intensity at 80 K which is much smaller than that observed for the vanadium terminated surface (Figure 5.1(b)). Indeed, the CO-induced peak in the spectrum of the vanadyl terminated surface at 80 K is smaller by a factor of 20 than the corresponding feature in the spectrum of the vanadium terminated surface.

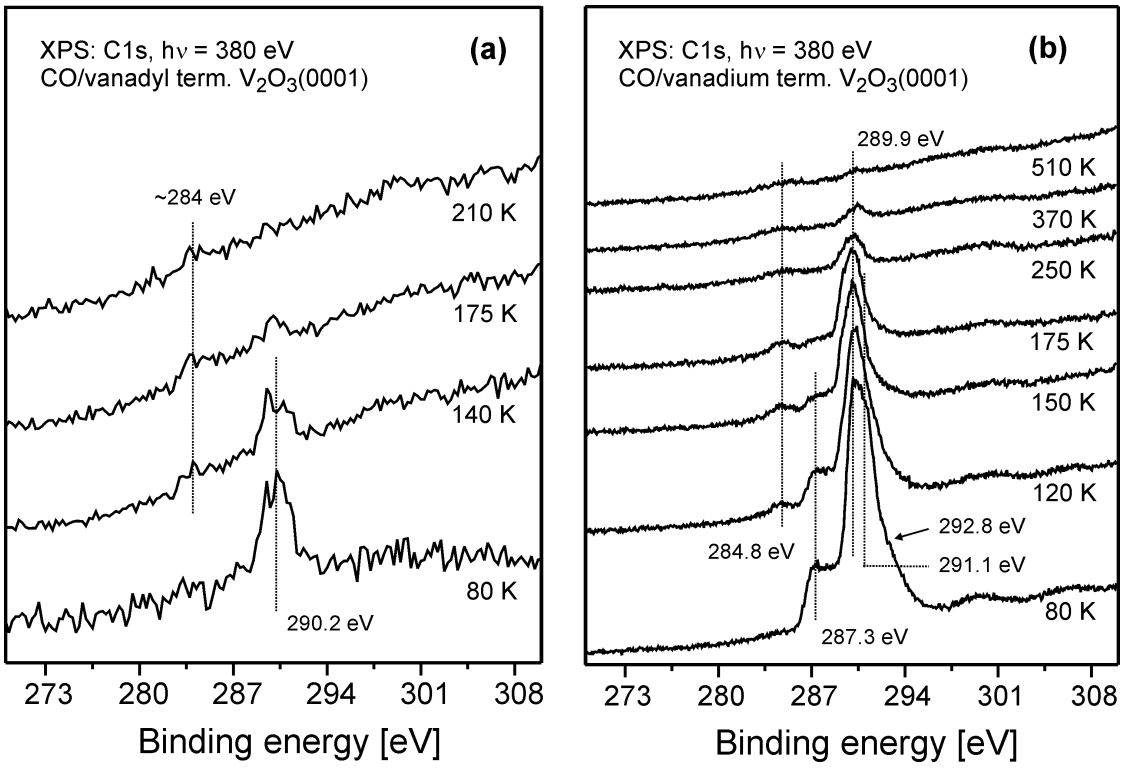

Figure 5.1: C 1s core level spectra of CO adsorbed on vanadyl terminated (left) and vanadium terminated (right) V_2O_3(0001)/W(110) as a function of the annealing temperature after dosing 15 L at 90K

In order to correlate the CO adsorption states and the V_2O_3(0001) surface structure, it is useful to discus the STM images of the V_2O_3(0001) surfaces. STM images of the vanadyl terminated and the vanadium terminated surfaces are displayed in

Figure 5.2 [132]. It should be mentioned, however, that the STM and the XPS experiments were performed in two different UHV systems. Therefore, these STM images may not fully represent the surfaces which were utilized in the XPS measurements. Moreover, the STM investigations clearly show that the $V_2O_3(0001)$ surface structure depends on the preparation conditions. Particularly, the concentration of defects may change from one preparation to another. Thus the correlation between the CO adsorption states and the STM images (as discussed below) may not be straightforward.

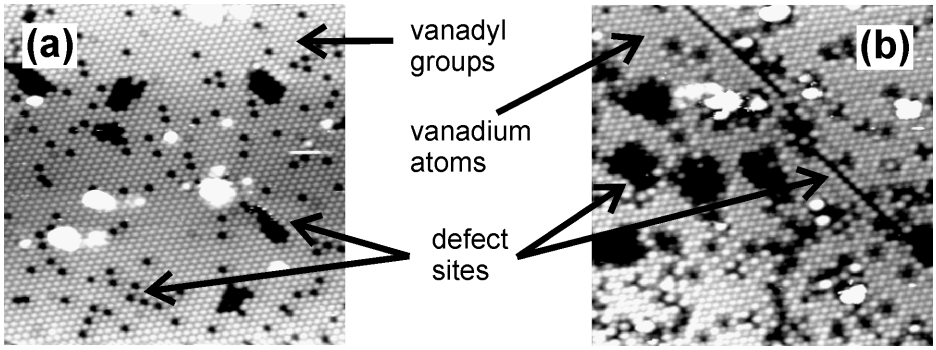

Figure 5.2 Left: STM image (20 nm x 20 nm, -1.5 V, 0.2 nA) of vanadyl terminated $V_2O_3(0001)$/Au(111). Right: STM image (20 nm x 20 nm, -1.0 V, 0.2 nA) of vanadium terminated $V_2O_3(0001)$/Au(111) [132].

Figure 5.2(a) displays a STM image of the vanadyl terminated $V_2O_3(0001)$ surface which consists of large flat terraces. The regular arrays of bright maxima are the vanadyl groups. The STM measurements indicate that the surface of the dark areas may be terminated by vanadyl groups. The boundaries of these dark areas are steps between two oxide layers. Additional defect sites are the dark points which may be associated with missing vanadyl oxygen atoms or missing vanadyl groups. The white areas are possibly due to vanadium-oxygen compounds which are not identified yet. These non-regular sites on the vanadyl terminated surface (i.e. point defects, steps and white areas in Figure 5.2(a)) may serve as adsorption sites for the CO molecules and, consequently, may induce the small peak at 290.2 eV in Figure 5.1(a). The small feature at about ~284 eV in Figure 5.1(a) may be attributed to atomic carbon on the surface.

Figure 5.2(b) shows a STM image of the vanadium terminated $V_2O_3(0001)$ surface which consists of flat terraces. In analogy to Figure 5.2(a), the regular arrays of bright maxima in Figure 5.2(b) are vanadium atoms and the surface of the dark areas is a vanadium terminated surface. The boundaries of these dark areas are steps between

two oxide layers. Other defect sites show up as dark points and dark lines in Figure 5.2(b). Bright spots and white areas, which may be due to unidentified vanadium-oxygen compounds, are also visible in Figure 5.2(b).

Figure 5.1(b) shows a series of XPS spectra taken for vanadium terminated V_2O_3(0001) after exposure to CO at 80 K as a function of the annealing temperature. The C 1s XPS spectrum recorded at 80 K exhibits a broad asymmetric peak at ~290.5 eV and a small peak in the low binding energy side. The broadness of the C ls feature at 80 K may be attributed to the presence of different CO species on different adsorption sites on the surface. The intense feature at 289.9 eV is possibly attributed to CO species adsorbed on regular surface sites. This species is stable on the surface up to at least 250 K. The binding energy of this species is very close to that observed for CO on the vanadyl terminated surface at 290.2 eV in Figure 5.1(a). This may indicate that both CO species are adsorbed on similar surface sites which expose vanadium atoms.

The correlation between the C 1s features (at 287.3, 291.1 and 292.8 eV) and the surface sites may not be straightforward. The difference in the binding energies and in the thermal behaviors of the C 1s features indicates that these features are associated with different adsorption sites. At this point, it is worth to mention that two CO adsorption states on regular Cr_2O_3(0001) surface sites were identified experimentally (by TDS and IRAS) and theoretically (by cluster calculations) [169]. Therefore, one of the features (at 287.3, 291.1 and 292.8 eV) may be due to CO adsorption on a regular V_2O_3(0001) surface site. The remaining features are possibly associated with CO species on non-regular surface sites such as steps, points, lines and white areas in Figure 5.2(b). In light of the present XPS and STM data, it is difficult to assign the features at 287.3, 291.1 and 292.8 eV to particular surface sites. It seems that the concentration of surface sites may not be the same in both cases.

Annealing the CO-covered surface reduces in the intensities of the C ls feature due to CO desorption or dissociation. Additionally, a small C ls peak is observed at 284.8 eV which may be attributed to atomic carbon on the surface [78]. The observation of the peak at 284.8 eV may indicate that a fraction of the adsorbed CO dissociates on the vanadium terminated surface. The small C 1s intensity at 370 K may be attributed to CO readsorption since the spectra were recorded at 80 K.

5.2.2 NEXAFS

Information on the molecular orientation of the adsorbed CO molecules can be provided by NEXAFS. Figure 5.3(a) displays C ls NEXAFS spectra recorded for CO on vanadium terminated $V_2O_3(0001)$ at 80 K. The spectra were recorded at two different light incidence angles: $\alpha = 0°$ (normal incidence) and $\alpha = 70°$ (grazing incidence). The NEXAFS spectra were normalized following an established procedure [76] which involves division of the spectra of the CO-covered surface by the spectra of the clean surface. The NEXAFS spectra (Figure 5.3(a)) exhibit three features at about 287.3, 300.2 and 305 eV. Other features (marked by arrows) are artifacts due to normalization problems. The light intensity of the beamline as a function of the photon energy appears to be slightly time-dependent, especially in the C 1s region. Since the spectra of the clean and the CO-covered surface were recorded at different times, it may be the case that the beamline characteristics changed in the meantime.

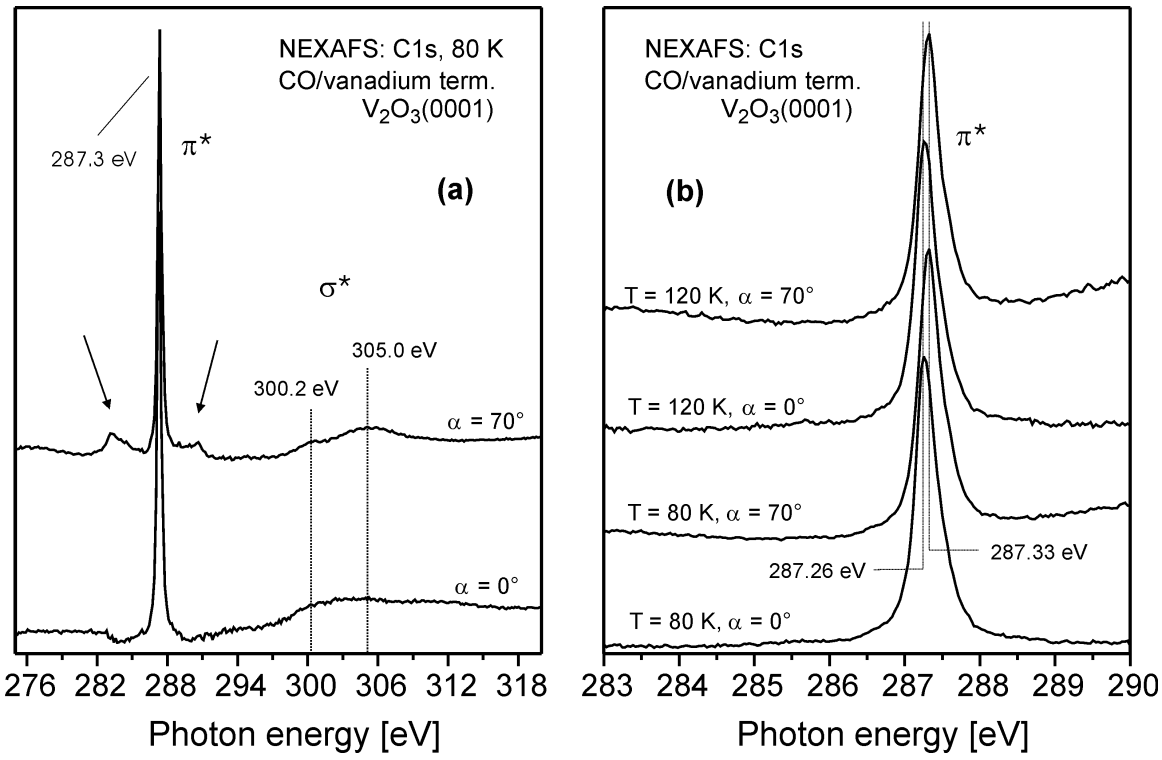

Figure 5.3: NEXAFS spectra of the vanadium terminated $V_2O_3(0001)$ after dosing 15 L CO at 80K; wide range of scanned photon energies (left) and a short range to show more details (right). NEXAFS spectra were recorded in two different light incidence angles as indicated.

Referring to the literature of NEXAFS data, the sharp feature at 287.3 eV in Figure 5.3(a) is identified as the well-known π* resonance of CO while the two broad features at about 300.2 and 305 eV correspond to σ* resonances [76]. The observation of two σ* resonances is possibly due to the presence of two adsorbed CO species in different environments on the surface. Indeed, inspection of Figure 5.3(b) reveals that the π* resonance shifts by ~70 meV when the light incidence angle is varied between 0° and 70°. This may suggest the presence of at least two different CO species on the surface. Indeed, there should be more than one CO adsorption state according to the IRAS data (section 5.2.3). Another possible explanation for the 70 meV shift is that the degeneracy of the 2π levels is lifted due to the tilting of the molecules. This means that the two peaks in the π* resonance regime may belong to different 2π final states of the same CO molecules. Although the 70 meV shift was reproducible, it cannot be fully excluded that this shift is due to monochromator instabilities. It may also play a role that the sample had to be rotated in order to change light incidence angle which means that different areas of the sample surface were probably investigated in different spectra.

Since the intensities of these resonances are governed by dipole selection rules, they can be used to get information concerning the adsorption geometry. According to the selection rules, the C1s → σ transition can only be excited with light polarized along the molecular axis. For CO molecules lying flat on the surface, this means that the sigma resonance should be strong for perpendicularly incident light whereas this resonance should be week for grazing light incidence. The π* resonance is only observed if the component of the electric field of the light perpendicular to the molecular axis is different from zero. If CO molecules are standing upright on the surface, the intensity of the π* resonance excitation should be the largest at normal incidence of the light whereas at grazing incidence the intensity should go towards zero. Obviously, the NEXAFS spectra reveal a significant π* resonance intensity also at α = 70° which means that the molecules must be somewhat tilted on the surface. A similar adsorption geometry of CO molecules was reported for CO on Cr_2O_3(0001) [168,169].

5.2.3 IRAS

Figure 5.4(a) compares the IRAS spectra taken after CO adsorption on vanadyl terminated (top spectrum) and on vanadium terminated $V_2O_3(0001)$ (bottom spectrum) at 90 K. No IR signal of CO is observed after CO adsorption on the vanadyl terminated surface. However, the XPS data for CO on the vanadyl terminated surface (Figure 5.1(a)) show a very small signal which may be attributed to CO adsorption on defect sites. These CO molecules may also exhibit a very weak IR intensity which is probably not observable with IRAS. On the other hand, the IRAS spectrum taken after CO adsorption on the vanadium terminated surface exhibit four peaks at about 2166 cm^{-1} (labeled P1), 2130 cm^{-1} (labeled P2), 2081 cm^{-1} (labeled P3) and 2038 cm^{-1} (labeled P4). This is fully consistent with observation of four C 1s features in the XPS data (see Figure 5.1(b). The observation of different peaks in the IR data is probably due to different interactions of CO molecules with neighboring CO molecules or with the surface. Different CO adsorption environments on the surface may also induce different IR peaks. These effects are already discussed in section 2.1.6.

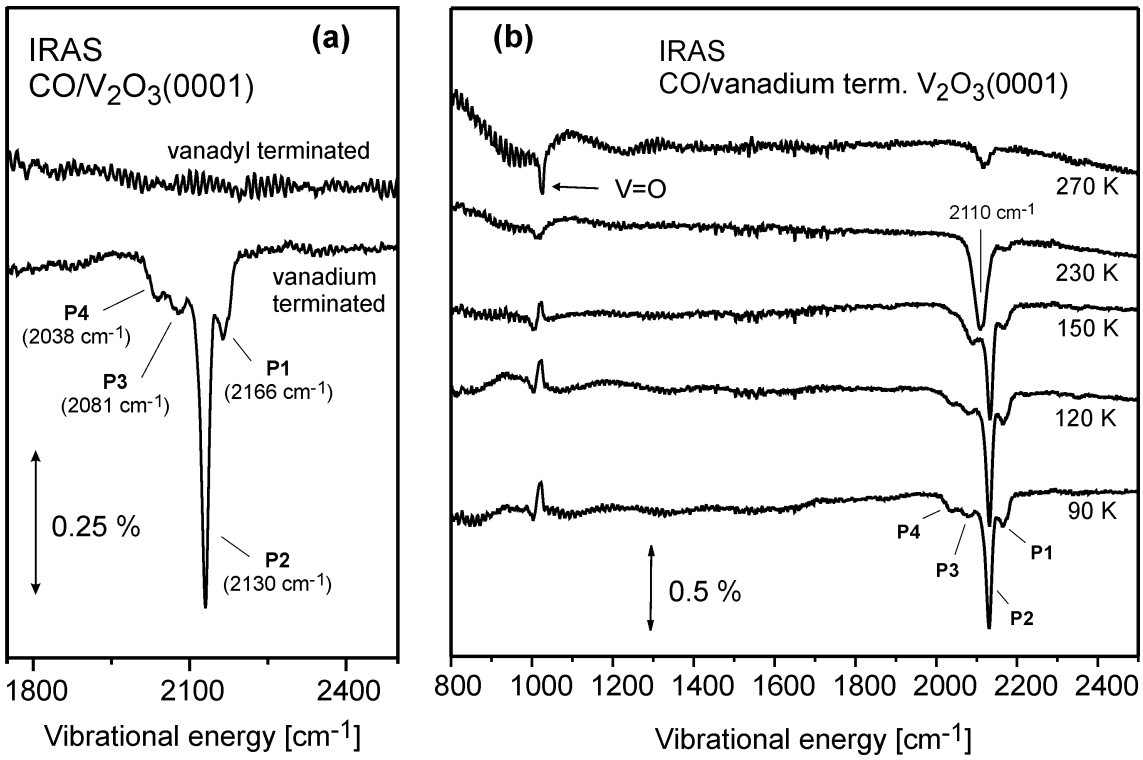

Figure 5.4: Left: IRAS spectra of CO adsorbed on vanadium terminated (bottom) and on vanadyl terminated $V_2O_3(0001)$/Au(111) (top). Right: IRAS spectra of CO adsorbed on vanadium terminated $V_2O_3(0001)$/Au(111) as a function of the annealing temperature. CO dosage (15 L) was performed at 90 K.

For CO on $Cr_2O_3(0001)$, two adsorption states were found (at 2170 and 2132 cm^{-1}) and were attributed to CO adsorption on regular surface sites. These states exhibit vibrational energies similar to the present IR features P1 (at 2166 cm^{-1}) and P2 (at 2130 cm^{-1}), respectively (see Figure 5.4). Thus, P1 and P2 may be attributed to CO species adsorbed on regular $V_2O_3(0001)$ surface sites. The other two IR features, P3 and P4, are probably attributed to CO species on non-regular $V_2O_3(0001)$ surface sites such as steps, points, lines and white areas in Figure 5.2(b). Unfortunately, the XPS and IRAS annealing experiments (Figures 5.1(b) and 5.4(b), respectively) provide no correlation between the features observed in both cases.

Figure 5.4(b) reveals that the peak P1 is blue-shifted with respect to the gas-phase value (2143 cm^{-1}) as frequently observed for CO on transition metal oxides [169]. This shift is possibly due to the Pauli repulsion between the carbon lone pair electrons and the surface charge distribution [164]. The other three peaks P2-P4 are red-shifted with respect to the gas-phase value which may be attributed to electron back-donation from the vanadium ions to CO. Davydov reported that metal cations which contain fully or partially filled d-orbitals can interact with the π^* orbital of CO via electron back-donation from the metal to CO [148]. A similar argument was used to explain the observed IR bands for V^{3+}–CO compounds [170].

Adsorbed CO may desorb or react when the sample temperature is increased. Figure 5.4(b) demonstrates the influence of annealing on the IRAS spectra. The temperature dependence of the IR spectra confirms the findings derived from the XPS data which show that CO interacts strongly with the vanadium terminated surface. The spectrum at 90 K in Figure 5.4(b) is the same as the one presented in Figure 5.4(a) for CO on the vanadium terminated surface. In addition to the features P1-P4, CO induces a signal with uncommon shape in the low frequency range (~1020 cm^{-1}). This signal may result from the interaction of CO with remaining vanadyl groups [171]. The origin of this uncommon shape is that the IRAS spectra (Figure 5.4(b)) are measured with respect to the clean vanadium terminated surface. In other words, each IR spectrum in Figure 5.4(b) represents the IR spectrum the CO-covered surface divided by the IR spectrum of the clean vanadium terminated surface recorded right before the CO exposure. The interaction of CO with the remaining vanadyl groups shifts the V=O stretching vibration frequency. This will lead to the observed uncommon shape in the IRAS spectra as a result of the above mentioned procedure. A similar CO-induced peak at a similar

vibrational energy was recently observed in IRAS spectra of CO on ferryl terminated Fe_2O_3(0001) [172]. After annealing the CO-covered surface at 150 K, the intensity of P4 is strongly attenuated due to CO desorption or dissociation (Figure 5.4(b)). A new peak at 2110 cm^{-1} develops after annealing to 230 K, suggesting the presence of a new state of adsorbed CO. The appearance of this new state may result from decreasing repulsive lateral interactions between adjacent CO molecules due to decreasing CO coverage or from occupation of new adsorption sites at 230 K. Furthermore, the IR spectrum at 230 K shows the appearance of a small structure at ~1020 cm^{-1} which becomes more obvious after annealing to 270 K. This peak can be attributed to the formation of vanadyl groups which may be considered as an indication for CO dissociation on the vanadium terminated surface. Similarly, CO was found to dissociate on reduced titania surfaces [166,167]. Finally, the fact that the peaks P1-P4 exhibit different thermal behaviors may also indicate that CO molecules are bonded to different sites on the vanadium terminated surface.

5.1 Summary

The results described above clearly demonstrate the influence of the V_2O_3(0001) surface termination on CO adsorption. CO interacts weakly with the vanadyl terminated surface and strongly with the vanadium terminated one, as indicated by IRAS and XPS. This means that CO is stabilized on the vanadium terminated surface after removing the O atoms of the V=O groups. The presented data provide an insight into the complex adsorption behavior of CO on the vanadium terminated surface. IRAS and XPS data suggest the presence of different CO species on different adsorption sites with different thermal stabilities. There are indications that a fraction of the adsorbed CO dissociates on the vanadium terminated surface. NEXAFS spectra reveal that at 90 K CO is adsorbed in a tilted geometry on the surface.

Chapter 6

Adsorption of Carbon Dioxide

This chapter describes the adsorption and reaction of CO_2 on vanadium terminated V_2O_3(0001). Utilizing TDS, UPS, XPS, IRAS, and NEXAFS, the adsorbed CO_2 species were identified and their molecular geometry was examined. The thermal stability and the reaction of different CO_2 species were also investigated.

6.1 Introduction

The interaction of CO_2 with metal and oxide surfaces is involved in a number of relevant catalytic processes [173]. So far, the interaction of CO_2 with metal surfaces has received more attention than the interaction of CO_2 with metal oxide surfaces. Generally, the chemisorption of CO_2 on oxide surfaces may lead to the formation of surface carbonate [174]. Moreover, the formation of $CO_2^{\delta-}$ species was also reported on many oxide surfaces such as Cr_2O_3(0001) [174] and RuO_2(110) [175]. The surface chemistry of CO_2 was extensively examined in reviews [176,177]

As pointed out by Freund and Roberts [176], the possible pathways for CO_2 reaction on transition-metal single-crystal surfaces involve the following key species: physisorbed CO_2, chemisorbed $CO_2^{\delta-}$, carbonate and oxalate compounds. Physisorption is found in almost all cases when the temperature approaches 80 K. The chemisorbed species is connected with the formation of the anionic $CO_2^{\delta-}$ molecule. The formation of $CO_2^{\delta-}$ upon CO_2 adsorption is a consequence of charge transfer from the substrate to the CO_2 molecule. As a result of such charge transfer, the linear CO_2 molecules change their molecular geometry and transform into bent $CO_2^{\delta-}$ species. Accordingly, the molecular orbital diagram of linear CO_2 is different from that of bent $CO_2^{\delta-}$ species [176]. The $CO_2^{\delta-}$ anions may be stabilized via solvation by neutral CO_2 molecules [176].

6.2 Results and Discussion

6.2.1 TDS

Figure 6.2 shows thermal desorption spectra measured after adsorption of CO_2 on vanadium terminated $V_2O_3(0001)$ at 90 K. Two desorption regimes are observed by monitoring mass 44: a low-temperature regime between 90 and 200 K followed by a high-temperature regime between 270 and 450 K. The high-temperature desorption feature can be assigned to strongly bonded (chemisorbed) species while the low temperature features can be assigned to weakly bonded (physisorbed) CO_2 species. A similar desorption behavior was observed in the case of $CO_2/Cr_2O_3(0001)$ in which the origin of the CO_2 desorption feature at high temperature was a chemisorbed CO_2^- carboxylate species, while the low temperature features were due to linear physisorbed CO_2 in different environments on the surface [174].

In order to follow the interaction of CO_2 with the vanadium terminated surface in more details, the desorption of CO (mass 28) was also monitored (see Figure 6.2). A certain amount of CO is always formed by cracking of CO_2 in the mass spectrometer. Another possible source for CO is its formation on the $V_2O_3(0001)$ surface via a reaction of the adsorbed CO_2 species. The pressure of CO formed by cracking of CO_2 in the mass spectrometer is a constant fraction of the CO_2 pressure. This fraction can be determined by admitting pure CO_2 to the mass spectrometer and determining the CO and CO_2 signal heights. Intensity in excess of this fraction in the TDS spectrum must be due to CO formed via a reaction of the adsorbed CO_2 species on the $V_2O_3(0001)$ surface. The CO spectrum in Figure 6.2 (labeled corrected 28) represents the spectrum of mass 28 after subtracting the contribution of mass 28 due to cracking of CO_2 in the mass spectrometer. The corrected CO spectrum clearly shows the formation of CO on $V_2O_3(0001)$, which implies CO_2 dissociation on the vanadium terminated surface. This substraction procedure is not necessarily fully correct since the fraction of CO formed by cracking of CO_2 in the mass spectrometer depends on the vibrational state of the CO_2 molecules. This method may induce errors if CO_2 desorbs in an excited state. However, the formation of CO on the $V_2O_3(0001)$ surface via CO_2 dissociation is further suggested by IRAS measurements which are discussed in the following section.

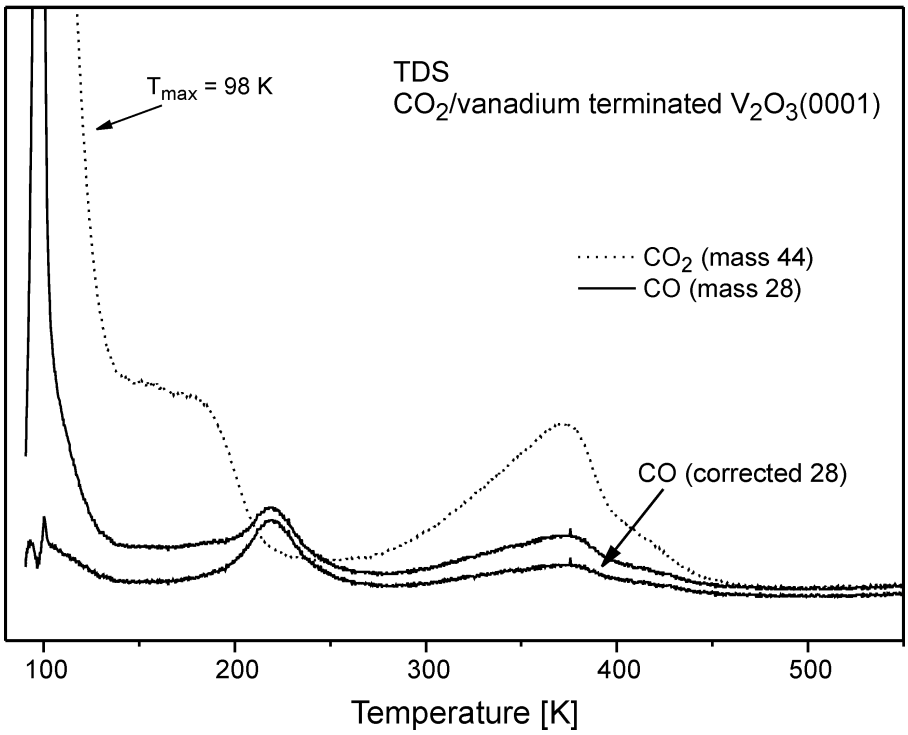

Figure 6.1: TDS spectra of CO_2 and CO after adsorption of CO_2 (saturation coverage) on vanadium terminated V_2O_3(0001)/Au(111) at 90 K. The heating rate was 0.5 Ks^{-1}. Partial pressures of masses 28 and 44 were recorded simultaneously. The lower spectrum represents the spectrum of mass 28 after subtracting the contribution of mass 28 due to CO_2 cracking in the mass spectrometer.

6.2.2 IRAS

IRAS measurements were performed to investigate the nature of the different adsorbed CO_2 species on vanadium terminated V_2O_3(0001) and to study the mechanism by which CO was formed. It is well known from the literature that chemisorbed and physisorbed CO_2 exhibit completely different vibrational properties [176]. The IR spectra are displayed in Figure 6.2. At low temperatures, three absorption regimes are observed at about 2370, 1300 and 1000 cm^{-1}. The first regime (at ~2370 cm^{-1}) is dominated by the signal of the asymmetric stretching vibration of linear physisorbed CO_2 [174,178]. This signal is possibly associated with CO_2 species desorbing in the low-temperature regime of Figure 6.1. A similar IR signal was found at ~2375 cm^{-1} for physisorbed CO_2 on Cr_2O_3(0001) [174]. Upon annealing, two peaks can be resolved at 2361 and 2378 cm^{-1}. The peak at 2361 cm^{-1} is detected at temperatures ≥ 350 K. At such temperatures, linear physisorbed CO_2 is not expected to be present on the surface as observed for CO_2/Cr_2O_3(0001) [174] and for CO_2/RuO_2(110) [175]. Since the spectra were recorded at 90 K, the peak at 2361 cm^{-1} at high temperatures may be induced by CO_2 readsorption.

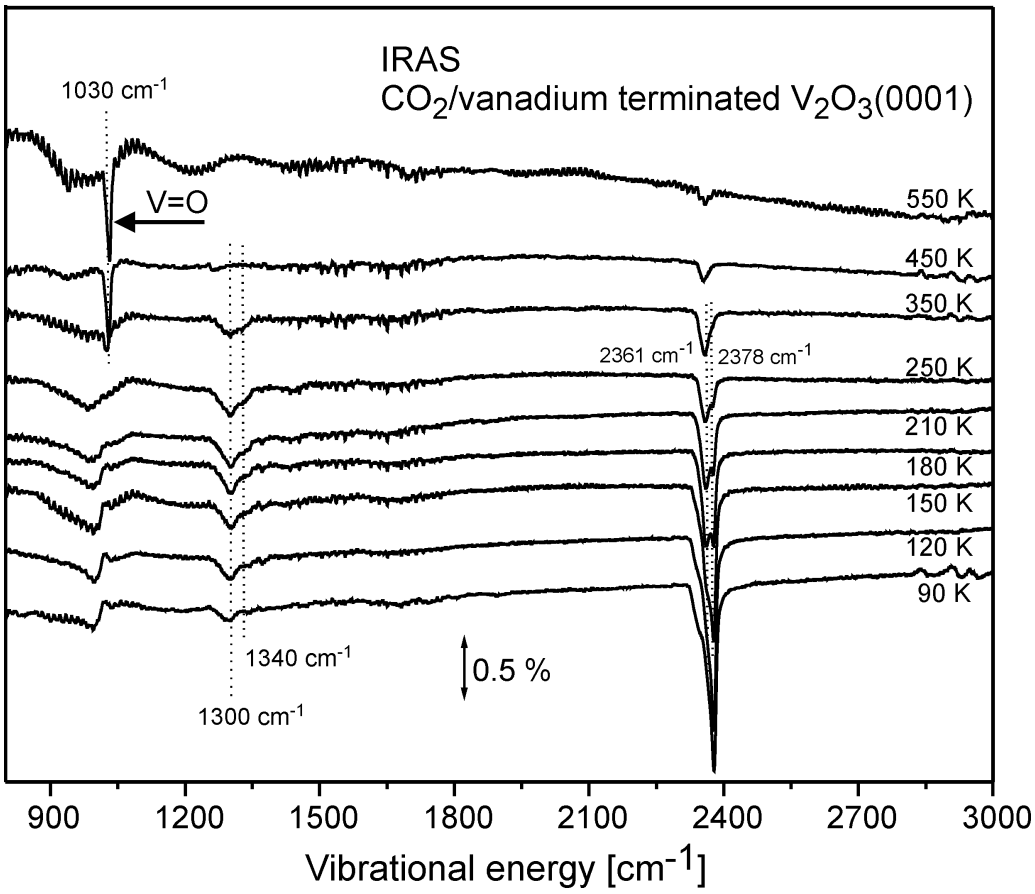

Figure 6.2: IRAS spectra of CO_2 adsorbed on the vanadium terminated V_2O_3(0001)/Au(111) surface as a function of the annealing temperature after dosing 20 L at 90 K.

In the second regime, a vibrational band at 1300 cm^{-1} is observed at 90 K. This band can be attributed to bent, negatively charged CO_2 species ($CO_2^{\delta-}$) [174]. An additional feature develops at 1340 cm^{-1} after annealing. This feature is possibly due to a $CO_2^{\delta-}$ species in a different environment on the surface. The $CO_2^{\delta-}$ induced features are detected up to at least 350 K and disappear at higher temperatures. Similar vibrational features were found at 1301 and 1342 cm^{-1} in the case of CO_2 on Cr_2O_3(0001) in which these features were also assigned to $CO_2^{\delta-}$ species in different environments [174]. Adsorbed $CO_2^{\delta-}$ species were also reported on other systems which are listed in Table 6.1. The band at 1300 cm^{-1} represents the symmetric OCO stretching vibration of $CO_2^{\delta-}$ [174]. No peak corresponding to the antisymmetric stretching vibration is observed at about 1600 cm^{-1}. The absence of any feature in this range suggests that the CO_2 species is adsorbed in C_{2v} symmetry with the O–O axis being parallel to the surface. The bending vibration is expected at ~800 cm^{-1}, which is not accessible by the employed IRAS set-up.

Table 6.1: Comparison of vibrational energies (in cm^{-1}) of chemisorbed $CO_2^{\delta-}$ observed here with those of other systems.

System	δ(OCO)	ν_s(OCO)	ν_{as}(OCO)	Reference
This work		1300/1340		
Cr_2O_3(0001)/Cr(111)		1301/1342		[174]
Na/Cr_2O_3(0001)/Cr(111)				[178]
RuO_2(110)	867	1225	1693	[175]
Ni(110)	750	1130/1390	1620	[179]
Re(0001)	650	1230	1625	[180]
Fe(111)	800	1064	1360/1600	[181]
Fe(100)		1232	1634	[182]
K/Rh(111)	840	1340	1630	[183]
Na/Pd(111)	744	1210	1530	[184]
K/Pt(111)	820	1340	1600	[185]
K/Ag	760	1260	1600	[186]

From the literature [176,187], it is known that $CO_2^{\delta-}$ may be stabilized via the formation of a $CO_2 \bullet CO_2^{\delta-}$ dimer which is formed via the solvation of a $CO_2^{\delta-}$ anion with a neutral CO_2:

$$CO_2^{\delta-} + CO_2 \rightarrow CO_2 \bullet CO_2^{\delta-}$$

Freund et al. [176] suggested that this species is a precursor for further surface reactions. Experimentally, however, little is known about the structure of $CO_2 \bullet CO_2^{\delta-}$ dimers. According to calculations [188], a stable T-shaped structure was suggested in which a linear CO_2 molecule is bonded via its carbon atom to an oxygen atom of a chemisorbed $CO_2^{\delta-}$ species as shown in Figure 6.3.

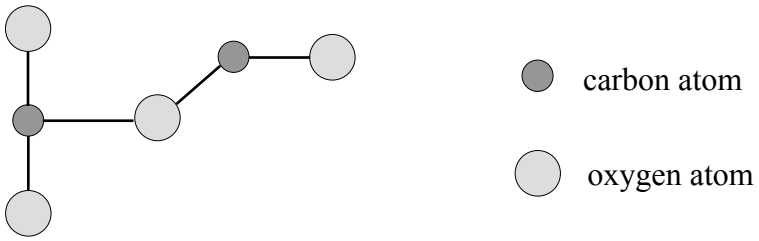

Figure 6.3: Schematic representation of the T-shaped structure of a $CO_2 \bullet CO_2^-$ dimer anion.

The desorption of CO_2 in the temperature range between 270 and 450 K is accompanied by CO desorption (Figure 6.1). A possible route for CO_2 desorption is the dissociation of the $CO_2 \bullet CO_2^{\delta-}$ dimer into CO_2 and $CO_2^{\delta-}$ species as follows:

$$CO_2 \bullet CO_2^{\delta-} \rightarrow CO_2 + CO_2^{\delta-}$$

where CO_2 desorbs to the gas phase and, simultaneously, the stability of the $CO_2^{\delta-}$ may get smaller as a result of CO_2 desorption. Consequently, $CO_2^{\delta-}$ may further react or dissociate.

It is worth to note that Figure 6.2 does not show any signal of CO. This is possibly due to a direct release of the CO into the gas phase which means that the formed CO did not adsorb on the $V_2O_3(0001)$ surface. In the high-temperature regime of the TDS spectra (270-450 K), an intensity ratio of 1:1 should be observed between mass 44 and mass 28 if $CO_2^{\delta-}$ dissociates completely to CO and O. Figure 6.1 shows that the intensity of CO_2 is higher than that of CO by a factor of ~5. This is probably due to an error in the calculation of the real intensity of CO. As explained earlier, the way of calculating the real intensity of the CO spectrum may not be fully accurate since the cracking pattern of CO_2 depends on its ro-vibrational state. Furthermore, one cannot exclude that part of the $CO_2^{\delta-}$ transforms into CO_2 (i.e. no $CO_2^{\delta-}$ dissociation) and desorbs which may explain why more CO_2 than CO desorb in the high-temperature regime. Another possible explanation is that one $CO_2^{\delta-}$ molecule is solvated by more than one CO_2 molecule [176].

The third regime in Figure 6.2 is the one at about 1000 cm^{-1} and exhibit broad structures. The interpretation of these structures at temperatures $\leq$ 250 K may not be straightforward since this regime is suffering from the instability of the IR spectrometer. However, one may speculate that these structures are associated with $CO_2^{\delta-}$ species interacting with the surface vanadium atoms through their oxygen atoms. If carbonate species are formed on the surface, peaks in this energy regime are to be expected as discussed in the following paragraph. Nevertheless, the interaction of CO_2 with remaining vanadyl groups is observed at low temperatures similar to the case of CO on $V_2O_3(0001)$ (see Figure 5.3(b)). Upon annealing at temperatures higher than 250 K, a sharp signal is observed at 1030 cm^{-1} which can be assigned to the formation of vanadyl (V=O) groups. This observation can be considered as an indication for the dissociation of the adsorbed $CO_2^{\delta-}$ on the vanadium terminated surface according to the following equation:

$$CO_2^{\delta-} \longrightarrow CO + O^{\delta-}$$

where CO is released into the gas phase as shown by TDS (Figure 6.1) and O reacts with surface vanadium atoms to form vanadyl groups as indicated by IRAS (Figure 6.2). At 550 k, 24% of the $V_2O_3(0001)$ surface is covered with vanadyl groups as revealed by comparing the intensity of the vanadyl feature in the IRAS spectrum recorded at 550 K (Figure 6.2) with that of the fully vanadyl terminated surface (Figure 3.4). This

coverage of vanadyl groups may indicate that not all the $CO_2^{\delta-}$ species dissociate, or that not on every surface vanadium atom a $CO_2^{\delta-}$ group is situated. Similarly, annealing CO_2-covered $Cr_2O_3(0001)$ up to 400 K was found to result in the formation of chromyl groups as revealed by IRAS measurements [174].

In general, CO_3^{2-} species might form upon CO_2 adsorption on oxide surfaces via CO_2 reaction with surface oxygen anions. On the basis of the presented IRAS spectra (Figure 6.2), the formation of CO_3^{2-} species on $V_2O_3(0001)$ cannot be entirely excluded. A general diagram of characteristic surface CO_3^{2-} vibrational frequencies is depicted in Figure 6.4 [174]. The diagram is divided into three regimes: a high-vibrational energy range (I), a medium-vibrational energy range (II) and a low-vibrational energy range (III). In typical IR spectra of carbonates on oxide surfaces, a signal in regime I should be expected [148]. Its intensity should exceed the signal of the counterpart in regime II [174]. The absence of any IR signals in regime I (Figure 6.4) may indicate that the dynamic dipole moment of CO_3^{2-} species is parallel to the surface. This may be expected for unidentate carbonate species laying flat on the surface. For bidentate carbonates standing upright on the surface, a signal is expected in regime I due to the high dynamic dipole moment perpendicular to the surface [174]. Therefore, the absence of any IR signals in regime I may indicate that bidentate carbonate species do not form on the surface.

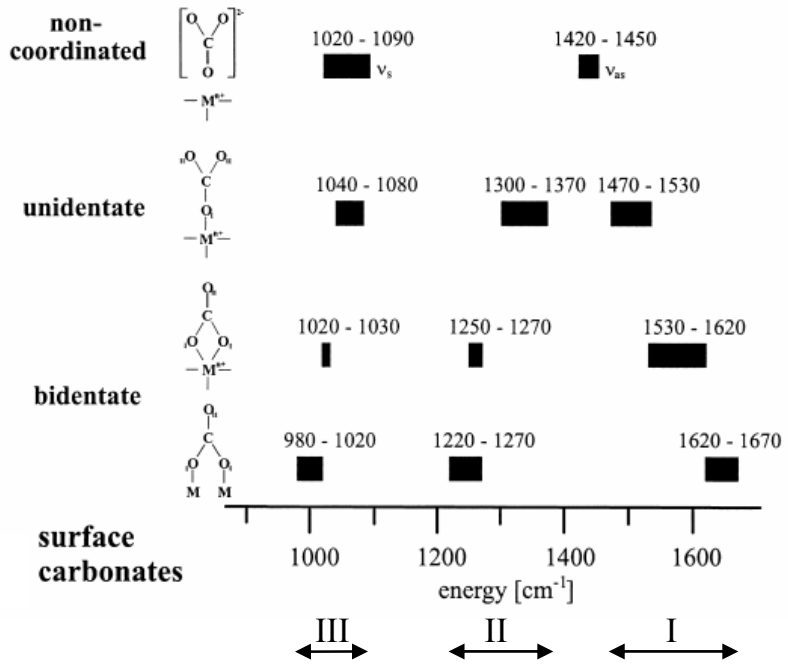

Figure 6.4: Correlation diagram of characteristic CO_3 vibration frequencies of surface carbonates [174].

Regarding regime III which suffers from the instability of the IR spectrometer, previously reported IR studies of cobalt (III) carbonate complexes [189-191] show much smaller intensities in regime III than in regimes I and II. Figure 6.2 reveals that the IR bands at ~1300 cm^{-1} exhibit relatively weak intensity (~0.2% in reflectance). Therefore, observing distinctive bands for carbonate species in regime III is expected to be troublesome [174]. Nevertheless, there is some intensity near to the vanadyl peak which goes away at a rather similar temperature as the structures around 1300 cm^{-1}. This may indicate that these IR bands are due to the same species.

As previously mentioned, carbonate species might form on an oxide surface via CO_2 reaction with a surface oxygen atom. Other routes for the formation of carbonate involve CO_2^- disproportionation [176,177] as the following:

$$2CO_2^- \rightarrow CO_3^{2-} + CO$$

or [178]:

$$CO_2 \bullet CO_2^- + e^- \rightarrow 2CO_2^- \rightarrow CO_3^{2-} + CO$$

6.2.3 UPS and XPS

Figure 6.5 compares valence band spectra of clean and CO_2-exposed vanadyl terminated $V_2O_3(0001)$ (left) with spectra of clean and CO_2-exposed vanadium terminated $V_2O_3(0001)$ (right). These spectra clearly show that more CO_2 molecules adsorb on the vanadium terminated surface than on the vanadyl terminated one. After CO_2 adsorption on the vanadium terminated surface at 80 K, three features appear at about 7.3, 11.6 and 13.0 eV which are characteristic for physisorbed CO_2 and can be assigned to the $1\pi_g$, $1\pi_u+3\sigma_u$ and $4\sigma_g$ levels, respectively [179,182,192].

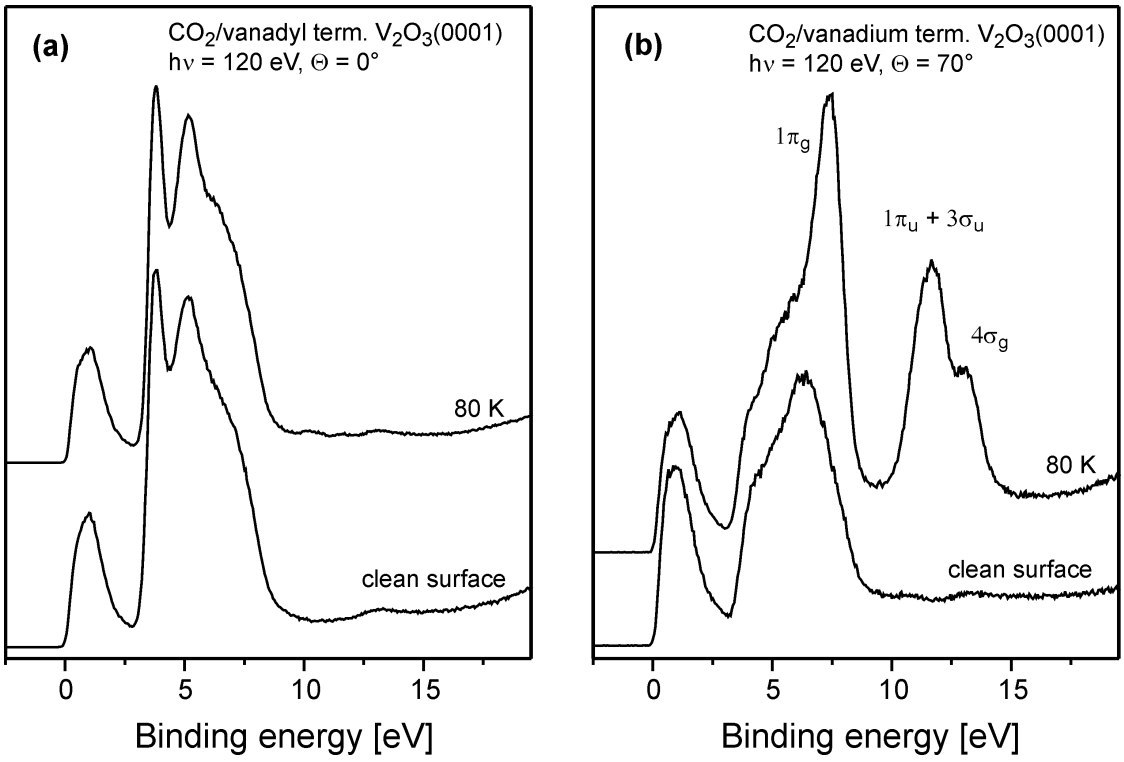

Figure 6.5: Valence band spectra of clean and CO_2-dosed vanadyl terminated V_2O_3(0001)/W(110) (left) and of clean and CO_2-dosed vanadium terminated V_2O_3(0001)/W(110) (right). CO_2 dosage (15 L) was performed at 80K.

More information about the interaction of CO_2 with the vanadium terminated surface is provided by a heating experiment in which the vanadium terminated surface was exposed to CO_2 at 80 K and subsequently annealed to the temperatures indicated in Figure 6.6(a). The difference spectra obtained with respect to the clean vanadium terminated surface are shown in Figure 6.6(b). Peaks at about 3.6, 5.2, 7.3, 11.6 and 13.0 eV can be distinguished at 80 K. As mentioned earlier, the peaks at about 7.3, 11.6 and 13.0 eV are attributed to the physisorbed CO_2. The other two peaks at 3.6 and 5.2 eV are partly due to the chemisorbed $CO_2^{\delta-}$ species. In addition to these two peaks, $CO_2^{\delta-}$ species should exhibit additional two peaks at higher binding energies [179,182,192,193] which are obviously hidden by the physisorbed CO_2-induced peaks at 80 K. The negative feature at about 0.6 eV points towards charge transfer from the V_2O_3(0001) surface to the adsorbed $CO_2^{\delta-}$ species.

Upon annealing to 120 K, the peaks induced by physisorbed CO_2 decrease in intensity and shift slightly to higher binding energies. Further annealing to 150 K desorbs more physisorbed CO_2. At 175 K, the peaks induced by physisorbed CO_2 are more or less gone. Based on the IRAS (Figure 6.2), XPS (Figure 6.7) and NEXAFS

(Figure 6.9) data, the remaining features may be attributed to chemisorbed species. Comparing the spectrum of $CO_2/V_2O_3(0001)$ at 175 K with that of $CO_2/Cr_2O_3(0001)$ at 170 K reveals that the spectral features in both cases are somewhat different. The authors [168] assigned the features in the $Cr_2O_3(0001)$ case to carbonate species. The spectra at 175 and 250 K (Figure 6.6(b)) are fairly similar except that the peak at 7.3 eV gains intensity at 250 K. CO_2 readsorption can be excluded after annealing to 250 K because the spectrum recorded at this temperature does not show any additional intensity at 11.6 and 13 eV which are associated with physisorbed CO_2. At 340 K, The spectrum exhibits peaks at 3.6, 5.2 and 10.1 eV which are probably associated with some surface species. The peak at 5.2 eV may also be attributed to the formation of vanadyl groups (see Figure 3.10), in agreement with the IRAS data (Figure 6.2).

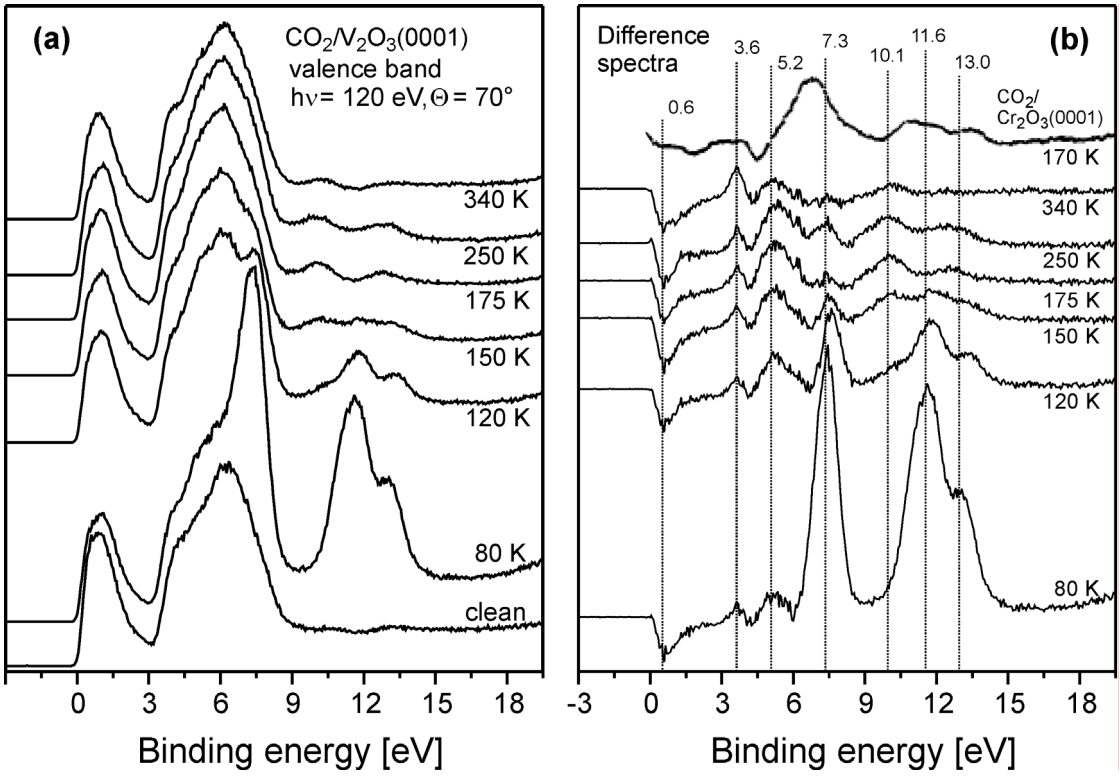

Figure 6.6: Left: Valence band spectra of CO_2 adsorbed on vanadium terminated $V_2O_3(0001)/W(110)$ as a function of the annealing temperature after dosing 15 L at 80 K. Right: difference spectra obtained from the valence band spectra shown in Panel (a) by subtraction of the spectrum of the vanadium terminated surface. At the top a spectrum of CO_2 on $Cr_2O_3(0001)$ after annealing at 170 K is shown [168].

The C 1s core level binding energies of adsorbed CO_2 provide another way for identifying the nature of the adsorbed CO_2 species on the $V_2O_3(0001)$ surface. The C1s core level spectra are displayed in Figure 6.7. The spectrum recorded at 80 K exhibits an intense peak at 291.6 eV which can be attributed to physisorbed CO_2. This peak

decreases in intensity upon annealing at 120 K and slightly shifts to 291.8 eV. Additionally, a new peak develops at 290.1 eV and it is detected up to 340 K. This peak can be attributed to $CO_2^{\delta-}$ species [177]. Figure 6.7 reveals that the peak induced by physisorbed CO_2 exhibits a higher binding energy than the peak induced by $CO_2^{\delta-}$, in good agreement with literature data [176,177].

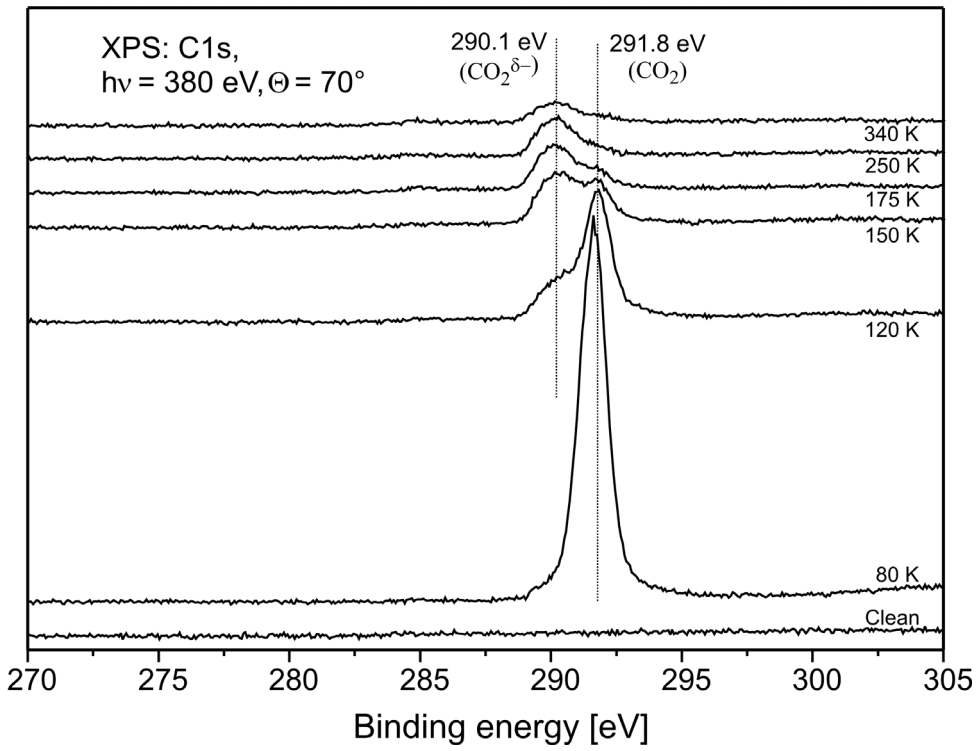

Figure 6.7: C1s core levels spectra of CO_2 adsorbed on vanadium terminated V_2O_3(0001)/W(110) as a function of the annealing temperature after dosing 15 L at 80 K.

6.2.4 NEXAFS

Figure 6.8 shows a C 1s NEXAFS spectrum of CO_2 on vanadium terminated V_2O_3(0001). After CO_2 adsorption at 85 K, features are observed at about 287.4, 290.9, 293.0, 300.6, 303.7 and 312.3 eV. The spectrum is fully consistent with the presence of adsorbed $CO_2^{\delta-}$ and CO_2 on the surface. The $CO_2^{\delta-}$ features appear at 287.4 eV (the π* resonance), and at 300.6 and 303.7 eV (σ* resonances). These peak positions are in good agreement with those reported for carboxylate (CO_2^-) species [76] and for $CO_2^{\delta-}$ species [194]. According to Stöhr et al. [76], the splitting of the σ* resonance features into two peaks (at 300.6 and 303.7 eV) is to be expected for carboxylates as a result of the interaction between the two adjacent C=O bonds.

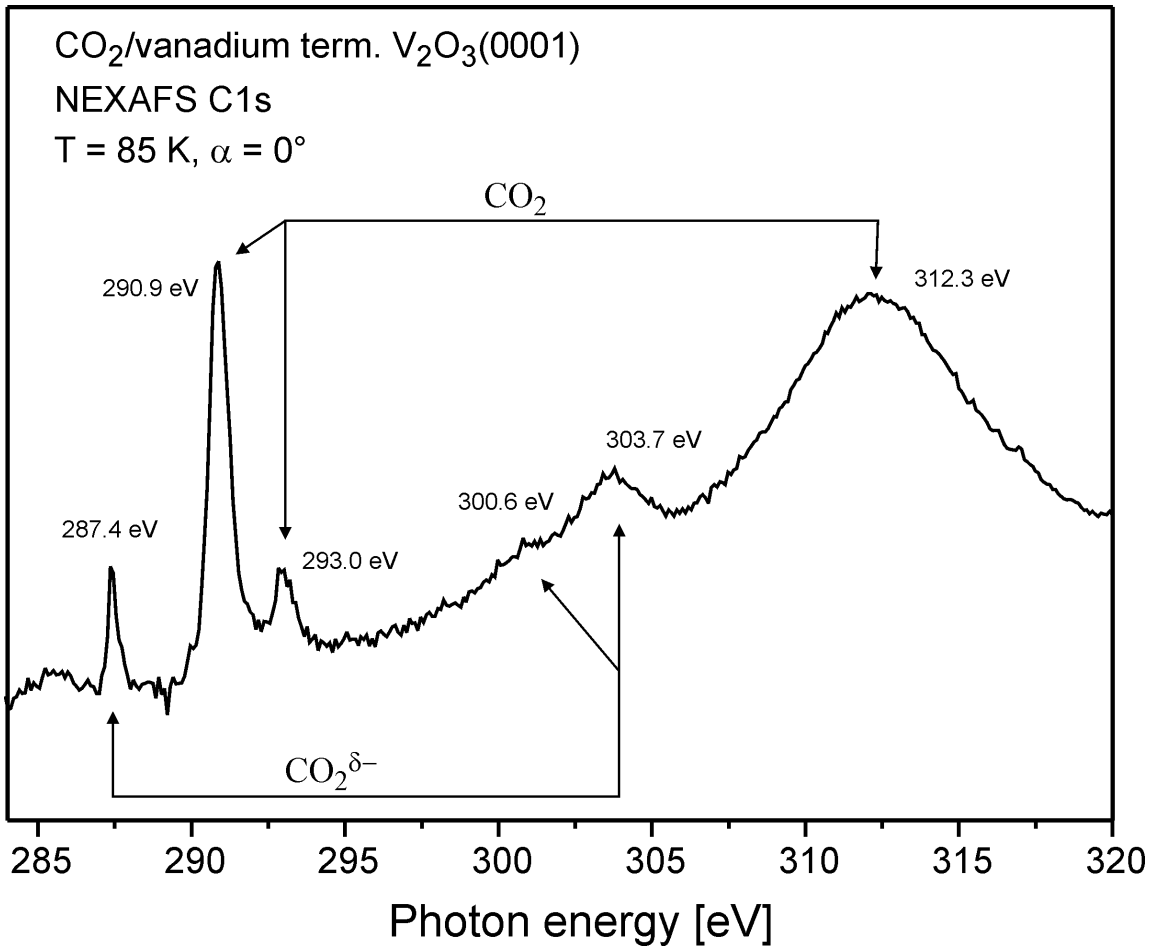

Figure 6.8: C1s NEXAFS spectrum of vanadium terminated V_2O_3(0001)/W(110) surface after dosing 15 L CO_2 at 85 K.

The features of the physisorbed CO_2 in Figure 6.8 appear at 290.9 and 312.3 eV and may be attributed to the π* and σ* resonances, respectively [168,194]. For CO_2 on Cr_2O_3(0001), two NEXAFS features at 286.9 and 290.2 eV were observed at 100 K [168]. The peak at 290.2 was attributed to physisorbed CO_2 while the peak at 286.9 was assigned to the π* resonance of $CO_2^{\delta-}$ adsorbed in C_{2v} symmetry [174], in agreement with the present NEXAFS data.

The interpretation of the peak at 293.0 eV (in Figure 6.8) is not that clear yet. It may be attributed to the presence of CO_2 species which are possibly involved in the formation of the CO_2•$CO_2^{\delta-}$ dimer. Another possible explanation is that the peak at 293.0 eV is due to a different 2π final state of the CO_2 molecules which induced the peak at 290.9 eV (i.e. these two peaks belong to the same CO_2 molecules). This is expected when the adsorbed CO_2 molecules are tilted which cause the degeneracy of the 2π levels to be lifted. According to the IRAS spectra (Figure 6.2) there should be a

number of different CO_2 adsorption states which may also lead to shifted 2π states. Whether the existence of the features at 290.9 and 293.0 eV is due to the splitting of the 2π state or due to the existence of different adsorbed species is not clear.

Figure 6.9(a) demonstrates the influence of annealing on the NEXAFS spectra. The spectrum at 85 K is the same as the one shown in Figure 6.8. After annealing at 174 K, the intensities of the peaks at 290.9 and 293.0 eV decrease while the intensity of the peak at 287.4 eV increases. It seems likely that the peaks at 290.9 and 293.0 eV belong to the same species since they exhibit a similar behavior upon annealing. The temperature dependence of the intensities of the peaks at 287.4 and 290.9 eV in the NEXAFS spectra (Figure 6.9(a)) corresponds quite well to the behavior of the peaks at 290.1 and 291.8 eV in the XPS data (Figure 6.7), respectively. This further indicates that the peaks at 290.9 and 293.0 eV in the NEXAFS data are due to π^* resonances of linear CO_2 whereas the peak at 287.4 is to be assigned to the π^* resonance of the bent $CO_2^{\delta-}$ species [194].

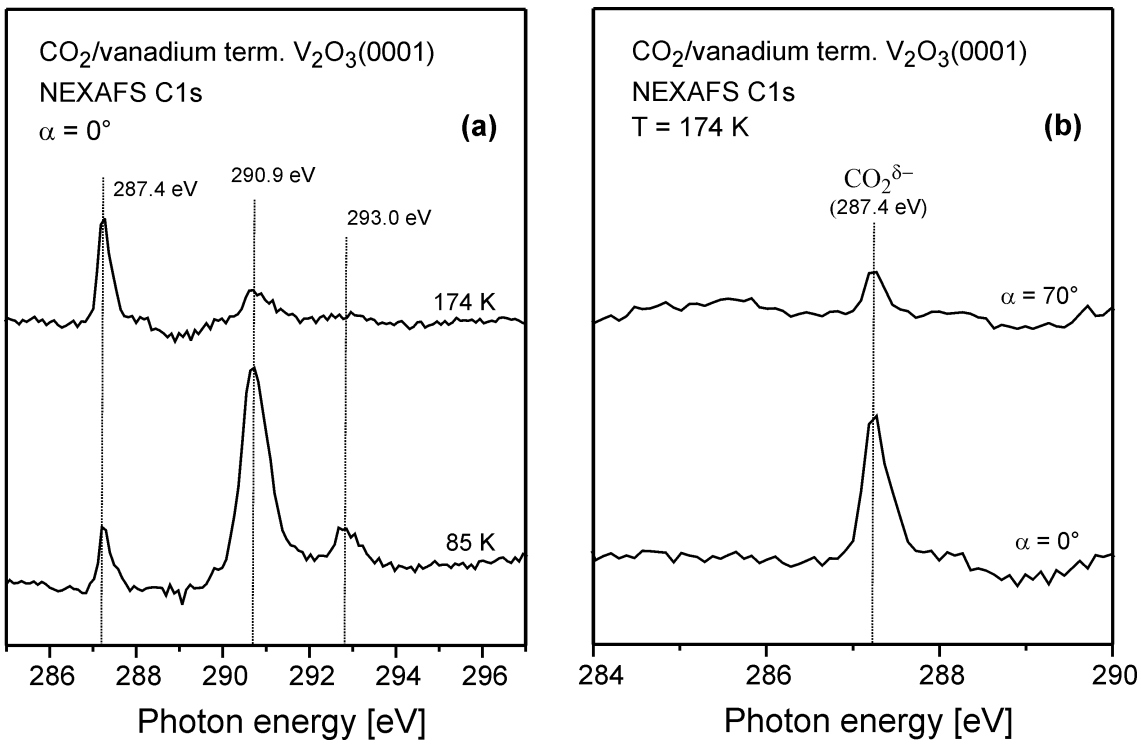

Figure 6.9: Left: C1s normal incidence NEXAFS spectra of vanadium terminated V_2O_3(0001)/W(110) after dosing 15 L CO_2 at 85 K (bottom) and after annealing to 160 K (top). Right: C1s NEXAFS spectra of CO_2 on vanadium terminated V_2O_3(0001)/W(110) recorded after annealing to 160 K as a function of the light incidence angle as indicated.

After annealing the CO_2-covered surface to 174 K, NEXAFS spectra were recorded at two different light incidence angles: $\alpha = 0°$ (normal incidence) and $\alpha = 70°$ (grazing incidence). The spectra are shown in Figure 6.9(b). The angular dependence of the π^* resonance at 287.4 eV can be used to obtain information on the orientation of the bent $CO_2^{\delta-}$ species on the $V_2O_3(0001)$ surface. In Figure 6.9(b), the intensity of the π^* resonance of the $CO_2^{\delta-}$ species is small when the incident radiation is at $\alpha = 0°$ whereas the intensity is higher at $\alpha = 70°$. The unoccupied π orbital in $CO_2^{\delta-}$ belongs to b_2 [194] which implies that the π^* resonance can be excited by the component of the electric vector perpendicular to the molecular plane. Consequently, the strong attenuation of the π^* resonance at grazing incidence indicates that the molecular plane of the $CO_2^{\delta-}$ species is perpendicular to the surface. This adsorption geometry of $CO_2^{\delta-}$ species agrees with the presented IRAS results (section 6.2.2) and NEXAFS results published in the literature [76,194].

6.2 Summary

The results and discussion presented above clearly demonstrate that CO_2 interacts strongly with the vanadium terminated $V_2O_3(0001)$ surface. The interaction of CO_2 with the $V_2O_3(0001)$ surface at 90 K leads to the formation of two different species: strongly bonded, bent $CO_2^{\delta-}$ species and weakly bonded, linear CO_2 species. For both species, the observed vibrations are essentially identical to those reported for adsorbed CO_2 species on $Cr_2O_3(0001)$. In addition to IRAS, the formation of $CO_2^{\delta-}$ species is confirmed by XPS and NEXAFS. This species adsorbs in C_{2v} symmetry with the O–O axis being parallel to the surface as revealed by IRAS and NEXAFS. This adsorption geometry is in agreement with that given for $CO_2^{\delta-}$ on $Cr_2O_3(0001)$. Solvation of $CO_2^{\delta-}$ with CO_2 leads to the formation of $CO_2 \bullet CO_2^{\delta-}$ dimers.

Upon annealing the CO_2-covered surface, CO_2 desorbs and $CO_2^{\delta-}$ decomposes according to the following equation:

$$CO_2^{\delta-} \longrightarrow CO_{(gas)} + O^{\delta-}_{(V=O)}$$

CO is released into the gas phase as shown by TDS whereas O reacts with the surface vanadium atoms to form V=O groups as indicated by IRAS.

In addition to the accessibility of the surface vanadium atoms, the electronic properties of the vanadium terminated $V_2O_3(0001)$ surface may be responsible for the formation of the $CO_2^{\delta-}$ species upon CO_2 adsorption. It seems that this surface provides electrons to the adsorbed CO_2 to initiate chemisorption leading to the formation of bent $CO_2^{\delta-}$ species.

Chapter 7

Adsorption of Water

This chapter describes the adsorption and growth of H_2O layers on $V_2O_3(0001)$ surfaces and explains the influence of the different surface terminations on the interaction with H_2O. The extent of H_2O dissociation on $V_2O_3(0001)$ surfaces was investigated using TDS, UPS, XPS, IRAS and HREELS.

7.1 Introduction

The adsorption of water on metal oxide surfaces is an important topic for surface scientists. This adsorption system is of fundamental importance for understanding many technologically important processes such as corrosion, geochemistry, atmospheric chemistry, electrochemistry and many heterogeneous catalytic reactions. The existing wealth of literature concerning H_2O adsorption on solid surfaces is summarized in the reviews given by Thiel and Madey [195] and Henderson [196].

The basic features of the interaction of H_2O molecules with oxide surfaces are summarized in the following lines. Generally, H_2O adsorbs on oxide surfaces in three possible scenarios, or combinations of them: (i) physisorption of molecular H_2O; (ii) chemisorption of molecular H_2O; and, (iii) chemisorption of molecular H_2O followed by dissociation. Physisorption represents weak interaction while chemisorption is much stronger and may lead to dissociation to H and OH species. The extent of dissociation may depend on the electronic properties, the surface structure and the surface temperature of the oxide. The conditions for dissociative or non-dissociative adsorption of H_2O were investigated on many oxide surfaces [11,195,196]. For example, the geometric arrangement of cations and anions as well as their ability to bind H_2O, OH and H are proposed to be the key factors in H_2O dissociation activity on an oxide surface.

7.2 Result and Discussion

7.2.1 UPS and XPS

Figure 7.1(a) and (b) presents a set of UPS and XPS spectra recorded after annealing multilayers of H_2O grown on vanadyl terminated $V_2O_3(0001)$ at 88 K. The typical levels of ice are obvious in the data at temperatures ≤ 165 K. Further annealing leads to desorption of the ice layer and the appearance of a feature at ~533.5 eV in the core level spectra, which is accompanied by corresponding features in the valence band spectra (marked by rectangles). These features are attributed to molecular H_2O [196] and they are detected up to ~288 K.

The same H_2O adsorption experiment was carried out for vanadium terminated $V_2O_3(0001)$. The photoelectron spectra are shown in Figure 7.1(c) and (d). After the removal of the ice layer (T ≥ 177 K), two O 1s features are observed at 531.3 and 533.2 eV in the core level spectra in Figure 7.1(d). The feature at 533.2 eV is due to molecular H_2O whereas the feature at 531.3 eV can be assigned to surface OH groups which are stable up to ~600 K. The molecular (H_2O) and hydroxyl (OH) features in the core level spectra are accompanied by corresponding features in the valence band spectra (marked by rectangles). According to the literature, hydroxyl species produce two features at about 11 eV (1π) and 7.5 eV (3σ) [197,198]. At the top of Figure 7.1(c) and (b), the spectra of the vanadium terminated surface before H_2O adsorption and after thermal removal of the OH groups are compared. Apart from subtle changes, the spectra are very similar which indicates that re-oxidation of the surface did not occur. This means that the water fragments are, more or less, completely removed from the surface after annealing at 597 K.

Figure 7.1(d) reveals that OH groups and molecular H_2O exist together on the vanadium terminated surface after ice desorption. This may indicate that mixed OH+H_2O overlayers were formed on the vanadium terminated surface as observed on Pt(111)+O [199,200] and $TiO_2(011)$ [201]. These layers are stabilized by OH-H_2O interactions. However, the IRAS data (section 7.2.2) show no change in the OH vibrational frequency after desorption of H_2O molecules. This would possibly indicate that OH-H_2O interactions are not significant on the $V_2O_3(0001)$ surface.

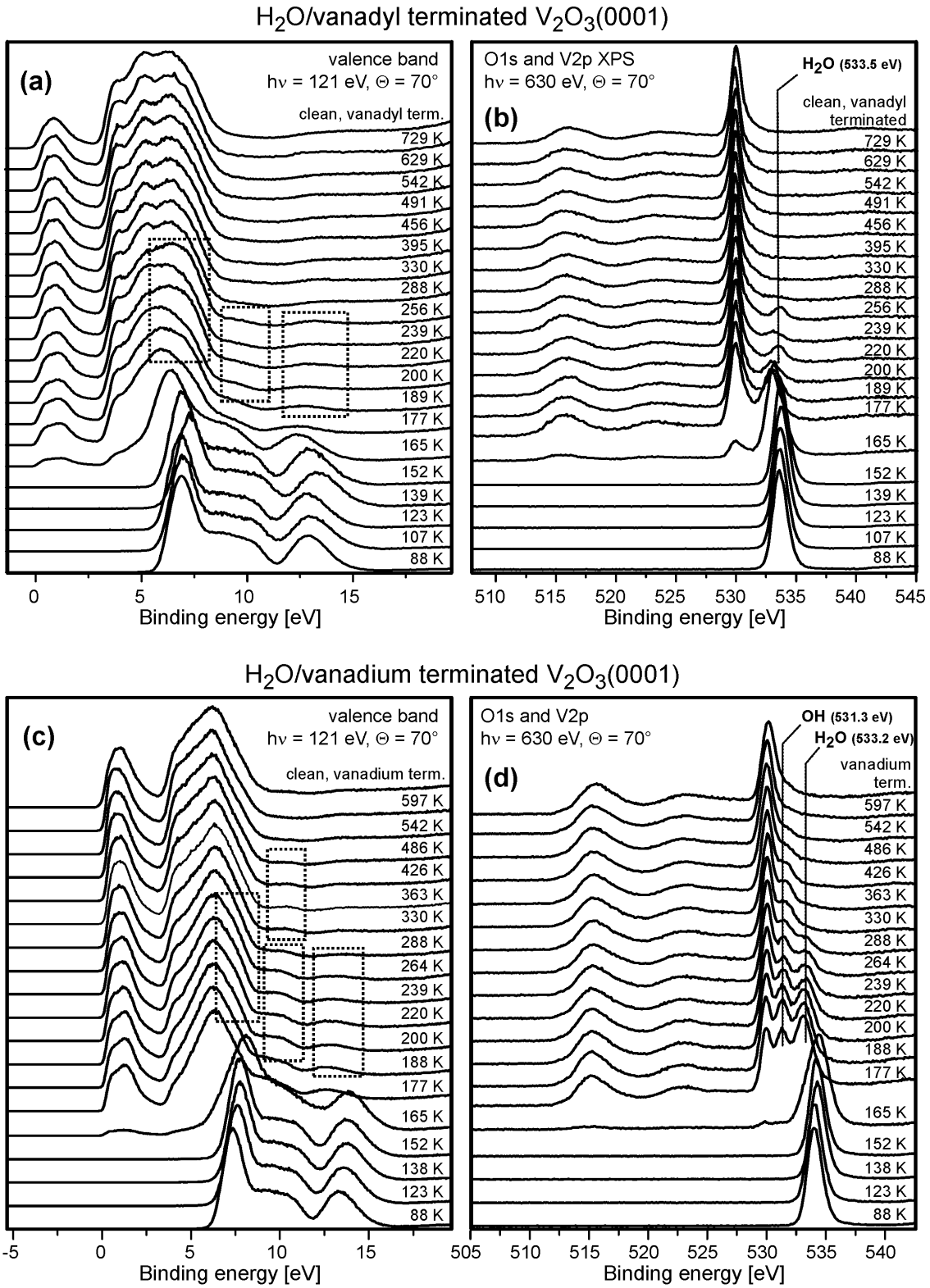

Figure 7.1: Valence band [(a) and (c)] and O1s+V2p core level [(b) and (d)] spectra of H_2O on vanadyl terminated V_2O_3(0001)/W(110) and vanadium terminated V_2O_3(0001)/Au(111) as a function of the annealing temperature. Multilayers of H_2O were adsorbed at 88 K. In each panel a spectrum of the respective clean surface is displayed at the top.

7.2.2 IRAS and HREELS

The findings of the photoelectron data concerning the state of adsorbed water, in terms of molecular or dissociative forms, can be confirmed using vibrational spectroscopy. Figure 7.2(a) shows the OH stretching regions of the infrared spectra taken from vanadyl terminated $V_2O_3(0001)$ after exposure to H_2O at 90 K. A broad band centered around 3400 cm^{-1} is observed at 90 K in addition to a small feature at 3694 cm^{-1}. The broad band is attributed to the OH stretching vibrations of hydrogen bonded OH in ice, whereas the small feature at 3694 cm^{-1} is assigned to the stretching vibration of dangling OH groups on the ice surface [202-204]. The intensity of the former peak increases with increasing the water coverage while the latter remains constant.

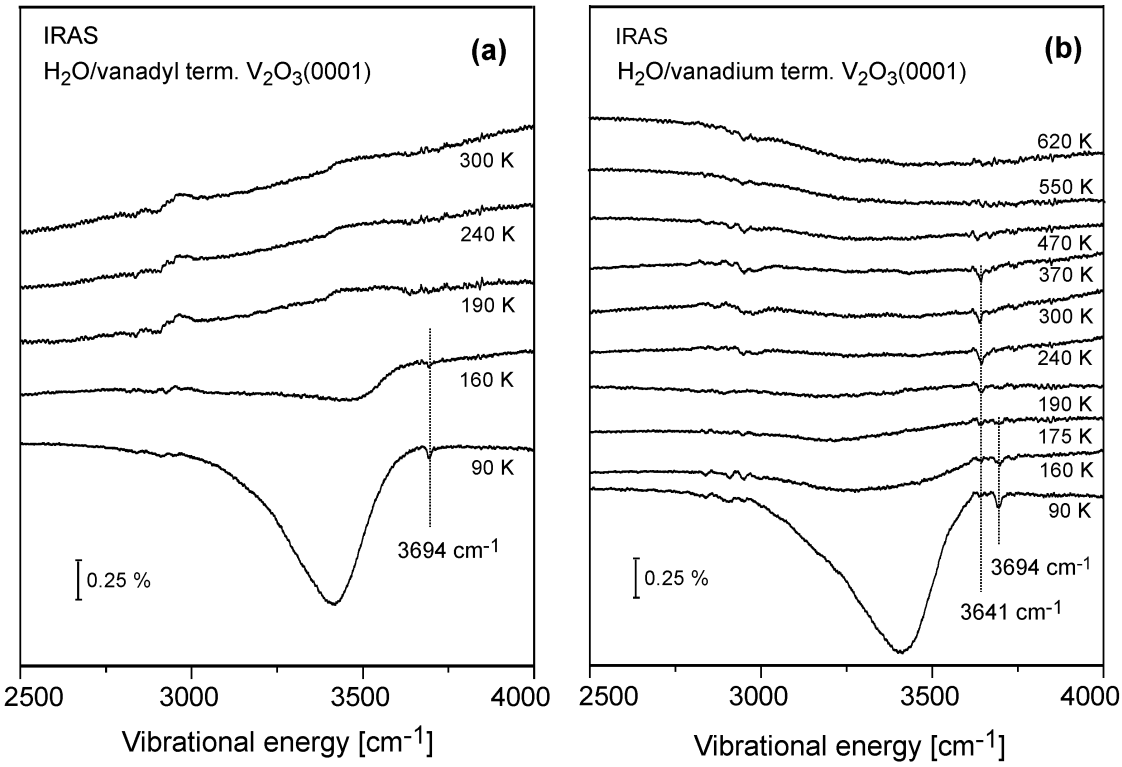

Figure 7.2: IRAS spectra of H_2O adsorbed on vanadyl terminated (left) and vanadium terminated $V_2O_3(0001)$/Au(111) (right) as a function of the annealing temperature after dosing 10 L at 90 K. Features at ~2900 cm^{-1} are artifacts of the infrared spectrometer.

Similar measurements were performed for the adsorption of H_2O on vanadium terminated $V_2O_3(0001)$. The spectra are displayed in Figure 7.2(b). Similar to the case of vanadyl terminated surface, two features are observed after H_2O on vanadium terminated $V_2O_3(0001)$ at 90 K. The broad feature is attributed to the OH stretching

vibrations of hydrogen bonded OH in ice while the small one is due to the vibration of dangling OH groups on the ice surface. Upon annealing, a vibration is observed at 3641 cm^{-1} which is detectable up to ~500 K. This feature is not observed in the spectra of H_2O on the vanadyl terminated surface (Figure 7.2(a)). Accordingly, it is assigned to the surface hydroxyl groups on the vanadium terminated surface. Busca et al. [205] reported a similar peak position (at 3645 cm^{-1}) for surface OH groups on V_2O_5 samples.

Two different OH groups are expected to form when H_2O decomposes to H and OH on an oxide surface. One group corresponds to the hydroxyl that results from the dissociation of H_2O and the other one originates from the adsorption of H. In the case of the existence of two chemically inequivalent hydroxyl groups, one would expect to observe two vibrational modes; one mode for each OH group. For example, Henderson and Chambers [206] reported that H_2O adsorption on $Cr_2O_3(0001)$ produced two different OH groups: a terminal OH group at 3600 cm^{-1} and a bridging OH group at 2885 cm^{-1}. The proton of the bridging OH group is hydrogen-bonded to the oxygen of the terminal OH group. In the present work, only one vibrational mode of the OH group on the vanadium terminated surface is observed at 3641 cm^{-1}. The same conclusion can be drawn from HREELS spectra which are taken from vanadium terminated $V_2O_3(0001)$ exposed to H_2O at 90 K and then annealed to 360 K (Figure 7.3). The spectrum at 360 K exhibits only a single peak at 3635 cm^{-1} due to surface OH groups, in agreement with the presented IRAS spectra. The observation of only one vibrational mode of the OH group may be caused by one of the following: (i) the vibrational energies of the two OH species are so similar that they cannot be resolved in the vibrational spectra, (ii) the two OH groups exhibit identical bonding to the substrate and, therefore, identical vibrational energies would be observed, or (iii) the dynamic dipole moment of one type of the OH groups is too weak to be observed by IRAS. Indeed, these explanations were previously suggested by a number of authors in order to explain the observation of only one vibrational mode of OH groups on other oxide surfaces. The observation of only one vibrational mode of hydroxyl groups was also reported after the dissociation of H_2O on oxide surfaces such as $Al_2O_3(0001)$ [207], $Fe_2O_3(012)$ [208], $TiO_2(110)$ [209] and MgO(100) [210].

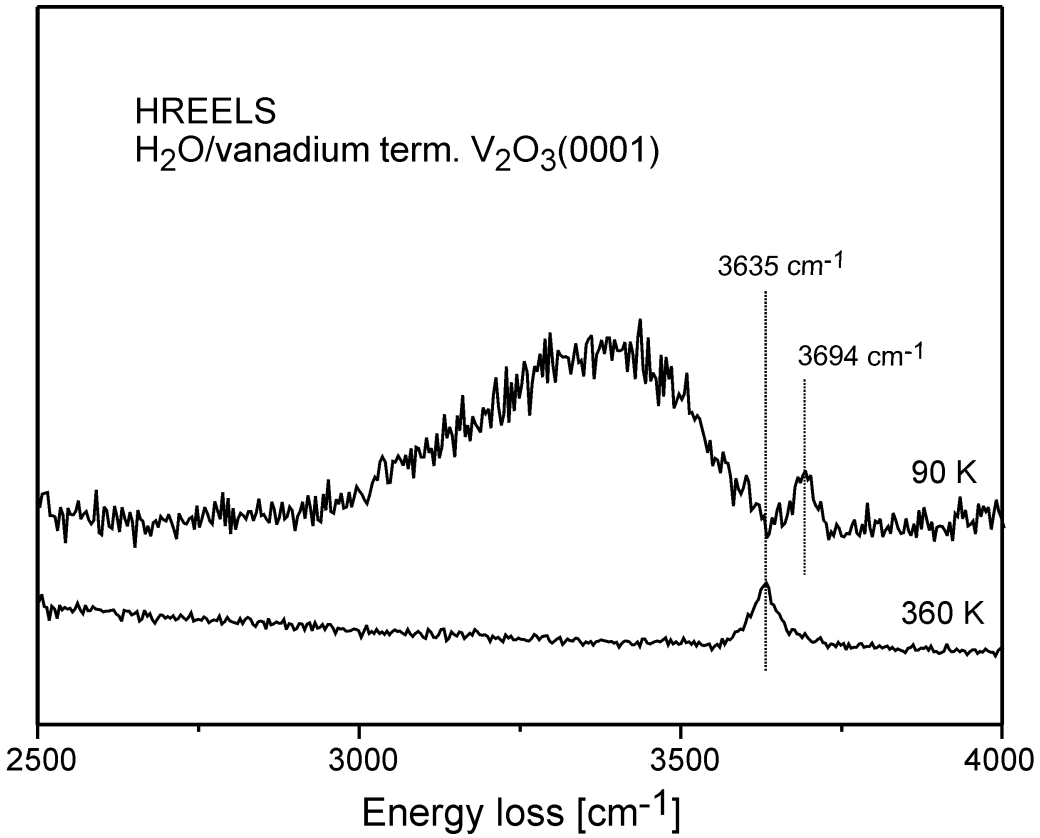

Figure 7.3: HREELS spectra of H_2O adsorbed on vanadium terminated $V_2O_3(0001)$ after dosing 10 L at 90 K (top) and after annealing to 360 K (bottom).

7.2.3 TDS

Additional insights into the processes occurring on $V_2O_3(0001)$ during water adsorption and desorption can be gained by TDS measurements. Figure 7.4(a) and (b) shows H_2O (mass 18) thermal desorption spectra from various exposures of H_2O at 90 K on vanadyl terminated and vanadium terminated $V_2O_3(0001)$, respectively. At low temperatures, the H_2O TDS peak positions and shapes for the vanadyl terminated and vanadium terminated surfaces are somewhat similar. There is a peak (labeled β) in the region of the multilayer desorption peak (labeled α). This peak may be attributed to desorption of the second water layer [196].

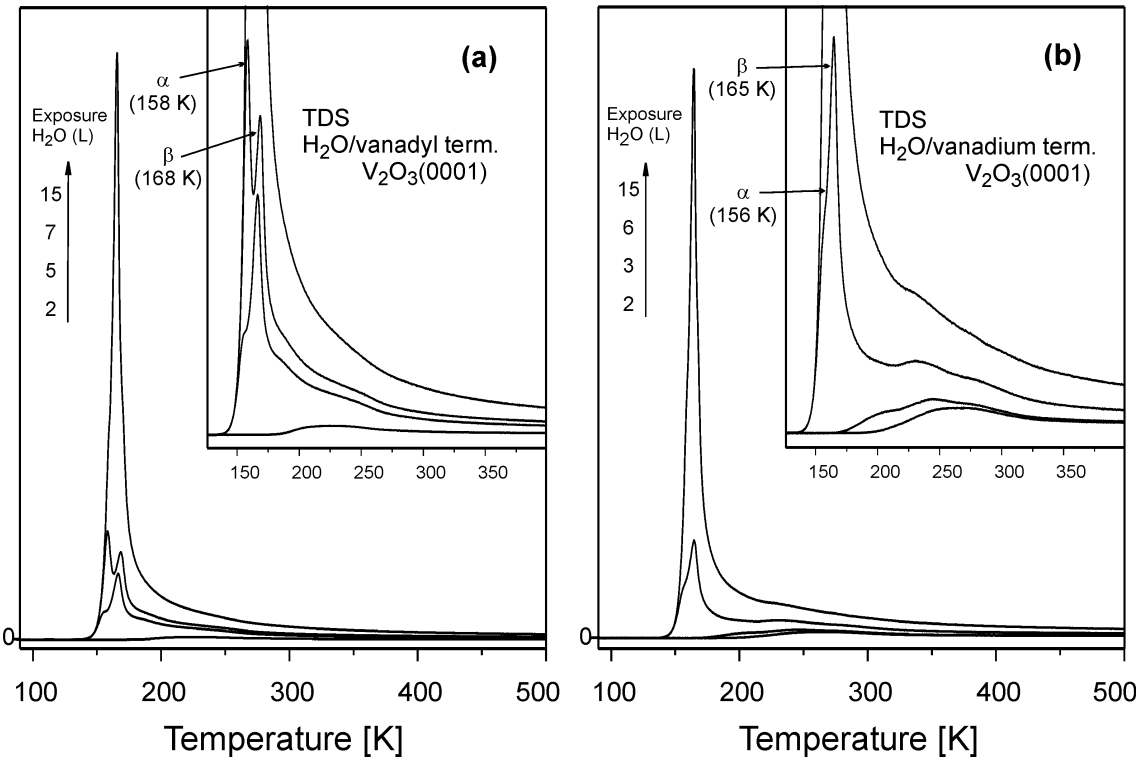

Figure 7.4: TDS spectra of H_2O (mass 18) adsorbed at 90 K on vanadyl terminated (left) and on vanadium terminated $V_2O_3(0001)/Au(111)$ as a function of the H_2O exposure. The heating rate was 0.7 Ks^{-1}.

Figure 7.5 displays the TDS spectra of 2 L of H_2O on the two differently terminated surfaces in more detail. Clearly, significant differences exist between the two TDS spectra. On one hand, the TDS spectrum of H_2O on the vanadyl terminated surface exhibits a desorption peak with a maximum at ~227 K which may be attributed to molecular submonolayer H_2O. This peak levels off towards higher temperatures and no additional structure appears. This is in agreement with the presented photoelectron spectra (Figure 7.1). On the other hand, Figure 7.5 shows that the desorption temperature of molecular water is clearly higher on the vanadium terminated surface (at ~268 K) than that on the vanadyl terminated one (at ~227 K). This points towards stronger H_2O bonding to the vanadium terminated surface than to the vanadyl terminated one. Moreover, additional broad desorption states are visible up to ~600 K suggesting the existence of more strongly adsorbed species. These states are most likely connected with the disappearance of the hydroxyl groups from surface upon annealing, as observed in Figure 7.1(b). Combining the information depicted in Figure 7.5 together with that derived from the XPS data clearly demonstrates that the hydroxyl groups recombine to form H_2O when the surface is warmed up. This scenario appears to be

consistent with what was observed for dissociative adsorption and recombinative desorption on other oxides surfaces:

$$H_2O_{(a)} \xrightarrow{dissociation} OH_{(a)} + H_{(a)} \xrightarrow{recombination} H_2O_{(g)}$$

The difference between the two terminations of $V_2O_3(0001)$ with respect to the interaction with H_2O might be linked to structural and electronic properties of both surfaces. These properties permit the dissociation of H_2O on the vanadium terminated surface only. The activity of H_2O dissociation on the vanadium terminated surface might be attributed to one or both of the following: (i) in the case of the vanadyl terminated surface, the access of H_2O molecules to the vanadium atoms is hindered since these vanadium atoms are capped by oxygen atoms, which is not the case for the vanadium terminated surface, and (ii) the oxidation state of the vanadium atoms on the vanadium terminated surface is smaller (see section 3.4) which means that the surface vanadium atoms have more 3d electron density to interact with H_2O molecules.

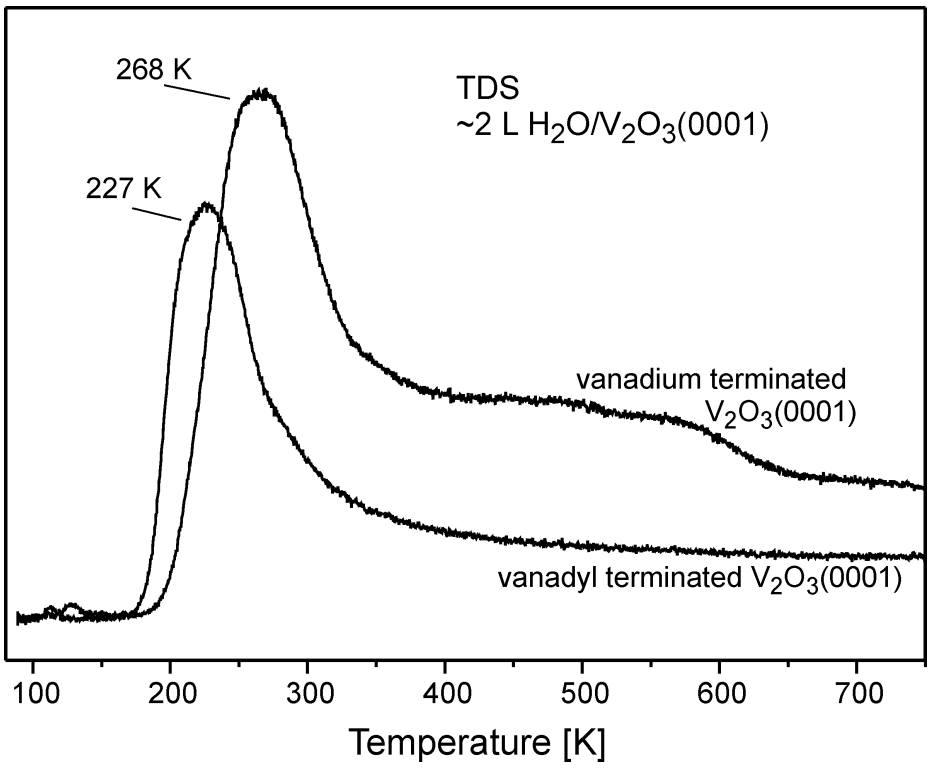

Figure 7.5: TDS spectra (mass 18) of 2 L H_2O on vanadium terminated and vanadyl terminated V23(0001/Au(111). The heating rate was 0.7 Ks^{-1}.

7.3 Crystalline water on $V_2O_3(0001)$

Ice can exist in a number of structurally different forms depending on pressure and temperature [211]. The deposition of H_2O vapor on a cold substrate (T<130 K) is known to lead to an amorphous ice phase, termed *amorphous solid water* (ASW), which is metastable with respect to crystalline ice [212]. Upon annealing, the ASW transforms irreversibly into crystalline ice. Figure 7.6 presents IRAS spectra recorded after annealing the ice layer on the vanadyl terminated $V_2O_3(0001)$ surface at different temperatures near to the multilayer desorption temperature. The sample was annealed with a heating rate of 0.7 Ks^{-1} and the spectra were recorded after cooling the sample to 90 K. The IR spectrum recorded at 90 K exhibits a broad band with a maximum at 3391 cm^{-1} and a shoulder in the low-energy side. This structure is characteristic for an amorphous ice film. Striking changes occur to the structure of the OH vibration band after annealing at 160 K. The OH vibration band exhibits a structure with a maximum at 3240 cm^{-1} and distinct shoulders at 3158 and 3348 cm^{-1}. Similar changes were previously observed by a number of authors and were attributed to a crystallization of the amorphous ice layer [203,204].

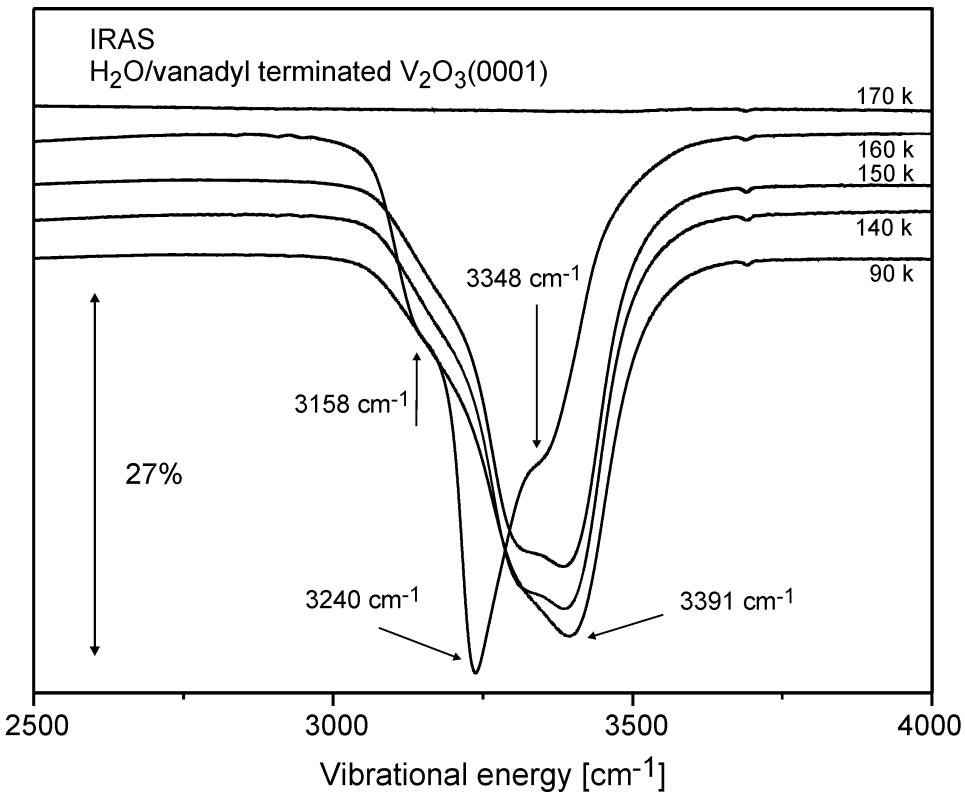

Figure 7.6: IRAS spectra of H_2O adsorbed on vanadyl terminated $V_2O_3(0001)$/Au(111) as a function of the annealing temperature. Multilayers of H_2O (200 L) were adsorbed at 88 K.

7.4 Summary

The results presented above clearly demonstrate the influence of the $V_2O_3(0001)$ surface termination on the H_2O adsorption path. At 90 K, H_2O adsorbs molecularly on the vanadyl terminated surface whereas it dissociates partially on the vanadium terminated surface forming OH groups, as demonstrated by XPS, UPS, IRAS and HREELS. The OH groups are removed completely from the vanadium terminated surface after annealing at ~600 K. TDS shows that annealing the OH-covered surface at temperatures higher than 300 K leads to the desorption of molecular H_2O as a result of the recombination of the OH groups. UPS data show no sign for surface oxidation after desoption of the OH groups.

The different reactivities of the vanadyl terminated and vanadium terminated $V_2O_3(0001)$ surfaces toward H_2O may be attributed to: (i) the surface vanadium atoms on the vanadium terminated surface are accessible for interaction with the H_2O molecules which might facilitate the dissociation of H_2O and the formation of V–OH bonds, whereas the capping of the surface vanadium atoms by oxygen atoms on the vanadyl terminated surface hinders the access to the vanadium atoms, and (ii) the vanadium atoms on the vanadium terminated surface are in a lower oxidation state compared to the vanadium atoms on the vanadyl terminated surface, which might facilitate the dissociation of H_2O on the vanadium terminated surface.

The amorphous ice transforms irreversibly to crystalline ice after annealing the amorphous ice layer near to the multilayer desorption temperature.

Chapter 8

Adsorption of Propane and Propene

This chapter deals with the adsorption of C_3H_8 on vanadium terminated V_2O_3(0001). TDS, UPS, XPS and NEXAFS were used to investigate the adsorption of C_3H_8 and to identify the adsorbed species. The adsorption of C_3H_6 was also examined.

8.1 Introduction

The oxidative dehydrogenation (ODH) of alkanes to alkenes offers an attractive route to convert the low cost saturated hydrocarbons into highly demanded chemicals. Particularly, the ODH of propane is a potential route to propene [213,214]. Extensive evaluations of catalyst compositions found that the most active and selective ones contain vanadium oxides as the active component [215-217]. However, the catalytic behavior of such catalysts can be influenced by a number of factors such as the presence of additives and the nature of both the support and the supported species. Consequently, the precise nature and concentration of the active sites remains most often a matter of speculation.

In propane ODH, propene is the primary product while carbon oxides (CO_x) form as byproducts via propane and propene combustion. Several studies addressed the primary and secondary reactions occurring during propane ODH but only few of them provided descriptions of the elementary steps involved. In analogy to other oxidation reactions, propane ODH is proposed to proceed via the Mars-van Krevelen mechanism, in which propane reacts with lattice oxygen in the catalyst [214]. The lattice oxygen is involved in the C–H bond activation step. Methylene C–H bonds in propane are weaker than those of the methyl groups. As a result, propane activation was proposed to occur by the initial cleavage of these weaker C–H bonds to form isopropoxide species [214]. Surface isopropoxide species were also proposed as surface reaction intermediates in the oxidative dehydrogenation reaction of propane to propene over supported vanadia catalysts [218-221].

8.2 Results and Discussion

8.2.1 TDS

Thermal desorption measurements were performed to obtain information about the adsorption and reaction of propane on the vanadium terminated $V_2O_3(0001)$ surface. Figure 8.1(a) shows a typical TDS spectrum of propane (mass 29) following the dosing of a saturation coverage of propane at 90 K on vanadium terminated $V_2O_3(0001)$ (solid line). The main peak in the TDS spectrum appears at about 120 K with a shoulder at about 105 K. No propane desorption was observed at temperatures higher than ~150 K. Figure 8.1(a) also presents a TDS spectrum measured to get information about the interaction of propane with O_2-predosed vanadium terminated $V_2O_3(0001)$ (dotted line). This was accomplished by predosing the vanadium terminated surface with 0.5 L of oxygen at 90 K followed by dosage propane. The question is, to what extent does the presence of oxygen influence the adsorption of propane? The effect of oxygen appears to be an increase of the intensity of the shoulder at ~105 K and a minor decrease of the intensity of the main peak.

TDS measurements were also conducted following propene adsorption on both, vanadium terminated and O_2-predosed vanadium terminated $V_2O_3(0001)$. Figure 8.1(b) shows TDS spectra recorded after propene adsorption at 90 K on clean vanadium terminated $V_2O_3(0001)$ (solid line) and on vanadium terminated $V_2O_3(0001)$ predosed with 0.5 L of oxygen (dotted line). Three features were observed by monitoring mass 41: intense and sharp features at 120 and 150 K followed by a very broad feature up to 300 K. The shoulder at ~105 K is more pronounced in the case of the O_2-predosed surface. Additionally, the overall desorption spectrum gains intensity in the case of the O_2-predosed surface. This increase in intensity is more pronounced in the temperature range between 90 and 140 K whereas the effect of oxygen at temperatures higher than 140 K is small. The desorption spectrum of the O_2-predosed surface is also slightly shifted to higher temperature compared to clean vanadium terminated surface.

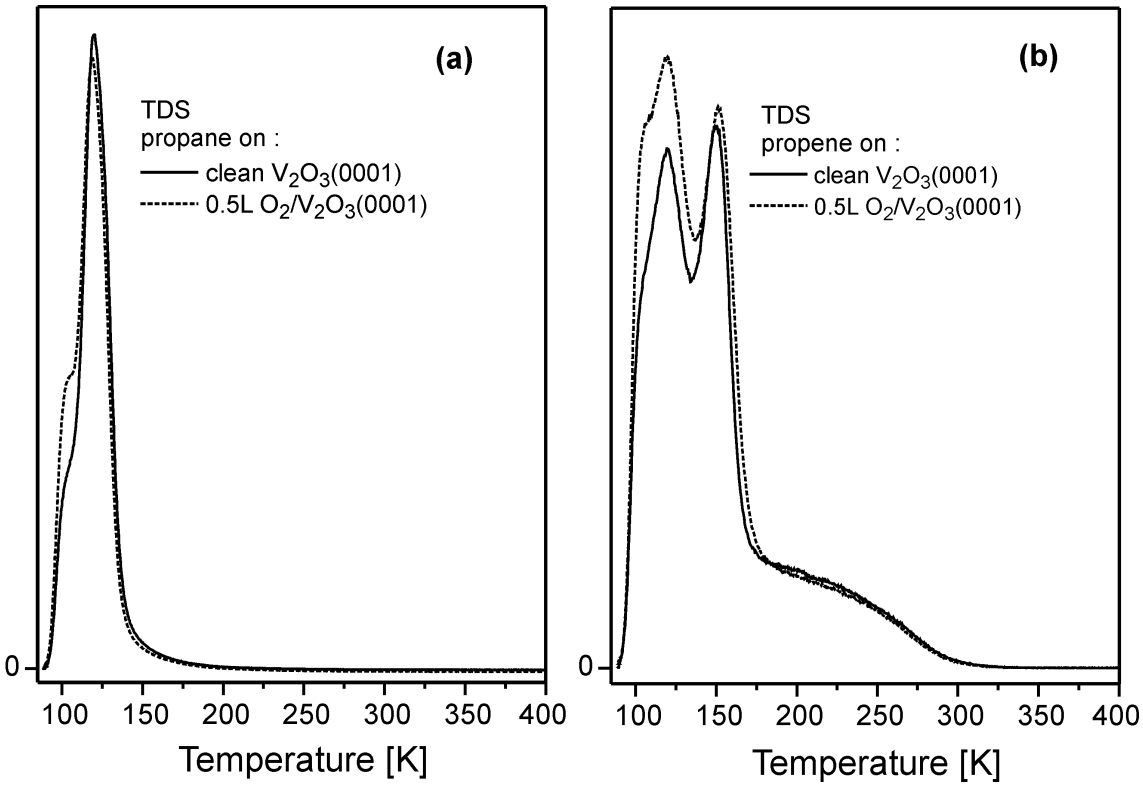

Figure 8.1: Left: TDS spectrum of C_3H_8 after adsorption of C_3H_8 on vanadium terminated V_2O_3(0001)/Au(111) (solid line) and vanadium terminated V_2O_3(0001)/Au(111) predosed with 0.5 L O_2 (dotted line). C_3H_8 dosage (30 L) was performed at 90K. The heating rate was 0.5 Ks^{-1}. Right: TDS spectrum of C_3H_6 after adsorption of C_3H_6 on vanadium terminated V_2O_3(0001)/Au(111) (solid line) and vanadium terminated V_2O_3(0001)/Au(111) predosed with 0.5 L O_2 (dotted line). C_3H_6 dosage (30 L) was performed at 90K. The heating rate was 0.5 Ks^{-1}

Figure 8.2 compares the desorption behavior of propane with that of propene on both the clean surface and the one predosed with oxygen. It is interesting to note that the desorption profiles of the low temperature shoulder at 105 K for both surfaces are the same. This may indicate that both molecules exhibit a similar interaction with the surface in this temperature range. Such an interaction is probably attributed to the interaction of the terminal methyl group with the same site on the surface since both molecules, propane ($CH_3CH_2CH_3$) and propene (CH_2=$CHCH_3$), have methyl groups in terminal positions.

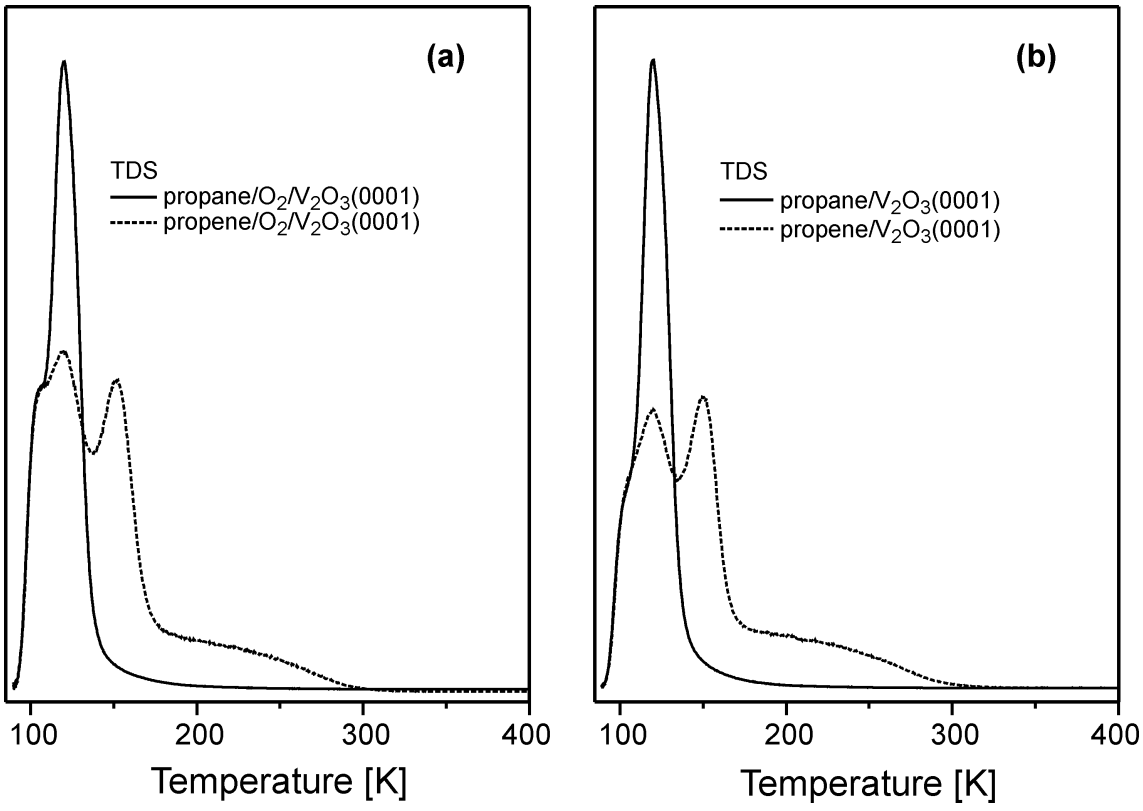

Figure 8.2: Left: TDS spectra of C_3H_8 (solid line) and C_3H_6 (dotted line) after adsorption of C_3H_8 and C_3H_6, respectively, on vanadium terminated $V_2O_3(0001)$/Au(111). Right: TDS spectra of C_3H_8 (solid line) and C_3H_6 (dotted line) after adsorption of C_3H_8 and C_3H_6, respectively, on vanadium terminated $V_2O_3(0001)$/Au(111) predosed with 0.5 L O_2. The spectra are the same as the ones shown in Figure 8.1.

8.2.2 XPS

Figure 8.3(a) shows a set of C 1s core level spectra obtained after propane adsorption on vanadium terminated $V_2O_3(0001)$ at 90 K followed by annealing at different temperatures. The spectra were plotted such that the details at small intensities are clearly visible. The spectrum recorded at 90 K exhibits an intense peak at 284.7 eV and a very small feature at 290.8 eV. This energetic difference of ~6 eV can be explained in terms of different chemical environments of the carbon atoms (chemical shift). The peak at the lower binding energy can be attributed to the adsorbed molecular propane. The intensity of this peak decreases significantly after annealing at 180 K. In contrast, the high energy C 1s feature gains intensity upon annealing and forms a broad feature in the binding energy range between 288.7 and 291.7 eV. On the basis of its binding energy, this feature can be attributed to a species containing a carbon-oxygen bond [78]. This species may be associated with an intermediate state for the formation

of propene or other compounds. One might at first think about the formation of alkoxide species or other oxidized hydrocarbons species, as illustrated in Figure 8.4.

Figure 8.3(b) shows a set of O 1s and V 2p core level spectra recorded after propane adsorption on vanadium terminated V_2O_3(0001) at 90 K followed by annealing at different temperatures. Upon annealing, a new structure develops at ~532 eV in the O 1s region. This structure is detected up to at least 427 K. The identification of this feature is not clear yet but it is pointing towards some kind of interaction between the oxygen of the oxide surface and the adsorbed species.

The observation of the high binding energy structures in Figure 8.3(a) and (b) is reproducible. These structures are not due to a surface contamination which may result from CO or H_2O adsorption from the background atmosphere. To confirm this, the following 'fast' experiment was performed: propane was adsorbed on vanadium terminated V_2O_3(0001) at 90 K, and then the sample was directly annealed to 295 K. The corresponding spectra are shown in Figure 8.3(a) and (b) (labeled fast). These spectra also exhibit the structures at ~290.5 and 532 eV. Another experiment was carried out in which water was adsorbed on V_2O_3(0001) at 90 K followed by annealing to 165 K. The corresponding spectrum is shown at the top of Figure 8.3(b) (labeled H_2O). In the O 1s region, this spectrum exhibits two features which are attributed to hydroxyl groups (OH) and molecular water (H_2O) as already discussed in section 8.2.1. Comparing the two spectra at the top in Figure 8.3(b) reveals that the structure in the O 1s region, which is obtained after annealing the C_3H_8/V_2O_3(0001) layer, is located between the binding energy of OH groups and that of H_2O. This clearly indicates that this structure is neither due to H_2O nor to OH. However, it is possibly due to a species that contains OH groups.

Figure 8.3(c) shows a set of C 1s core level spectra obtained after C_3H_8 adsorption on vanadium terminated V_2O_3(0001) predosed with 0.5 L of oxygen. Similar to the case of C_3H_8 adsorption on the clean vanadium terminated sutface, the spectrum at 90 K exhibits an intense peak at 283.4 eV and a very small feature at 289.6 eV (Figure 8.3(c)). The peak induced by C_3H_8 decreases in intensity upon annealing due to C_3H_8 desorption. The intensity of the high binding energy feature increases after annealing to 179 K. This feature may also be attributed to an oxygen containing species.

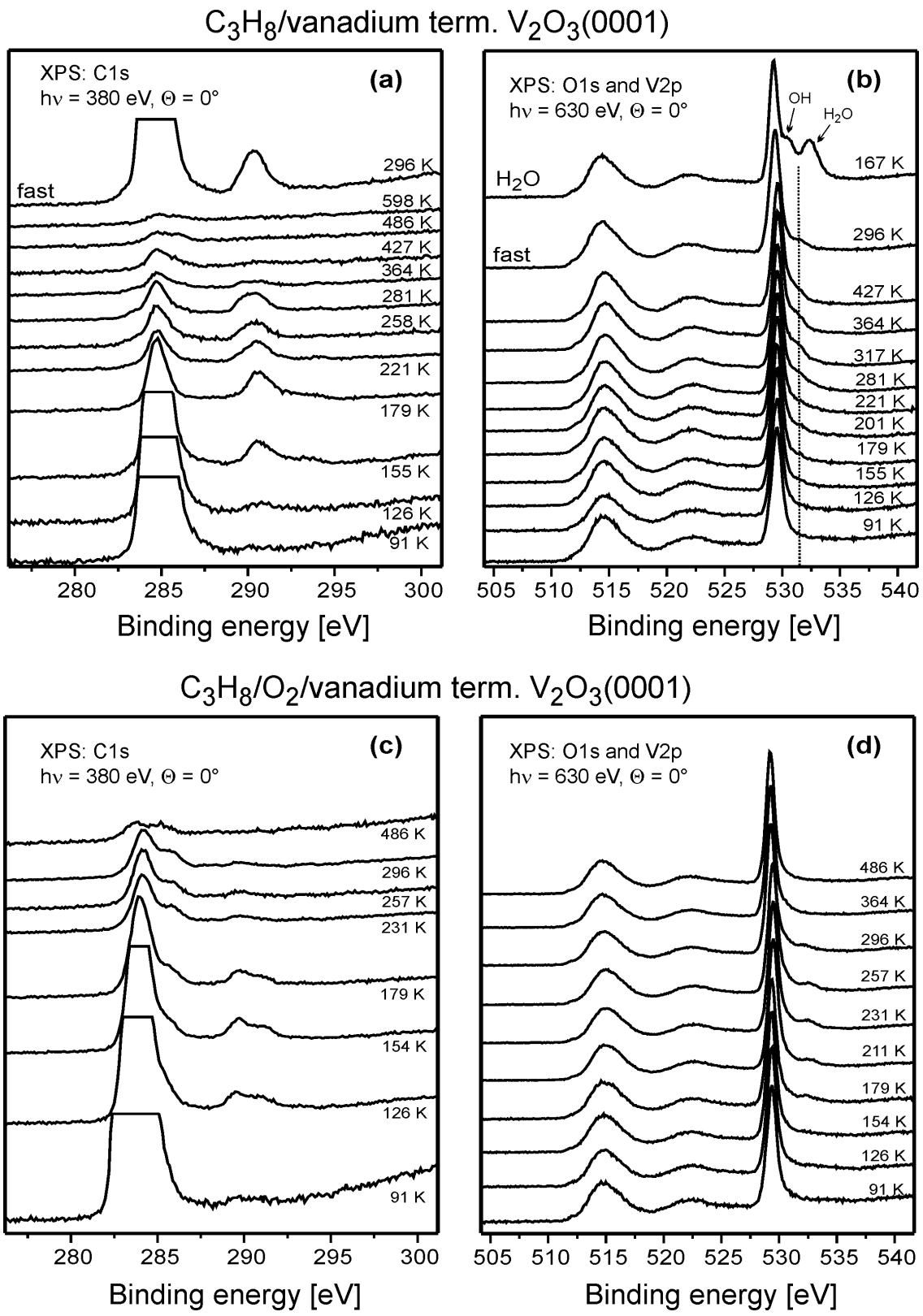

Figure 8.3: C 1s [(a) and (c)] and O1s+V2p [(b) and (d)] core level spectra of C_3H_8 on vanadium terminated V_2O_3(0001)/Au(111) and vanadium terminated V_2O_3(0001)/Au(111) predosed with 0.5 L O_2 as a function of the annealing temperature. C_3H_8 dosage (saturation coverage) was performed 91 K.

Figure 8.3(d) shows the O ls and V 2p core level spectra corresponding to the same experiment as Figure 8.3(c). No change occurrs in the O ls region except for the appearance of a small structure at 532.7 eV which can be attributed to molecular water adsorbed from the background atmosphere.

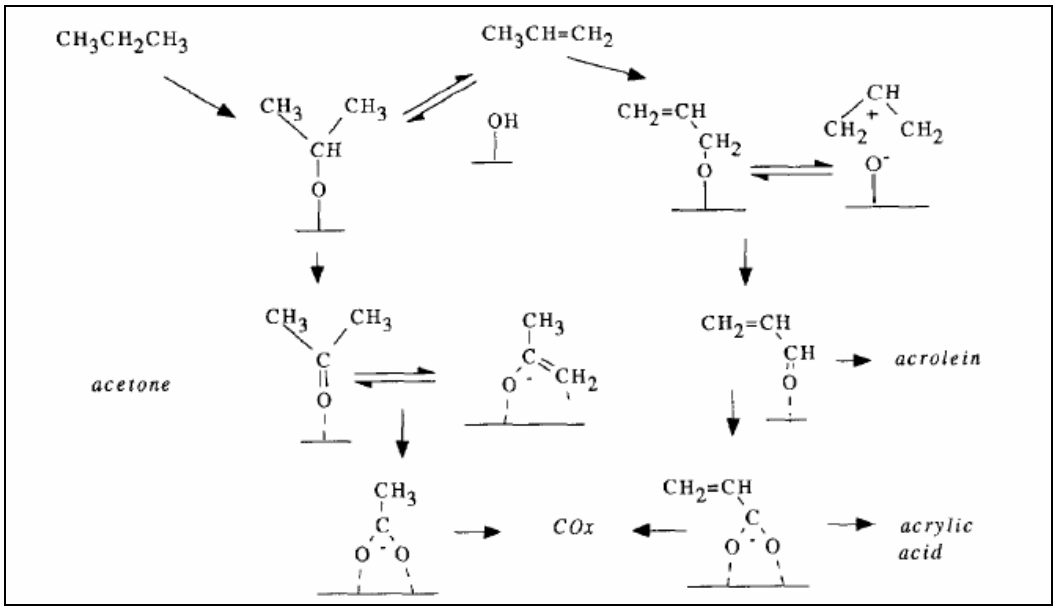

Figure 8.4: Surface reaction pathway for propane and propene oxidation over metal oxides [222].

In order to get more information about the effect of O_2-preadsorption, it is useful to compare the C 1s XPS spectra taken after propane adsorption on the clean vanadium terminated surface and the one predosed with O_2 (Figure 8.3(a) and (c)). Clearly, predosed O_2 significantly influences the interaction of propane with the $V_2O_3(0001)$ surface. The most pronounced effect is related to the oxygen containing species which is found to be less stable in the case of O_2-predosed surface since the corresponding C 1s intensity decreases at lower temperatures. The effect of oxygen is also obvious in the O ls and V 2p core levels spectra (Figure 8.3(b) and (d)). The structure at ~532 eV in the case of $C_3H_8/V_2O_3(0001)$ is not observed for the case of $C_3H_8/O_2/V_2O_3(0001)$. This may indicate that the predosed oxygen blocks the adsorption site responsible for the structure at 532 eV. Moreover, the structure at 532 eV and the high energy C1s peaks are probably not due to the same species. The C 1s core level spectra at high temperatures exhibit some intensity which is possibly due to propane adsorbed on defect sites or due to propane readsorption since the spectra were recorded at 90 K.

Similarly, the adsorption of propene on the clean surface and the one predosed with O_2 was also investigated. The XPS spectra are presented in Figure 8.5. Briefly, a high binding energy peak (at ~290.2 eV) is observed in the C 1s spectra which may be attributed to a species containing oxygen. This peak is detected up to 364 K. The corresponding V 2p and O 1s core level spectra show a peak in the O 1s region. These results are somewhat similar to the case of propane on vanadium terminated V_2O_3(0001).

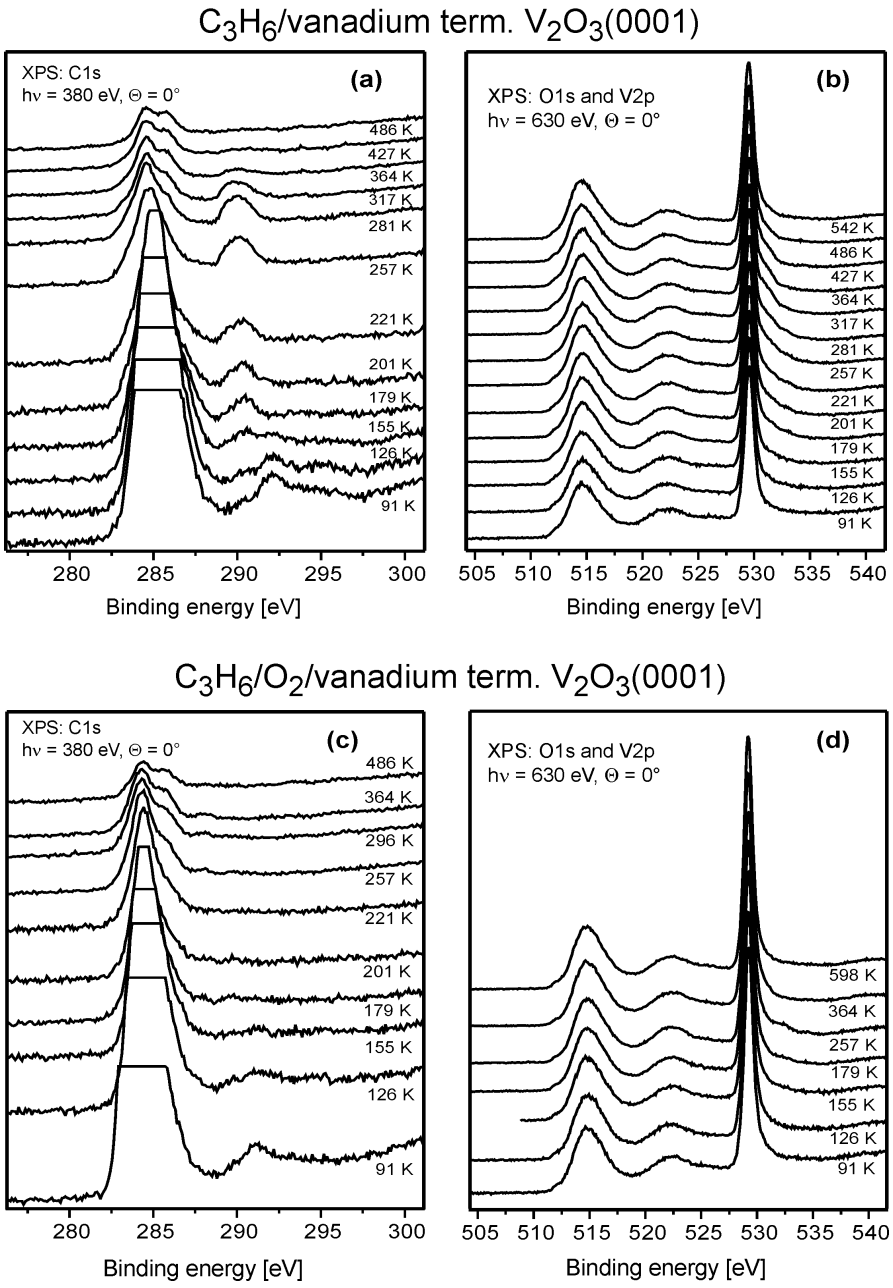

Figure 8.5: C 1s [(a) and (c)] and O1s+V2p [(b) and (d)] core level spectra of C_3H_6 on vanadium terminated V_2O_3(0001)/Au(111) and vanadium terminated V_2O_3(0001)/Au(111) predosed 0.5 L O_2 as a function of the annealing temperature. C_3H_6 dosage (saturation coverage) was performed 91 K.

8.2.3 NEXAFS

Figure 8.6 shows NEXAFS spectra recorded after propane adsorption on vanadium terminated V_2O_3(0001) at 91 K. These spectra were recorded at two different photon incidence angles: normal ($\alpha = 0°$) and grazing ($\alpha = 70°$). At 91 K, the NEXAFS spectra exhibit two broad resonances (labeled A and B) which are typical for hydrocarbons [76]. The A and B resonances are assigned to transitions into C–H and C–C antibonding orbitals, respectively [76]. The NEXAFS spectra recorded at 91 K agree nicely with measured spectra of gaseous propane [76] and with calculated NEXAFS spectra of propane [223]. Obviously, the resonance B consists of two peaks (labeled B1 and B2). The lower energy peak B1 is excited by the component of the electric field vector perpendicular to the CCC plane while the higher energy peak B2 is excited by the component parallel to the propane chain [76,224]. The enhanced intensity of the B1 peak at grazing incidence indicates that the propane is almost lying flat on the surface. Additional shoulders at about 287 and 286.5 eV (indicated by arrows) are more obvious at $\alpha = 70°$ than at $\alpha = 0°$. A particular interpretation of these structures is not very clear. Indeed, Stöhr et al. [225] demonstrated theoretically that the C–H resonance range of the central carbon atom of propane exhibits two states, namely the C–H π^* and σ^* states. One has to consider, of course, that the propane molecule contains two CH_3 and one CH_2 groups, which produce complex NEXAFS spectra [226]. These different groups should contribute to the C–H and the C–C resonances [223].

Obvious changes in the NEXAFS spectra are found after annealing to 179 K. At this temperature, the C_3H_8-induced resonance structures disappear due to propane desorption as indicated by the TDS data (Figure 8.1(a)). Additionally, two new structures at about 287.2 and 289.6 eV are found for $\alpha = 0°$, while three structures at about 287.2, 288.8 and 289.3 eV are found for $\alpha = 70°$. Based on the XPS data (Figure 8.3(a)), these structures are most likely associated with the oxygen containing species. However, the feature at 287.2 eV may also be attributed to the same species which induced the shoulder at about 287 eV in the spectrum at 91 K in Figure 8.6(b). Moreover, C_3H_8-induced structures at 179 K cannot be fully excluded especially in Figure 8.6(b), since the features at 179 K exhibit similar photon energies to those found for propane at 91 K.

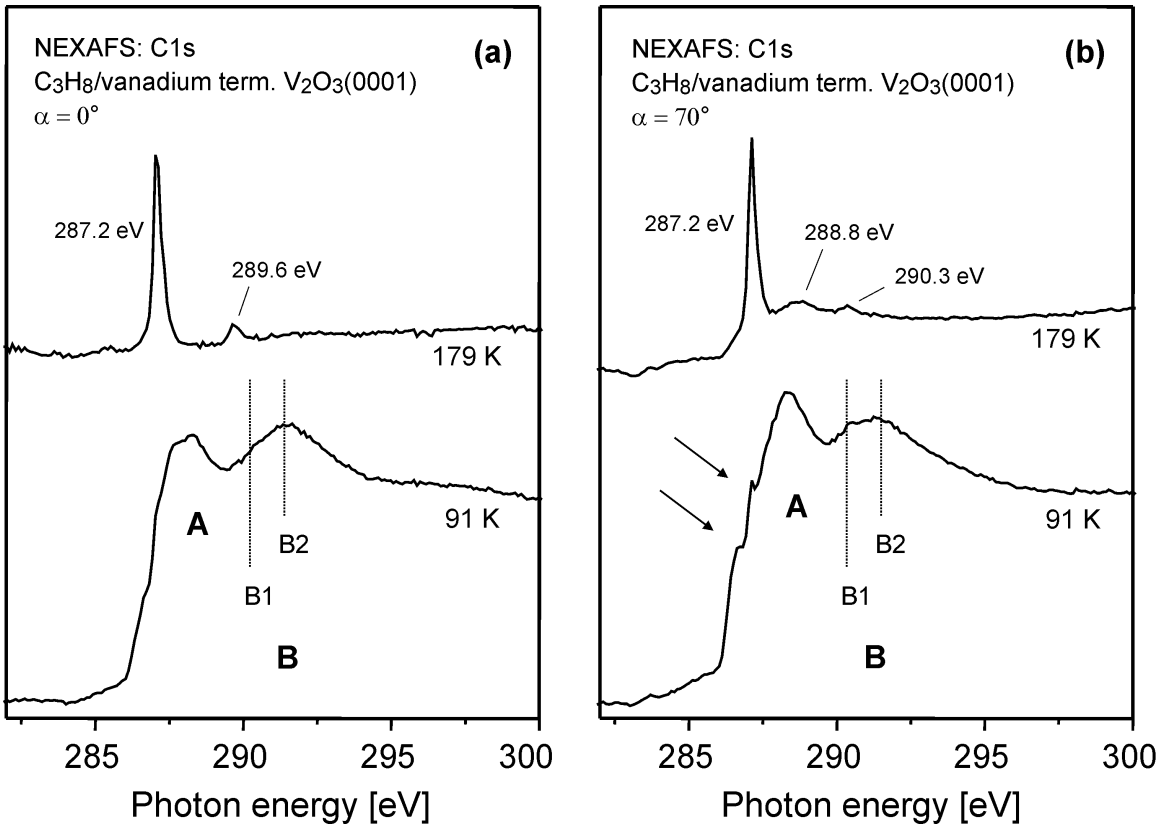

Figure 8.6: Left: C 1s NEXAFS spectra of vanadium terminated V_2O_3(0001)/Au(111) after C_3H_8 adsorption (saturation coverage) as a function of the annealing temperature. The NEXAFS spectra were recorded for two different light incidence angles as indicated.

In order to get more information from the NEXAFS spectra at 179 K, it is useful to compare these spectra with NEXAFS data of other oxygen containing species. In this context, similar NEXAFS spectra were reported for acetone on ZnO(0001) [227]. The spectra of acetone on ZnO(0001) exhibit structures at 287.6 and 289.0 eV which are in fair agreement with the features observed in Figure 8.6(a). As reported by several authors, the formation of acetone as intermediate is expected in the course of the propane oxidation reaction. However, the similarity of the NEXAFS data obtained for acetone on ZnO(0001) and the data obtained in the present study may also suggest the formation of an acetone-like species such as enolate. Interestingly, the structure at 289.6 is not present at α = 70°. This is possibly due to the molecular orientation of the oxygenate species. On the other hand, the structures at 288.8 and 290.3 eV, which may be attributed to C–H and C–C resonances of the oxygenate species, are not present at α = 0°. This may also be due to the molecular orientation of the oxygenate species.

8.3 Summary

The interaction of propane, as well as propene, with the vanadium terminated $V_2O_3(0001)$ surface was discussed. Based on the results presented above, it is concluded that propane adsorption on $V_2O_3(0001)$ gives rise to the formation of oxidized hydrocarbon species at low temperatures. Oxygen preadsorption may block certain adsorption sites as suggested by XPS. In spite of this, the formation of oxidized hydrocarbon species is observed. In the literature one can find a number of chemical reactions that occur at temperatures lower than 300 K. For example, Zaera and Chrysostomou reported the formation of propane at 210 K after the adsorption of propene on Pt(111) [228]. Similar findings were reported for propene on Mo(100) [229]. Other examples of low-temperature reactivities on metals and metal oxides are available in the literature [173,230-232]. However, comparative adsorption experiments for oxygen containing compounds on vanadium terminated $V_2O_3(0001)$ are needed to confirm (or to identify) the nature of the oxidized hydrocarbon species.

Chapter 9

Summary and outlook

The exploration of the structure–activity relationships observed for heterogeneous catalysts is necessary to understand how these materials function. However, technical catalysts and the chemical reactions occurring on their surfaces are usually very complex. Additionally, there are many experimental difficulties related to the application of surface science techniques to these systems. Therefore little is known about the microscopic details underlying the catalytic processes. An approach to handle these difficulties is to investigate simplified systems, so-called *model systems*, under UHV conditions. This approach permits the application of many well-established and powerful experimental methods of surface science to investigate the model catalysts as well as the chemical processes on their surfaces. Particularly, surface chemistry studies are essential to improve the understanding of the fundamental mechanisms in heterogonous catalysis.

The purpose of the present thesis was to contribute to the field of vanadium oxide catalysis via the study of the well-defined $V_2O_3(0001)$ model catalyst. A detailed description of various aspects of the $V_2O_3(0001)$ system was presented; beginning with the preparation, moving on to the characterization, and ending with the reactivity of this model system. Experiments were carried out under UHV conditions using a variety of surface science techniques such as low energy electron diffraction (LEED), thermal desorption spectroscopy (TDS), X-ray photoelectron spectroscopy (XPS), ultraviolet photoelectron spectroscopy (UPS), near-edge X-ray absorption fine structure (NEXAFS), infrared reflection-absorption spectroscopy (IRAS), and high resolution electron energy loss spectroscopy (HREELS). The application and combination of these surface sensitive techniques was found to be extremely valuable for studying the $V_2O_3(0001)$ model catalyst. Under typical UHV conditions, the $V_2O_3(0001)$ surface is terminated by a layer of vanadyl groups which can be reduced by electron irradiation to a layer of vanadium atoms. Comparative spectroscopic data were collected for both terminations. Each termination was found to exhibit characteristic electronic, geometric

and chemical properties. Correlations between the differently terminated $V_2O_3(0001)$ surfaces and their chemical activities could be established.

Conclusions that can be drawn from the preceding chapters are summarized in the following paragraphs.

The preparation of the $V_2O_3(0001)$ model catalyst

Well-ordered $V_2O_3(0001)$ thin films with a thickness of about 100 Å were grown on W(110) and Au(111) substrates. Usually ~50 Å of vanadium were deposited onto the respective substrate at 600 K in 1×10^{-7} mbar O_2 followed by annealing at 670 K in 1×10^{-7} mbar O_2 and then annealing in vacuum at 850 K. Under these conditions, the $V_2O_3(0001)$ films were found to be terminated by a layer of vanadyl groups. These groups are stable on the surface up to temperatures higher than 1000 K. The oxygen atoms of the vanadyl layer can be removed by electron irradiation in UHV leading to a surface terminated by vanadium atoms. Annealing the vanadium terminated surface in an oxygen atmosphere fully restores the vanadyl layer.

The characterization of the $V_2O_3(0001)$ model catalyst

Results obtained in the present work for $V_2O_3(0001)$ using LEED, XPS, UPS, IRAS, HREELS and NEXAFS are in good agreement with results reported previously in the literature for V_2O_3 single-crystals and thin films. The sharp reflexes observed by LEED indicate a high degree of a long-range order of the $V_2O_3(0001)$ films. IRAS and HREELS spectra of the vanadyl terminated surface exhibit a peak at 1040 cm^{-1} due to the excitation of vanadyl (V=O) stretching vibrations. This peak disappears after electron irradiation as a result of the removal of the vanadyl oxygen atoms.

Under very surface sensitive conditions, a V 2p surface state is observed in XPS spectra of the vanadyl terminated surface. This state vanishes after reduction of the surface by electron irradiation. The binding energy of this state indicates that the oxidation state of the surface vanadium atoms on the vanadyl terminated surface is higher than the oxidation state of the bulk vanadium atoms. This result is corroborated by ARUPS spectra which show that the V 3d induced intensity is smaller for the vanadyl terminated surface than for the vanadium terminated one. UPS spectra of the vanadyl terminated surface reveal a band at about 5 eV binding energy due to vanadyl groups.

The $V_2O_3(0001)$ surface states are also observed in NEXAFS spectra. In addition to the V 2p surface state, the NEXAFS spectra exhibit intensity due to a O 1s surface state which is associated with the vanadyl oxygen atoms on the vanadyl terminated surface. Features associated with other oxygen species in the surface region, namely threefold and fourfold coordinated oxygen species, are also observed in the NEXAFS spectra.

The work function is found to be 5.3 eV for the vanadium terminated surface and 6.3 eV for the vanadyl terminated one. The lower work function of the vanadium terminated surface is a result of the removal of the vanadyl oxygen atoms. Finally, the metal-insulator transition (MIT) of the $V_2O_3(0001)$ film is observed in UPS, NEXAFS and HREELS data. Theoretical calculations may be needed to explain the details of the data.

The reactivity of the $V_2O_3(0001)$ model catalyst

As the first adsorption system, oxygen on vanadium terminated $V_2O_3(0001)$ was studied. Oxygen adsorption at 90 K was found to occur both dissociatively and molecularly, as indicated by IRAS and HREELS. In addition to the formation of vanadyl groups, negatively charged adsorbed oxygen species in the form of peroxo (O_2^{2-}) species are also formed. Upon annealing the peroxo species dissociate and their oxygen atoms bond to the surface vanadium atoms forming vanadyl groups. As indicated by IRAS, the vanadyl terminated surface is fully recovered after annealing the O_2-dosed vanadium terminated surface.

The adsorption of carbon monoxide on $V_2O_3(0001)$ surfaces was also probed. The presented IRAS and XPS data clearly demonstrate that the interaction with CO depends on the $V_2O_3(0001)$ surface termination. CO was found to interact weakly with the vanadyl terminated surface and strongly with the vanadium terminated one. The presented data provide an insight into the complex adsorption behavior of CO on the vanadium terminated surface where different CO species are observed. These species exhibit different thermal stabilities. NEXAFS spectra recorded at 90 K reveal that CO is adsorbed in a tilted geometry on the vanadium terminated surface. Finally, IRAS show that vanadyl groups form when the CO-covered surface is annealed, indicating dissociation of part of the CO molecules.

Carbon dioxide was found to interact strongly with the vanadium terminated surface. Adsorption of CO_2 at 90 K leads to the formation of strongly bonded bent

$CO_2^{\delta-}$ species and weakly bonded linear CO_2 species. The formation of these species is confirmed by IRAS, XPS and NEXAFS. The $CO_2^{\delta-}$ is adsorbed in C_{2v} symmetry with the O–O axis being parallel to the surface as indicated by IRAS and NEXAFS. Solvation of $CO_2^{\delta-}$ with CO_2 leads to the formation of $CO_2 \bullet CO_2^{\delta-}$ dimers.

When the CO_2-covered surface is annealed, CO_2 desorbs and $CO_2^{\delta-}$ decomposes completely or partially according to the following equation:

$$CO_2^{\delta-} \longrightarrow CO + O^{\delta-}$$

TDS shows that CO is released into the gas phase, whereas O reacts with the surface vanadium atoms to form V=O groups as indicated by IRAS.

For water adsorption on $V_2O_3(0001)$ surfaces, the presented results clearly demonstrate the influence of the surface termination on the H_2O adsorption path. It was found that at 90 K H_2O adsorbs molecularly on the vanadyl terminated surface and dissociates partly on the vanadium terminated surface. Hydroxyl groups are formed on the vanadium terminated surface as evidenced by XPS, UPS, HREELS and IRAS. These OH groups are removed completely from the surface after annealing at temperatures higher than 600 K. TDS data show that the OH groups recombine and desorb as H_2O after annealing the OH-covered surface at temperatures higher than 300 K. This scenario appears to be consistent with that observed for dissociative adsorption and recombinative desoption on other oxide surfaces:

$$H_2O_{(a)} \xrightarrow{dissociation} OH_{(a)} + H_{(a)} \xrightarrow{recombination} H_2O_{(g)}$$

An amorphous ice layer is grown on the vanadyl terminated surface at 90 K. This layer transforms irreversibly into crystalline ice after annealing close to the H_2O multilayer desorption temperature.

The interaction of propane, as well as propene, with the vanadium terminated surface was also examined. Based on the presented data, the formation of oxidized hydrocarbon species at low temperatures is observed after propane (or propene) adsorption on the surface. Oxygen preadsorption may block certain adsorption sites as suggested by XPS. In spite of this, the formation of oxidized hydrocarbon species is observed. Further adsorption experiments on oxygen containing compounds on the vanadium terminated surface are needed to identify the nature of the oxidized hydrocarbon species.

At this point, the question that can be raised is: How do the adsorbates interact with the vanadium- and the vanadyl terminated $V_2O_3(0001)$ surface? Indeed, one essential conclusion that can be drawn from the present work is that the surface termination of $V_2O_3(0001)$ significantly influences its chemical activity. The vanadyl terminated $V_2O_3(0001)$ surface is chemically inert towards all the investigated molecules, whereas the vanadium terminated $V_2O_3(0001)$ surface is chemically active. Dissociative adsorption was only observed on the vanadium terminated surface. This difference between the chemical activities can be traced back to the electronic and geometric properties of the two surface terminations. These properties permit strong interactions with the vanadium terminated surface only.

The adsorption studies show that the chemical activity of the $V_2O_3(0001)$ surface is related to the accessibility of the surface vanadium atoms. The vanadium atoms on the vanadyl terminated surface are capped by oxygen atoms which hinder the access of adsorbate molecules to these vanadium atoms. On the other hand, the surface vanadium atoms on the vanadium terminated surface are not capped by oxygen atoms and therefore the adsorbates can approach these sites more closely which may lead to a stronger interaction. In addition to this, the vanadium atoms on the vanadium terminated surface are in a lower oxidation state compared to the vanadium atoms on the vanadyl terminated surface. This may facilitate the charge transfer from the vanadium atoms to the adsorbed molecules, which may lead to a stronger adsorbate-substrate bond or even to adsorbate dissociation.

Further investigations of the $V_2O_3(0001)$ model catalyst are required in order to deepen the understanding of this system. For instance, the interaction of $V_2O_3(0001)$ with other molecules which are relevant to industrial processes could be an area of research. When vanadium oxides are used in technical applications, they are often modified through doping with traces of metals or through combination with other oxides. Using the information gained for pure $V_2O_3(0001)$, one can step further by adding dopants to this model catalyst and then examining its chemical activity. Furthermore, reactivity studies in high pressure environments could be performed. The photoactivity of $V_2O_3(0001)$ model catalysts could also be examined. A combination of experimental measurements and theoretical calculations could be helpful to obtain further insights on the physical and chemical properties of $V_2O_3(0001)$ model catalysts.

Appendix A

Abbreviations:

ARUPS	Angular Resolved Ultraviolet Photoelectron Spectroscopy
AEY	Auger Electron Yield
ESCA	Electron Spectroscopy for Chemical Analysis
HREELS	High Resolution Electron Energy Loss Spectroscopy
FY	Fluorescent Yield
IRAS	Infrared Reflection-Absorption Spectroscopy
KE	Kinetic Energy
LEED	Low Energy Electron Diffraction
MCT	Mercury Cadmium Telluride
MIT	Metal-Insulator Transition
NEXAFS	Near-Edge X-ray Absorption Fine Structure
PES	Photoelectron Spectroscopy
PYD	Partial Yield Detector
UPS	Ultraviolet Photoelectron Spectroscopy
TDS	Temperature Desorption Spectroscopy
TEY	Total Electron Yield
TYD	Total Yield Detection
STM	Scanning Tunneling Microscopy
UHV	Ultra-high Vacuum
XAS	X-Ray Absorption Spectroscopy
XPS	X-Ray Photoelectron Spectroscop

Appendix B

Overview of reactions catalyzed by vanadium oxide based catalysts [43]:

- Selective oxidation of alkanes and alkenes
- Selective catalytic reduction of NO*x* with NH_3
- Oxidation of *o*-xylene to phthalic anhydride
- Ammoxidation of aromatics and methylaromatics
- Selective oxidation of methanol to formaldehyde
- Oxidation of SO_2
- Decomposition of isopropylalcohol
- Oxidation of aliphatic and aromatic hydrocarbons
- Photo-oxidation of CO
- Photo-isomerization of butene
- Partial oxidation of methane to formaldehyde
- Oxidation of H_2S
- Synthesis of isobutyraldehyde from methanol and ethanol
- Selective oxidation of 4-methylanisole
- Selective oxidation of *p*-methoxytoluene
- Alkylation of aldehydes with methanol
- Oxidative coupling of methane
- Synthesis of 2,6-dimethylphenol from methanol and cyclohexanone
- Synthesis of isobutyraldehyde from methanol and *n*-propylalcohol
- Total oxidation of benzene
- Dehydrocyclodimerization of isobutene to xylene
- Polymerization of olefins
- Selective oxidation of alkanes with peroxides
- Oxidative dehydrogenation of alkanes
- Isomerization of *m*-xylene
- Epoxidation of alkenes with peroxides
- Hydroxylation of phenol
- Direct conversion of methane to aromatics

Bibliography

[1] P.A. Cox, *Transition Metal Oxides: An Introduction to their Electronic Structure and Properties,* Clarendon Press, Oxford, 1992.

[2] D.P. Woodruff, *The Chemical Physics of Solid Surfaces: Oxide Surfaces*, Elsevier Science, 2001.

[3] G. Ertl, Knözinger, J. Weitkamp, *Handbook of heterogeneous Catalysis*, Wiley VCH, Weinheim, 1997.

[4] G.A. Somorjai, Surf. Sci. 299 (1994) 849.

[5] H.-J. Freund, M. Bäumer, J. Libuda, G. Rupprechter and S. Shakhudinov, J. Catal. 216 (2003) 223.

[6] H.-J. Freund, Surf. Sci. 500 (2002) 271.

[7] H.-J. Freund, M. Bäumer and H. Kuhlenbeck, Adv. Catal. 45 (2000) 333.

[8] P.L.J. Gunter, J.W.H. Niemantsverdriet, F.H. Ribeiro and G.A. Somorjai. Catal. Rev. Sci. Eng. 39 (1997) 77.

[9] C.T. Campbell, Surf. Sci. Rep. 27 (1997) 1.

[10] D.W. Goodman, Surf. Sci. Rev. Lett. 2 (1995) 9.

[11] V.E. Henrich and P.A. Cox, *The Surface Science of Metal Oxides,* Cambridge University Press, Cambridge, 1994.

[12] G.A. Somorjai, *Introduction to Surface Chemistry and Catalysis*, Wiley, New York, 1994.

[13] H.-J. Freund, H. Kuhlenbeck, J. Libuda, G. Rupprechter, M. Bäumer and H. Hamann, Topics Catal. 15 (2001) 201.

[14] D.W. Goodman, J. Catal. 216 (2003) 213.

[15] H.-J. Freund, Faraday Discuss. 114 (1999) 1.

[16] M. Bäumer and H.-J. Freund, Prog. Surf. Sci. 61 (1999) 127.

[17] J. Middeke, R.-P. Blum, M. Hafemeister and H. Niehus, Surf. Sci. 587 (2005) 219.

[18] C.H.F. Peden, G.S. Herman, I.Z. Ismagilov, B.D. Kay, M.A. Henderson, Y.-J. Kim and S.A. Chambers, Catal. Today 51 (1999) 513.

[19] S.C. Street and D.W. Goodman, Ann. Rev. Phys. Chem. 48 (1997) 37.

[20] H.-J. Freund, H. Kuhlenbeck and V. Staemmler, Rep. Prog. Phys. 59 (1996) 283.

[21] H-J. Freund, B. Dillmann, D. Ehrlich, M. Haßel, R.M. Jaeger, H. Kuhlenbeck, C.A Ventrice Jr, F. Winkelmann, S. Wohlrab, C. Xu, Th. Bertrams, A. Brodde and H. Neddermeyer, J. Mol. Catal. 82 (1993) 143.

[22] F. Zaera, Prog. Surf. Sci. 69 (2001) 1.

[23] H.-J. Freund, Catal. Today 100 (2005) 3.

[24] H-J. Freund, Angew. Chem. Int. Ed. Engl. 36 (1997) 542.

[25] K.B. Lewis, S.T. Oyama and G.A. Somorjai, Surf. Sci., 233 (1990) 75.

[26] G.H. Vurens, D.R. Strongin, M. Salmeron and G.A. Somorjai, Surf. Sci., 199 (1988) L387.

[27] H.K. Kim, T.Y. Seong and Y.S. Yoon, J. Vac. Sci. Technol. B 21 (2003) 754.

[28] Y. Naik, G.A.R. Rao and V. Venugopal, J. Rad. Nucl. Chem. 247 (2001) 11.

[29] K. Hermann and M. Witko, *Theory of physical and chemical behaviour of transition metaloxides: Vanadium and molybdenum oxides,* in D.A. King and D.P. Woodruff (Eds.), *Oxide Surfaces,* volume 9 of *The Chemical* Physics *of Solid Surfaces*, pages 136– 191, Elsevier, 2001.

[30] G. Micocci, A. Serra, A. Tepore, S. Capone, R. Rella and P. Siciliano, J. Vac. Sci. Technol. A 15 (1997) 34.

[31] D. Manno, A. Serra, M. D. Giulio, G. Micocci, A. Taurino, A. Tepore and D. Berti, J. Appl. Phys. 81 (1997) 2709.

[32] G.C. Granqvist, Solid State Ionics 70 1994 678.

[33] S.D. Hansen and C.R. Aita, J. Vac. Sci. Technol. A 3 (1986) 660.

[34] V.S. Pankajakshau, K. Neelakanden and C.S. Menon, Thin Solid Films 215 (1992) 196.

[35] O.B. Ajaya, A.A. Anani and A.O. Obabueki, Thin Solid Films 82 (1981) 151.

[36] T. Yoshino, N. Baba and Y. Konda, Jpn. J. Appl. Phys. 26 (1987) 782.

[37] G.T. Chandrappa. N. Steunou, S. Cassaignon, C. Bauvais, P.K. Biswas and J. Livage, J. Sol-Gel Sci. Technol. 26 (2003) 593.

[38] G.T. Chandrappa, N. Steunou and J. Livage, Nature, 416 (2002) 702.

[39] J.P. Schreckenbach and P. Strauch, Appl. Surf. Sci. 143 (1999) 6.

[40] V. Luca., D.J. MacLachlan, J.M. Hook and R. Withers, Chem. Mater. 7 (1995) 2220.

[41] F. Chaput, B. Dunn, P. Fuqua and K. Salloux, J. Non-Cryst. Sol. 188 (1995) 11.

[42] S. Surnev, M.G. Ramsey and F.P. Netzer, Prog. Surf. Sci. 73 (2003) 117.

[43] B.M. Weckhuysen and D.E. Keller, Catal. today 78 (2003) 25.

[44] B. Grzybowska-Swierkosz, Appl. Catal. A: Gen. 157 (1997) 409, and references cited therein.

[45] G. G. Cortez and M. A. Banares, J Catal. 209 (2002) 197.

[46] K.B. Lewis, S.T. Oyama and G.A. Somorjai, Surf. Sci. 233 (1990) 75.

[47] A.-C. Dupuis, M. Abu Haija, B. Richter, H. Kuhlenbeck and H.-J. Freund, Surf. Sci. 539 (2003) 99.

[48] K. Kishi, K. Hirai and T. Yamamoto, Surf. Sci. 290 (1993) 309.

[49] H. Niehus, R.P. Blum and D. Ahlbehrendt, Surf. Rev. Lett. 10 (2003) 353.

[50] K. Kishi, Y. Hayakawa and K. Fujiwara, Surf. Sci. 356 (1996) 171.

[51] F.P. Leisenberger, S. Surnev, L. Vitali, M.G. Ramsey and F.P. Netzer, J. Vac. Sci. Technol. A 17 (1999) 1743.

[52] S. Surnev, G. Kresse, M. Sock, M.G. Ramsey and F.P. Netzer, Surf. Sci. 495 (2001) 91.

[53] S. Surnev, L. Vitali, M. G. Ramsey and F. P. Netzer, G. Kresse and J. Hafner, Phys. Rev. B 61 (2000) 13945.

[54] J. Schoiswohl, M. Sock, S. Surnev, M.G. Ramsey, F.P. Netzer, G. Kresse and J.N. Andersen, Surf. Sci. 55 (2004) 101.

[55] J. Schoiswohl, S. Surnev, F.P. Netzer and G. Kresse, J. Phys. Condens. Matter 18 (2006) R1.

[56] J. Biener, M. Bäumer and R.J. Madix, Surf. Sci. 432 (1999) 178.

[57] M. Sambi, M. Della Negra and G. Granozzi, Surf. Sci. 470 (2000) L116.

[58] J. Biener, M. Bäumer, R.J. Madix, P. Liu, E. Nelson, T. Kendelewisz and G. Brown, Surf. Sci. 449 (2000) 50.

[59] G.S. Wong and J.M. Vohs, Surf. Sci. 498 (2002) 266.

[60] A.D. Rata, A.R. Chezan, M.W. Haverkort, H.H. Hsieh, H.-J. Lin, C.T. Chen, L. H. Tjeng and T. Hibma, Phys. Rev. B 69 (2004) 075404.

[61] I. Czekaj, K. Hermann and M. Witko, Surf. Sci. 525 (2003) 33.

[62] I. Czekaj, K. Hermann and M. Witko, Surf. Sci. 525 (2003) 46

[63] I. Czekaj, K. Hermann and M. Witko, Surf. Sci. 545 (2003) 85.

[64] G. Kresse, S. Surnev, J. Schoiswohl and F.P. Netzer, Surf. Sci. 55 (2004) 118.

[65] M. Abu Haija, S. Guimond, A. Uhl, H. Kuhlenbeck and H.-J. Freund, Surf. Sci. 600 (2006) 1040

[66] M. Abu Haija, S. Guimond, Y. Romanyshyn, A. Uhl, H. Kuhlenbeck, T.K. Todorova, M.V. Ganduglia-Pirovano, J. Döbler, J. Sauer and H.-J. Freund, Surf. Sci., accepted.

[67] P.K. Ghosh, *Introduction to Photoelectron Spectroscopy,* John Wiley & Sons, 1983.

[68] G. Ertl and J. Küppers. *Low Energy Electrons and Surface Chemistry.* VCH Verlagsgesellschaft, Weinheim, Germany, 1985.

[69] D.P. Woodruff and T.A. Dechar, *Modern Techniques of Surface Science*, Cambridge University Press, Cambridge, UK, 1986.

[70] L.C. Feldman and J.W. Mayer, *Fundamentals of Surface and Thin Film Analysis,* Elsevier Science, New York, 1986.

[71] C.N. Chitten, E.D. Pylant, A.L. Schwaner and J.M. White, *Thermal Desorption Mass Spectroscopy*, A.T. Hubbard (Ed.) *The Handbook of Surface Imaging and Visualization*, Chapter 59, CRC Press, Tokyo, 1995.

[72] P.A Redhead, Vacuum 12 (1962) 203.

[73] S. Hüfner, *Photoelectron Spectroscopy: Principles and Applications,* Springer, Berlin, 2003.

[74] F. Reinert and S. Hüfner, New J. Phys. 7 (2005) 97.

[75] D. Norman, J. Phys. C: Solid state Phys. 19 (1986) 3273.

[76] J. Stöhr, *NEXAFS Spectroscopy*, in: R. Gomer (Ed.), *Springer Series in Surface Science*, Vol. 25, Springer, Berlin, 1992.

[77] J. Kawai, *Absorption Techniques in X-ray Spectrometer,* in: R.A. Meyers (Ed.), *Encyclopedia of Analytical Chemistry*, pages 13288– 13315, John Wiley & Sons, 2000.

[78] J.F. Moulder, W.F. Sickle, P.E. Sobol and K.D. Bomben, *Handbook of X-ray Photoelectron Spectroscopy*, J. Chastain (Ed.), Perkin-Elmer Corporation, Eden Prairie (Minnesota), 1992.

[79] F.M. Hoffmann, Surf. Sci. Rep. 3 (1983) 107.

[80] P. Hollins, Vacuum 45 (1994) 705.

[81] B.E. Hayden, *Reflection Absorption Infrared Spectroscopy*, in: Jr.J.T. Yates and T. E. Madey (Eds.), *Vibrational Spectroscopy of Molecules on Surfaces*, volume 1 of *Methods of Surface Characterization*, Plenum Press, 1987.

[82] H. Ibach and D.L. Mills, *Electron Energy Loss Spectroscopy and Surface Vibrations*, Academic Press, 1982.

[83] M. Eremtchenko, F.S. Tautz, R. Öttking, V.M. Polyakov, F. Schwierz, G. Cherkashinin and J.A. Schaefer, Surf. Sci. 582 (2005) 159.

[84] www.bessy.de

[85] P. Feulner and D. Menzel, J. Vac. Sci. Technol. 17 (1980) 662.

[86] N.F. Mott and Contem. Phys. 14 (1973) 401.

[87] J.B. Goodenough, in: H. Reiss (Ed.), *Progress in solid state chemistry*, vol. 5, Pergamon, New York, 1971, p. 145.

[88] G. Keller, K. Held, V. Eyert, D. Vollhardt and V. I. Anisimov, Phys. Rev. B 70 (2004) 205116.

[89] P. Pfalzer, J. Will, A. Nateprov, Jr., M. Klemm, V. Eyert, S. Horn, A.I. Frenkel, S. Calvin and M.L. denBoer, Ohys. Rev B. 66 (2002) 085119.

[90] U. Schwingenschlögl, V. Eyert and U. Eckern, Europhys. Lett. 61 (2003) 361.

[91] H. Jhans and J.M. Honig, F.A. Chudnovskiy and V.N. Andreev, J. Solid State Chem. 159 (2000) 41.

[92] S. Mederle-Hoffmeister, S. Klimm, M. Klemm and S. Horn, Physica B 259 (1999) 851.

[93] J.W. Taylor, T.J. Smith, K.H. Andersen, H. Capellmann, R.K. Kremer, A. Simon, O. Schärpf, K-U. Neumann and K.R.A. Ziebeck, Eur. Phys. J. B 12 (1999) 199.

[94] M. Demeter, M. Neumann and W. Reichelt, Surf. Sci. 454–456 (2000) 41.

[95] K.E. Smith and V.E. Henrich, Phys. Rev. B 38 (1988) 5965.

[96] K.E. Smith and V.E. Henrich, Phys. Rev. B 38 (1988) 9571.

[97] G.A. Sawatzky and D. Post, Phys. Rev. B 20 (1979) 1546.

[98] P.J. Brown, M.M.R. Costa and K.R.A. Ziebeck, J. Phys. Condens. Matter 10 (1998) 9581.

[99] T. Uozumi, K. Okada, A. Kotani, R. Zimmermann, P. Steiner, S. Hufner, Y. Tezuka and S. Shin, J. Electron Spectrosc. Relat. Phenom. 83 (1997) 9.

[100] V.A. Gubanov, N.I. Lazukova and E.Z. Kurmaev, J. Solid State Chem. 19 (1976) 1.

[101] S. Shin, S. Suga, M. Taniguchi, M. Fujisawa, H. Kanzaki, A. Fujimori, H. Daimon, Y. Ueda, K. Kosuge and S. Kachi, Phys. Rev. B 41 (1990) 4993.

[102] V.M. Cherkashenko, V.E. Dolgih, E.Z. Kurmaev and A.A. Fotiev, J. Solid State Chem. 22 (1977) 217.

[103] R.L. Kurtz and V.E. Henrich, Phys. Rev. B 28 (1983) 6699.

[104] M. Catti, G. Sandrone and R. Dovesi, Phys. Rev. B 55 (1997) 16122.

[105] M. Catti and G. Sandrone, Faraday Discuss. 106 (1997) 189.

[106] L. F. Mattheiss, J. Phys.: Condens. Matter 6 (1994) 6477.

[107] A. Julbe, D. Farrusseng, D. Cot and C. Guizard, Cataly. Today 67 (2001) 139.

[108] G. A. Zenkovets, G. N. Kryukova, S. V. Tsybulya, V. F. Anufrienko, and V. Yu. Gavrilov, Kinetics and Catalysis, 42 (2001) 132

[109] B. P. Barbero, L. E. Cadús and L. Hilaire, Appl. Catal. A: Gen. 246 (2003) 237.

[110] Z. Chao and E. Ruckenstein, Cataly. Lett. 88 (2003) 147.

[111] Z. Chao and E. Ruckenstein, Catal. Lett. 94 (2004) 217.

[112] S. Shin, J. Phys. Soc. Jpn. 64 (1995) 1230.

[113] A.E. Bocquet, T. Mizokawa, K. Morikawa, A. Fujimori, S.R. Barman, K. Maiti, D.D. Sarma, Y. Tokura and M. Onoda. Phys. Rev. B 53 (1996) 1161.

[114] R. Zimmermann, R. Claessen, F. Reinert, P. Steiner and S. Hüfner, J. Phys. Condens. Matter 10 (1998) 5697.

[115] T. Uozumi, K. Okada and A. Kotani, J. Phys. Soc. Jpn. 62 (1993) 2595.

[116] D.S. Toledano, P. Metcalf and V.E. Henrich, Surf. Sci., 449 (2000) 19.

[117] K.E. Smith, Solid State Sci. 4 (2002) 359.

[118] P.W. Tasker, J. Phys. C: Soild State Phys. 12 (1979) 4977.

[119] C. Rehbein, N.M. Harrison and A. Wander, Phys. Rev. B 54 (1996) 14066.

[120] F. Rohr, M. Bäumer, H.J. Freund, J.A. Mejias, V. Staemmler, S. Müller, L. Hammer and K. Heinz, Surf. Sci. 372 (1997) L291.

[121] M. Wilde, O. Seiferth, K. Al-Shamery and H.J. Freund, J. Chem. Phys. 111 (1999) 1158.

[122] S. Wang, K. Murata, T. Hayakawa, S. Hamakawa and K. Suzuki, Appl. Catal. A 196 (2000) 1.

[123] A.-C. Dupuis, PhD thesis, Humboldt Universität Berlin, 2002, (English language).

[124] H.-J. Freund, B. Dillmann, O. Seiferth, G. Klivenyi, M. Bender, D. Ehrlich, I. Hemmerich and D. Cappus, Catal. Today 32 (1996) 1.

[125] B. Dillmann, F. Rohr, O. Seiferth, G. Klivenyi, M. Bender, K. Homann, I. N. Yakovkin, D. Ehrlich, M. Bäumer, H. Kuhlenbeck and H.-J. Freund, Faraday Disc. 105 (1996) 295.

[126] Z. Zhang and V.E. Henrich, Surf. Sci. 321 (1994) 133.

[127] C. Kolczewski and K. Hermann, Theo. Chem. Acc. 114 (2005) 60

[128] C.M. Kim, B.D. DeVries, D. Fröhberger and J.G. Chen, Surf. Sci. 327 (1995) 81.

[129] J.G. Chen, C.M. Kim, B. Fröhberger, B.D. DeVriesand and M.S. Touvelle, Surf. Sci. 321 (1994) 145.

[130] M. Abbate, H. Pen, M.T. Czyóyk, F.M.F. de Groot, J.C. Fuggle, Y.J. Ma, C.T. Chen, F. Sette, A. Fujimori, Y. Ueda and K. Kosuge, J. Electron Spectrosc. Relat. Phenom. 62 (1993) 185.

[131] B. Sass, C. Tusche, W. Felsch, N. Quaas, A. Weismann and M. Wenderoth, J. Phys.: Condens. Matter 16 (2004) 77.

[132] S. Guimond, M. Naschitzki, M. Abu Haija, H. Kuhlenbeck and H.-J. Freund, in preparation.

[133] D.S. Toledano, P. Metacalf and V.E. Henrich, Surf. Sci. 472 (2001) 21

[134] F. Pfuner, J. Schoiswohl, M. Sock, S. Surnev, M.G. Ramsey and F.P. Netzer, J. Phys.: Condens. Matter 17 (2005) 4035.

[135] H.-D. Kim, H. Kumigashira, A. Ashihara and T. Takahashi, Phys. Rev. B 57 (1998) 1316.

[136] O. Müller, J.P. Urbach, E. Goering, T. Weber, R. Barth, H. Schuler, M. Klemm, S. Horn and M.L. denBoer, Phys. Rev. B 56 (1997) 15056.

[137] W. Theis and K. Horn, Phys. Rev. B. 47 (1993) 16060.

[138] L. Hedin and A. Rosengren, J. Phys. F: Metal Phys. 7 (1977) 1339.

[139] P.H. Citrin, P. Eisenberger and D.R. Hamann, Phys. Rev. Lett. 33 (1974) 965.

[140] H. Abe, M. Terauchi, M. Tanaka and S. Shin, Jpn. J. Appl. Phys. 37 (1998) 584.

[141] H. Abe, M. Terauchi, M. Tanaka and S. Shin, Jpn. J. Appl. Phys. 38 (1999) 1403.

[142] J.-H. Park, L. H. Tjeng, A. Tanaka, J.W. Allen, C.T. Chen, P. Metcalf, J.M. Honig, F.M.F. de Groot and G.A. Sawatzky, Phys. Rev. 61 (2000) 11506.

[143] B. Sass, C. Tusche, W. Felsch, N. Quaas, A. Weismann and M. Wenderoth, J. Phys.: Condens. Matter 16 (2004) 77.

[144] H.H. Kung, *Oxidative dehydrogenation of light (C2 to C6) alkanes*, in: D. Riley, H. Pines, and W. Haag (Eds.), *Advances in Catalysis*, volume 40, page 1, Elsevier, 1994.

[145] A. Bielański and J. Haber, *Oxygen in Catalysis*, Marcel Dekker, New York,1991.

[146] M. Iwamoto and J.H. Lunsford, J. Phys. Chem. 84 (1980) 3079.

[147] V.E. Henrich, Rep. Prog. Phys. 48 (1985) 1481.

[148] A.A. Davydov, *Infrared Spectroscopy of Adsorbed Species on the Surfaces of Transition MetalOxides*, Wiley&Sons, Chichester, United Kingdom, 1990.

[149] C. Louis, T.L. Chang, M. Kermarec, T.L. Van, J.M. Tatiboüet and M. Che, Coll. Surf. A 72 (1993) 217.

[150] M. Haneda, T. Mizushima and N. Kakuta, J. Chem. Soc. Faraday Trans. 91 (1995) 4459.

[151] D. Barreca, F. Morazzoni, G.A. Rizzi, R. Scotti and E. Tondello, Phys. Chem. Chem. Phys. 3 (2001) 1743.

[152] T. Kawabe, K. Tabata, E. Suzuki, Y. Yamaguchi and Y. Nagasawa, J. Phys. Chem. B 105 (2001) 4239.

[153] V.V. Pushkarev, V.I. Kovalchuk and J.L. d'Itri, J. Phys. Chem. B 108 (2004) 5341.

[154] M. Che and A.J. Tench, *Characterization and reactivity of molecular oxygen species on oxide surfaces,* in: D.D. Eley, H. Pines, and P. B. Weisz (Eds.), *Advances in Catalysis*, volume 31, page 77, Elsevier, 1982.

[155] M. Che and A.J. Tench, *Characterization and reactivity of molecular oxygen species on oxide surfaces*, in: D.D. Eley, H. Pines, and P. B. Weisz (Eds.), *Advances in Catalysis*, volume 32, page 1, Elsevier, 1983.

[156] N. Sheppard, *Vibrational spectroscopy of adsorbates*, in: R.F. Willis (Ed.), *Springer Series in Chemical Physics*, , Vol. 15, Page 165, Springer Verlag, Berlin, 1980.

[157] C. Li, K. Domen, K. Maruya and T. Onishi, J. Am. Chem. Soc. 111 (1989) 7683.

[158] V.M. Bermudez and V.H. Ritz, Chem. Phys. Lett. 73 (1980) 160.

[159] J.P.S. Badyal, X. Zhang and B.M. Lambert, Surf. Sci. 225 (1990) L15.

[160] A.F. Carely, S.D. Jackson, B.M. Lambert and J.O'Shea, Chem. Phys. Lett. 545 (2000) 141.

[161] G. Busca, Catal. Today 41 (1998) 191.

[162] G. Blyholder, J. Phys. Chem. 68 (1964) 2772.

[163] J.C. Lavalley, Catal. Today 27 (1996) 377.

[164] G. Pacchioni, G. Cogliandro and P. Bagus, Surf. Sci. 255 (1991) 344.

[165] G. Pacchioni, T. Minerva and P. Bagus, Surf. Sci. 275 (1992) 450.

[166] G.B. Raupp and J.A. Dumesic, J. Phys. Chem. 89 (1985) 5240.

[167] M.A. Vannice and C. Sudhakar, J. Phys. Chem. 88 (1984) 2429.

[168] H. Kuhlenbeck, C. Xu, B. Dillmann, M. Haßel, B. Adam, D. Ehrlich, S. Wohlrab, H-J. Freund, U.A. Ditzinger, H. Neddermeyer, M. Neuber and M. Neumann, Ber. Bunsenges. Phys. Chem. 96 (1992) 15.

[169] M. Pykavy, V. Staemmler, O. Seiferth and H.-J. Freund, Surf. Sci. 479 (2001) 11.

[170] P. Concepción, H. Knözinger, J.M. López Nieto and A. Martíez-Arias, J. Phys. Chem. B 106 (2002) 2574.

[171] N. Magg, J.B. Giorgi, A. Hammoudeh, T. Schroeder, M. Bäumer and H.-J. Freund, J. Phys. Chem. B, 107 (2003) 9003.

[172] C. Lemire, S. Bertarione, A. Zecchina, D. Scarano, A. Chaka, S. Shaikhutdinov and H.-J. Freund, Phys. Rev. Lett. 94 (2005) 166101.

[173] G. Pacchioni, Surf. Sci. 281 (1993) 207.

[174] O. Seiferth, K. Wolter, B. Dillmann, G. Klivenyi, H.-J. Freund, D. Scarano and A. Zecchina, Surf. Sci. 421 (1999) 176.

[175] Y. Wang, A. Lafosse and K. Jacobi, J. Phys. Chem. B, 106 (2002) 5476.

[176] H.-J. Freund and M. W. Roberts, Surf. Sci. Rep. 25 (1996) 225.

[177] F. Solymosi, J. Mol. Catal. 65 (1991) 337.

[178] O. Seiferth, K. Wolter, H. Kuhlenbeck and H.-J. Freund, Surf. Sci. 505 (2002) 215.

[179] B.Bartos, H.-J. Freund, H. Kuhlenbeck, M. Neuman, H. Lindner and K. Müller, Surf. Sci. 179 (1987) 59.

[180] H. Peled and M. Asscher, Surf. Sci. 183 (1987) 201.

[181] G. Hess, H. Froitzheim and Ch. Baumgartner, Surf. Sci. 331–333 (1995) 138.

[182] M. Nassir and D. Dwyer, J. Vac. Sci. Technol. 11 (1993) 2104.

[183] F. Solymosi and G. Klivenyi, Surf. Sci. 315 (1994) 255.

[184] D. Ehrlich, S. Wohlrab, J. Wambach, H. Kuhlenbeck and H.-J. Freund, Vacuum 41 (1990) 157.

[185] J. Segner, C.T. Campbell, G. Doyen and G. Ertl, Surf. Sci. 138 (1984) 505.

[186] K.J. Maynard and M. Moskovits, Surf. Sci. 225 (1990) 40.

[187] H.-J. Freund and R.P. Messmer, Surf. Sci. 172 (1986) 1.

[188] A.R. Rossi and K.D. Jordan, J. Chem. Phys. 70 (1979) 4422.

[189] K. Nakamoto, *Infrared and Raman Spectra of Inorganic and Coordination Compounds*, Wiley, New York, 1978.

[190] J.A. Goldsmith and S.D. Ross, Spectrochim. Acta 24A (1968) 993.

[191] B.M. Gatehouse and S.E. Livingstone, R.S. Nyholm, J. Chem. Soc. (1958).

[192] H.-J. Freund, H. Behber, B.Bartos, G. Wedler, H. Kuhlenbeck and M. Neuman, Surf. Sci. 180 (1987) 550.

[193] J. Kiss, K. Revesz and F. Solymosi, Surf. Sci. 207 (1988) 36.

[194] G. Illing, D. Heskett, E.W. Plummer, H.-J. Freund, J. Somers, Th. Lindner, A.M. Bradshow, U. Stake, K. Heinz, P.L. Deandres, D. Saldin and J.B. Pendry, Surf. Sci. 206 (1988) 1.

[195] P.A. Thiel and T.E. Madey, Surf. Sci. Rep. 7 (1987) 211.

[196] M.A. Henderson, Surf. Sci. Rep. 46 (2002) 1.

[197] C.A. Muryn, P.J. Hardman, J.J. Crouch, G.N. Raiker, G. Thornton and D.S.L. Law, Surf. Sci. 251-252 (1991) 747.

[198] R.L. Kurtz, R. Stockbauer, T.E. Madey, E. Roman and J.L. De Segovia, Surf. Sci. 218 (1989) 178.

[199] C. Clay, S. Haq and A. Hodgson, Phys. Rev. Lett. 92 (2004) 046102.

[200] G.S. Karlberg and G. Wahnström, J. Chem. Phys. 122 (2005) 194705.

[201] T.J. Beck, A. Klust, M. Batzill, U. Diebold, C.D. Valentin, A. Tilocca and A. Selloni, Surf. Sci. 591 (2005) L267.

[202] S.J. Bushby, B.W. Callen, K. Griffiths, F.J. Esposto, R.S. Timsit and P.R. Norton, Surf. Sci. 298 (1993) L181.

[203] S. Hawkins, G. Kumi, S. Malyk, H. Reisler and C. Wittig, Chem. Phys. Lett. 404 (2005) 19.

[204] U. Leist, W. Ranke and K. Al-Shamery, Phys. Chem. Chem. Phys. 5 (2003) 2435.

[205] G. Busca, G. Ramis and V. Lorenzelli, J. Mol. Catal. 50 (1989) 231.

[206] M.A. Henderson and S.A. Chambers, Surf. Sci. 449 (2000) 135.

[207] V. Coustet and J. Jupille, Surf. Sci. 307-309 (1994) 1161.

[208] M.A. Henderson, S.A. Joyce and J.R. Rustad, Sur. Sci. 417 (1998) 66.

[209] M.A. Henderson, Surf. Sci. 355 (1996)151.

[210] Y.Yu, Q. Guo, S. Liu, E. Wang and P.J. Møller, Phys Rev. B 68 (2003) 115414.

[211] C. Lobban, J.L. Finney and W. F. Kuhs, Nature 391 (1998) 268.

[212] R.S. Smith and B.D. Kay, Nature 398 (1999) 788.

[213] T. Blasko and J.M. López Nieto, Appl. Catal. A 157 (1997) 117.

[214] H.H. Kung, Adv. Catal. 40 (1994) 1.

[215] E.A. Mamedov and V. Cortés-Corberán, Appl. Catal. A 127 (1995) 1.

[216] S. Albonetti, F. Cavani and F. Trifiró, Catal. Rev. Sci. Eng. 38 (1996) 413.

[217] B. Grzybowska-Swiekkosz, Appl. Catal. A 157 (1997) 409.

[218] E. Finocchio, G. Busca, V. Lorenzelli and R.J.Willey, J. Catal. 151 (1995) 204.

[219] K. Chen, A.T. Bell and E. Iglesia, J. Catal. 209 (2002) 35.

[220] G. Busca, E. Finocchio, V. Lorenzelli, G. Ramis and M. Baldi, Catal. Today 49 (1999) 453.

[221] M. Panizza, C. Resini, F. Raccoli, G. Busca, R. Catani and S. Rossini, Chem. Eng. J. 93 (2003) 181.

[222] G. Busca, E. Finocchio, G. Ramis and G. Ricchiardi, Catal. Today 32 (1996) 133.

[223] P. Väterlein, R. Fink, E. Umbach, and W. Wurth, J. Chem. Phys. 108 (1998) 3313.

[224] A. Imanishi, K. Isawa, F. Matsui, T. Tsuduki, T. Yokoyama, H. Kondoh, Y. Kitajima and T. Ohta, Surf. Sci. 407 (1998) 282.

[225] J. Stöhr, D.A Outka, K. Baberschke, D. Arvanitis and J.A. Horsley, Phys. Rev. B 36 (1987) 2976.

[226] S.G. Urquhart and R. Gillies, J. Phys. Chem. A 109 (2005) 2151.

[227] A. Gutiérrez-Sosa, T.M. Evans, S.C. Parker, C.T. Campbell and G. Thornton, Surf. Sci. 497 (2002) 239.

[228] F. Zaera and D. Chrysostomou, Surf. Sci. 457 (2000) 89.

[229] G. Wu and W.T. Tysoe, Surf. Sci. 391 (1997) 134.

[230] D.T.P. Watson, S. Titmuss and D.A. King, Sur. Sci. 505 (2002) 49.

[231] M.A. Henderson, S. Otero-Tapia and M.E. Castro, Faraday Discuss. 114 (1999) 313.

[232] S.A. Chambers, M.A. Henderson, Y.J. Kim and S. Thevuthasan, Surf. Rev. Lett. 5 (1998) 381.

Kurzzusammenfassung

Es werden die Ergebnisse einer systematischen Studie von verschiedenen Aspekten des wohldefinierten $V_2O_3(0001)$ Modellkatalysator-Systems präsentiert. Diese Studie behandelt die Präparation, die Charakterisierung und die chemische Reaktivität des $V_2O_3(0001)$ Modellkatalysators. Die Experimente wurden unter UHV-Bedingungen ausgeführt, wobei eine Reihe von oberflächensensitiven Methoden wie LEED, TDS, XPS, UPS, NEXAFS, IRAS, und HREELS zum Einsatz kamen .

In der vorliegenden Arbeit wurde der $V_2O_3(0001)$-Modellkatalysator als dünner Film von ~100 Å Schichtdicke auf Au(111)- und W(110)-Substraten präpariert. Die Oberfläche von $V_2O_3(0001)$ kann durch eine Lage von Vanadylgruppen oder durch eine Lage von Vanadiumatomen terminiert sein. Diese Oberflächen wurden charakterisiert, wobei der Fokus auf ihren geometrischen und elektronischen Eigenschaften lag, welche mit den chemischen Reaktivitäten verknüpft sind. Die chemischen Reaktivitäten der unterschiedlich terminierten $V_2O_3(0001)$-Oberflächen wurden durch Adsorption einer Reihe von Probenmolekülen untersucht. Die chemisorbierten Spezies wurden identifiziert und im Hinblick auf Stabilität, geometrische und elektronische Eigenschaften sowie mögliche vorliegende Reaktionskanäle untersucht. Die untersuchten Moleküle waren Sauerstoff, Kohlenmonoxid, Kohlendioxid, Wasser, Propan und Propen. Bei den Untersuchungen wurde speziell auf den Einfluss der Oberflächenterminierung auf die Adsorption und die Reaktivität dieser Moleküle eingegangen. So konnte eine Beziehung zwischen Struktur und Reaktivität aufgestellt werden.

Die vanadylterminierte $V_2O_3(0001)$-Oberfläche hat sich als chemisch inert gegenüber allen untersuchten Molekülen erwiesen, wohingegen für die vanadiumterminierte $V_2O_3(0001)$-Oberfläche chemische Reaktivität gefunden wurde. Der Unterschied zwischen den chemischen Reaktivitäten der beiden Oberflächenterminierungen resultiert aus den unterschiedlichen geometrischen und elektronischen Eigenschaften. Diese Eigenschaften erlauben starke Wechselwirkungen ausschließlich mit der vanadiumterminierten Oberfläche, was in manchen Fällen zu dissoziativer Adsorption führt. Anders als die Oberflächen-Vanadiumatome der vanadylterminierten Oberfläche sind die Oberflächen-Vanadiumatome der vanadiumterminierten Oberfläche ungehindert für die adsorbierten Moleküle zugänglich und liegen in einem niedrigeren Oxidationszustand vor. Die Adsorption von O_2 auf der vanadiumterminierten Oberfläche führt zur Bildung von Vanadylgruppen und negativ geladenen Peroxospezies (O_2^{2-}). Tempern der peroxo-bedeckten Oberfläche stellt die Vanadylterminierung wieder her. CO wechselwirkt stark mit der vanadiumterminierten Oberfläche und adsorbiert in einer gekippten Geometrie auf der Oberfläche. Tempern der CO-bedeckten Oberfläche führt zur Bildung von Vanadylgruppen, höchstwahrscheinlich über CO-Dissoziation. Die Adsorption von CO_2 auf der vanadiumterminierten Oberfläche induziert die Bildung stark gebundener, gewinkelter $CO_2^{\delta-}$ Spezies zusätzlich zu schwach gebundenen, linearen CO_2 Spezies. $CO_2^{\delta-}$ adsorbiert in C_{2v}-Symmetrie, wobei die O–O-Bindungsachse parallel zur Oberfläche liegt. Nach einem Tempervorgang zerfällt es zu CO und O, wobei die Sauerstoffatome Vanadylgruppen ausbilden. H_2O dissoziiert auf der vanadiumterminierten Oberfläche und bildet OH-Spezies aus, die bis ~600 K stabil sind. Die Adsorption von C_3H_8 und C_3H_6 auf der vanadiumterminierten Oberfläche zieht die Bildung einer oxidierten Kohlenwasserstoff-Spezies nach sich.

Acknowledgements

I would like to express my deep and sincere gratitude to Professor Hans-Joachim Freund for supervising this thesis. He gave me the opportunity to do this research in his group and to work in an excellent scientific environment in the department of Chemical Physics at the Fritz Haber Institute. His wide knowledge and logical way of thinking were of great value to me.

I gratefully acknowledge Professor Gerhard H. Findenegg for co-supervising this work.

I am deeply grateful to Dr. Helmut Kuhlenbeck. His active cooperation and extensive discussions were very helpful for the accomplishment of this study. His valuable comments and suggestions were essential to materialize the thesis in the present form. I warmly thank him and Sebastien Guimond for the perfect teamwork and support at BESSY. My thanks are also due to Alexander Uhl for his support during the vibrational spectroscopic measurements.

I wish to thank all those who helped me with my work. I am particularly grateful to Dr. Ayman Hammoudeh, Dr. Boonchuan Immaraporn, Hadj-Mohamed Benia, Ismail Abu Haija, Dr. Rafat Ahmad, Sarp Kaya, Samer Aburous, Dr. Thomas Schröder and Tobias Schalow. I also wish to thank Erika Popovic and Klaus Peter Vogelgesang for their help at the beginning of my work.

The financial support of the Deutsche Forschungsgemeinschaft through their Sonderforschungsbereich 546 is gratefully acknowledged.

I wish to extend my thanks to my friends in Jordan. My deepest appreciation goes to my parents and sisters for their love and support. Their unending prayers for my success were a true inspiration throughout my life.

I owe my special gratitude to the woman I love, my dear wife Maram Hammadeen, for her generous understanding and continuous support during this work.

Publications

- A.-C. Dupuis, **M. Abu Haija**, B. Richter, H. Kuhlenbeck and H.-J. Freund, V_2O_3(0001) on Au(111) and W(110): Growth, Termination and Electronic Structure, Surf. Sci. 539 (2003) 99.

- **M. Abu Haija**, S. Guimond, A. Uhl, H. Kuhlenbeck and H.-J. Freund, Adsorption of Water on Thin V_2O_3(0001) Films, Surf. Sci. 600 (2006) 1040.

- **M. Abu Haija**, S. Guimond, Y. Romanyshyn, A. Uhl, H. Kuhlenbeck, T.K. Todorova, M.V. Ganduglia-Pirovano, J. Döbler, J. Sauer and H.-J. Freund, Low Temperature Adsorption of Oxygen on Reduced V_2O_3(0001) Surfaces, Surf. Sci., 600 (2006) 1497.

- S. Guimond, **M. Abu Haija**, S. Kaya, J. Lu, J. Weissenrieder, S. Shaikhutdinov, H. Kuhlenbeck, H.-J. Freund and J. Sauer, Vanadium Oxide Surfaces and Supported Vanadium Oxide Nanoclusters, Topics Catal. 38 (2006) 117.

- A. Bandara, **M. Abu Haija**, F. Höbel, H. Kuhlenbeck, G. Rupprechter and H.-J. Freund, Molecular Adsorption on V_2O_3(0001)/Au(111) Surfaces, Topics Catal., submitted.